Model Predictive Control for Hybrid Annealing Furnace at Tata Steel IJmuiden

Formulation and validation of model and controller

D.R. Nusman

Master of Science Thesis

TU Delft Delft University of Technology

Delft Center for Systems and Control

Model Predictive Control for Hybrid Annealing Furnace at Tata Steel IJmuiden

Formulation and validation of model and controller

Master of Science Thesis

For the degree of Master of Science in Systems and Control at
Delft University of Technology

D.R. Nusman

September 27, 2017

Faculty of Mechanical, Maritime and Materials Engineering (3mE)
Delft University of Technology

The work in this thesis was supported by Tata Steel IJmuiden. Their cooperation is hereby gratefully acknowledged.

Delft University of Technology
Department of
Delft Center for Systems and Control (dcsc)

The undersigned hereby certify that they have read and recommend to the Faculty of Mechanical, Maritime and Materials Engineering (3mE) for acceptance a thesis entitled

Model Predictive Control for Hybrid Annealing Furnace at Tata Steel IJmuiden

by

D.R. Nusman

in partial fulfillment of the requirements for the degree of

Master of Science Systems and Control

Dated: September 27, 2017

Supervisor(s):

MSc. Hai Wu

Prof.dr.ir. Bart De Schutter

Reader(s):

Dr.ir. Ton van den Boom

Dr. Riccardo Ferrari

Abstract

The demand from the automotive industry for thinner, stronger and more ductile steels led to development of the so called Advanced High Strength Steel (AHSS). These new steel grades are produced at one of the hot dip galvanizing lines, "Dompel Verzinklijn 3" (DVL3), at Tata Steel IJmuiden. The annealing furnace in DVL3 consists out of a number of consecutive sections. One of these sections is the Slow-Cooling Section.

The Slow-Cooling Section, a so-called hybrid furnace, is installed with both heating and cooling capabilities to effectively adjust the temperature required by the metallurgical prescription of a specific steel strip product. The required temperature and associated cooling or heating demand can vary from strip to strip, depending on the desired mechanical properties and strip dimensions, which complicates the control of the Slow-Cooling Section. This is further complicated by process variations in production speed and system delays in control instrumentation. It becomes apparent that in order to produce these high quality steel grades, an improved solution to achieve precise temperature control in the slow cooling process has to be found.

In this research a Model Predictive Control (MPC) is developed for the control of the Slow-Cooling Section of DVL3. This advanced control system is based on a mathematical model, developed in the first part of this research, incorporating the heat transfer from and to the steel strips inside the Slow-Cooling Section. The nonlinear furnace model is validated with historical furnace data, showing good agreement for various process conditions. MPC is applied using two different methods. The first method is based on one linear internal model. The second method approximates the nonlinear mathematical model by the use of piecewise affine models. Case studies are performed to test the performance of the new controllers. The performance of the new controllers are compared with the current temperature control of DVL3.

A critical discussion is presented based on the results of both Model Predictive Controllers. It is shown that the predictive ability, especially in transient conditions is improved with the newly developed MPC and more accurate temperature control is achieved. Recommendations are given to further improve the control performance.

Table of Contents

List of Figures

List of Tables

Chapter 1

Introduction

Tata Steel is Europe's second largest steel producer. Many demanding markets are served, including aerospace, automotive, construction and packaging. Tata Steel in Europe annually produces more than 10 million tonnes of steel of which 5 million tonnes is cold rolled steel. After cold rolling, the steel strips undergo a heat treatment, better known as annealing. During the annealing treatment the desired microstructure and mechanical properties of the steel are produced. Tata Steel IJmuiden has many continuous annealing and hot dip galvanizing lines, designed for this purpose. These lines are primarily suited for stable operating conditions. However, the product portfolio is subject to diversification. This results in rapidly changing operating conditions for the annealing furnaces.

One of the hot dip galvanizing lines of Tata Steel IJmuiden focuses on steel for the automotive industry. The automotive industry requests thinner, stronger and more ductile steel than conventional low- to high-strength steels. These stronger and more ductile steel products are also known as Advanced or Ultra High Strength Steels. To produce steel products that are both strong and ductile, the cooling process in the annealing furnace becomes increasingly important, due to the phase transformations taking place during the cooling. The cooling process takes place in two sections in the annealing furnace. The first cooling section, called the Slow-Cooling Section, is the focus of this research. In order to obtain strong and ductile steel, accurate temperature control throughout the annealing furnace is required. Both the required accurate temperature control and the product batches getting smaller and more diverse lead to the demand for an advanced control system.

The steel industry in Europe is suffering from fierce competition, high raw material prices and low product prices. So besides the production complexity, the influence of the steel market demands a more efficient use of the plants also. More efficient use of the plants can be realised by implementing a more advanced control system.

Model Predictive Control (MPC) is seen as a suitable successor of conventional control systems to control the annealing furnaces and make this process more efficient [7, 17, 32, 41, 47]. MPC is an umbrella name for a range of control methods [27]. These control methods, based on a process model, calculate the optimal control action by solving, at every time step,

a receding prediction horizon open-loop optimisation problem. The optimisation problem starts, iteratively, at the current state of the plant and returns the optimal control sequence for the finite horizon, while respecting process constraints. The control system uses a process model to predict the dynamics of the associated plant. The performance of the control system depends on the quality of this process model.

1-1 Research Objective

The development of a model-based predictive controller, to improve the temperature control performance of the Slow-Cooling Section, is studied in this research. It also includes the development of a suited process model as required in a model-based predictive controller. The Slow-Cooling Section contains both cooling and heating elements and can therefore be seen as a hybrid set-up. The process in the annealing furnaces is subject to varying operating conditions, which also complicates the modelling and control. The research goal is therefore defined as follows:

"How can the hybrid set-up of the Slow-Cooling Section be modelled and controlled, while respecting all process variations, such that precise temperature control can be achieved"

The research question can be split into two major parts. The first part includes the modelling of the Slow-Cooling Section to mathematically describe the dynamics of the thermal process, with respect to the process constraints and varying process conditions. The nonlinear model is validated against process data. The second part covers the development of the model-based predictive controller. The performance of the controller is tested using simulations. The goal of the new controller is to obtain accurate temperature control, while maximising efficiency of the Slow-Cooling Section and respecting the constraints.

1-2 Structure of the Thesis

In Chapter 2 some background on the annealing process and more specific information on the Slow-Cooling Section is given. The literature review in Chapter 3 leads to the selection of the type of controller, which sets further requirements for the type of process model, to take into account multiple process parameters, constraints and disturbances. The process model of the Slow-Cooling Section is developed in Chapter 4. The nonlinear process model is prepared in the first part of Chapter 5, so that it can be applied in an MPC framework. Two approaches are used in Chapter 5 for the development of two Model Predictive Controllers. The control systems are tested in Chapter 6 by performing simulations, using historical production data. A critical discussion is presented based on the results of both Model Predictive Controllers. Finally, in Chapter 7 conclusions that can be drawn and recommendations for future research are given.

The nonlinear process model requires knowledge on heat transfer. Basic theory on heat transfer is explained in Appendix A. The physical and chemical behaviour of steel is explained in Appendix B.

Chapter 2

Process Background

2-1 Introduction

In the steel industry it is a common practice to cast steel into slabs. These slabs are rolled to a thinner strip. To produce the desired mechanical properties and to apply a zinc layer as protective layer, the steel undergoes a series of treatments in the hot dip galvanizing lines. Tata Steel has a number of strip processing lines designed for this purpose, including "Dompel Verzink Lijn 3" (DVL3) at IJmuiden, schematically depicted in Figure 2-1. Cold rolled steel strips arrive at the hot dip galvanizing line in coils. The steel strips are welded to each other to ensure a continuous process. Besides cleaning and surface corrections, the annealing treatment in DVL3 is designed to produce the desired mechanical properties. The annealing furnace is highlighted in red in Figure 2-1. This research focusses on one of the sections of the annealing furnace.

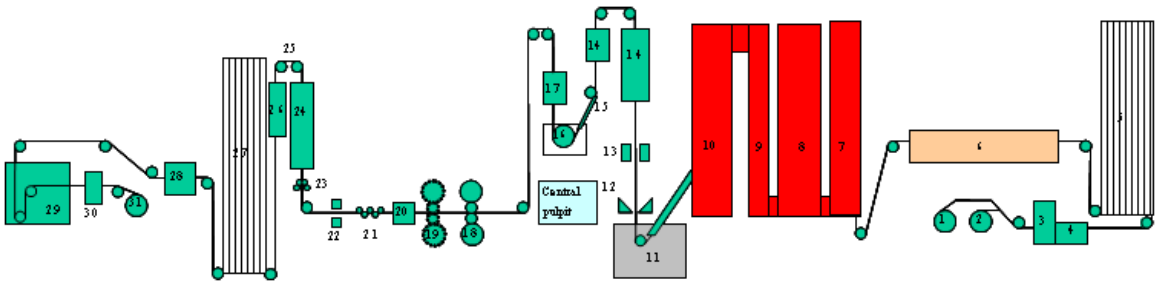

Figure 2-1: Schematic overview of DVL3.

2-2 Annealing Furnace

One of the most important parts of DVL3 is the annealing furnace. Annealing is a heat treatment process, applied to cold rolled steel, to produce the desired mechanical properties.

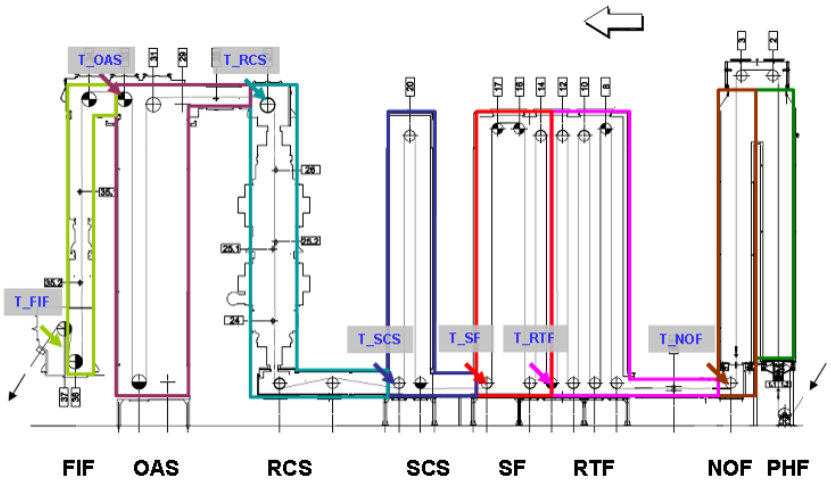

Figure 2-2: Schematic overview of the annealing furnace in DVL3.

The most important mechanical properties of steel are strength and ductility. Modern steel types combine these two properties. However, steel that is both strong and ductile is very difficult to produce. Therefore, besides the chemical composition and crystal structure of the material, the annealing treatment plays an important role to obtain these properties also. The annealing treatment occurs in a number of consecutive sections, depicted in Figure 2-2. The temperature of the steel throughout the annealing furnace is predefined by an annealing recipe. An example of an annealing recipe is depicted in Figure 2-3.

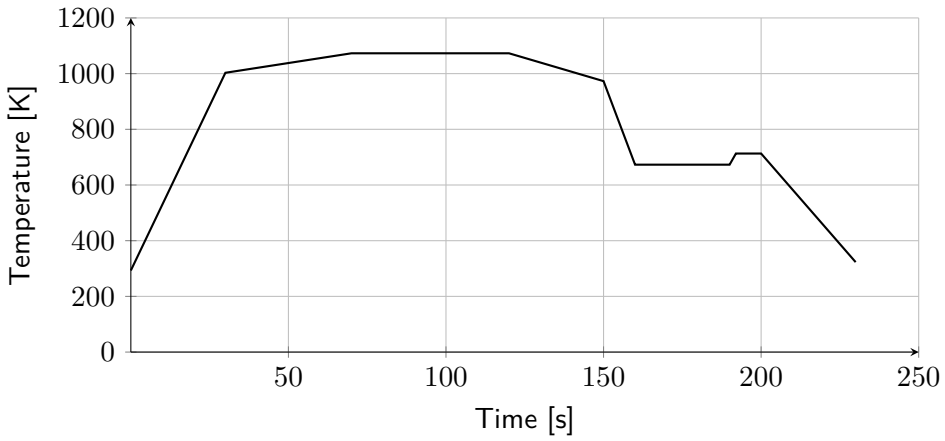

Figure 2-3: Example of an annealing recipe.

2-3 Slow-Cooling Section

The focus of this thesis is on the Slow-Cooling Section in DVL3. The steel strip traverses the Slow-Cooling Section in two passes. The strip enters the furnace at a temperature between 1133 - 1033 K and leaves at a temperature between 1073 - 923 K. The Slow-Cooling Section contains both cooling and heating elements, divided in an upper and lower cooling zone. Fans

provide the circulation of the protective gas. The protective gas is cooled in water-cooled heat exchangers. The heating is done by electric heating elements to compensate for the heat losses to the surroundings and to keep and / or raise the furnace temperature to a desired level. The key parameters of the Slow-Cooling Section are depicted in Table 2-1.

Table 2-1: Key parameters of the Slow-Cooling Section.

Parameter	Value	Unit
Strip width	900 - 2.050	mm
Strip thickness	0,6 - 2,5	mm
Line speed (max.)	180	m/min
Number of recirculation fans	2	-
Number of heating elements	21	-
Number of transport rolls	3	-
Throughput of steel	550	kt/y

2-3-1 Recirculation Fans

The most important components in the Slow-Cooling Section are the recirculation fans. The protective gas, a mixture of hydrogen and nitrogen, is circulated by the fans. The fans rotate with a certain rotational speed to propel the protective gas into the Slow-Cooling Section. This results in heat transfer via convection. If the heat transfer coefficient belonging to the heat transfer from the strip to the protective gas can be expressed as a function of the rotational speed, then it can be used as an input to the control system. The fan affinity laws [20] describe the affine relation between rotational speed and flow.

2-3-2 Electric Heating Elements

The steel strip is cooled in the Slow-Cooling Section. Although the furnace is insulated to high standards, heat is still lost to the surroundings. In order to maintain the desired temperature in the Slow-Cooling Section, multiple electric heating elements are installed in the furnace.

In the upper and lower part of the Slow-Cooling Section, 3 and 6 electric heaters are installed, respectively, to keep the transport rolls at same temperature as the strip. The transport rolls and strip have to be at the same temperature to prevent the strip from buckling. In the middle part 12 additional electric heaters are installed for line starts and process control. The heating elements are placed directly on the furnace walls. The heating elements convert electricity into heat via resistive heating. When the relation between supplied power and generated heat is known, the supplied power can be used as an input to the control system.

2-3-3 Process and Instrumentation Diagram

In Figure 2-4 the process and instrumentation diagram of the Slow-Cooling Section is depicted. The locations of the heating elements are an approximation of the reality. Figure 2-4a is seen from the previous section in the annealing furnace. The black lines indicate the direction of

the protective gas. Figure 2-4b shows the Slow-Cooling Section from the operator side. The strip comes in from the previous section at the right and leaves the Slow-Cooling Section at the bottom left to the next section. The direction of the strip is indicated by the black arrow. The small red dots near the bottom transport rolls indicate the location of the pyrometers.

2-4 Conclusions

In this chapter important background information on the process inside the hot dip galvanizing line, "Dompel Verzink Lijn 3" is given. More specific, information on the Slow-Cooling Section and its components is given. The Slow-Cooling Section is one of the sections of the annealing furnace. Inside the annealing furnace a heat treatment is applied to the steel strips to produce the desired mechanical properties, i.e. strength and ductility. The recirculation fans and the electric heating elements are the actuators available for temperature control inside the Slow-Cooling Section. A process and instrumentation diagram is given for the reader to get a complete overview of the set-up of the Slow-Cooling Section.

In order to describe the Slow-Cooling Section, while respecting all the process variations, depicted in Table 2-1, it is important to obtain specifications on the recirculation fans and heating elements. Besides the recirculation fans and the electric heating elements, heat exchangers are also present in the Slow-Cooling Section. Due to the limited availability of specifications and drawings it is decided that the dynamics of the heat exchanger falls outside the scope of this research.

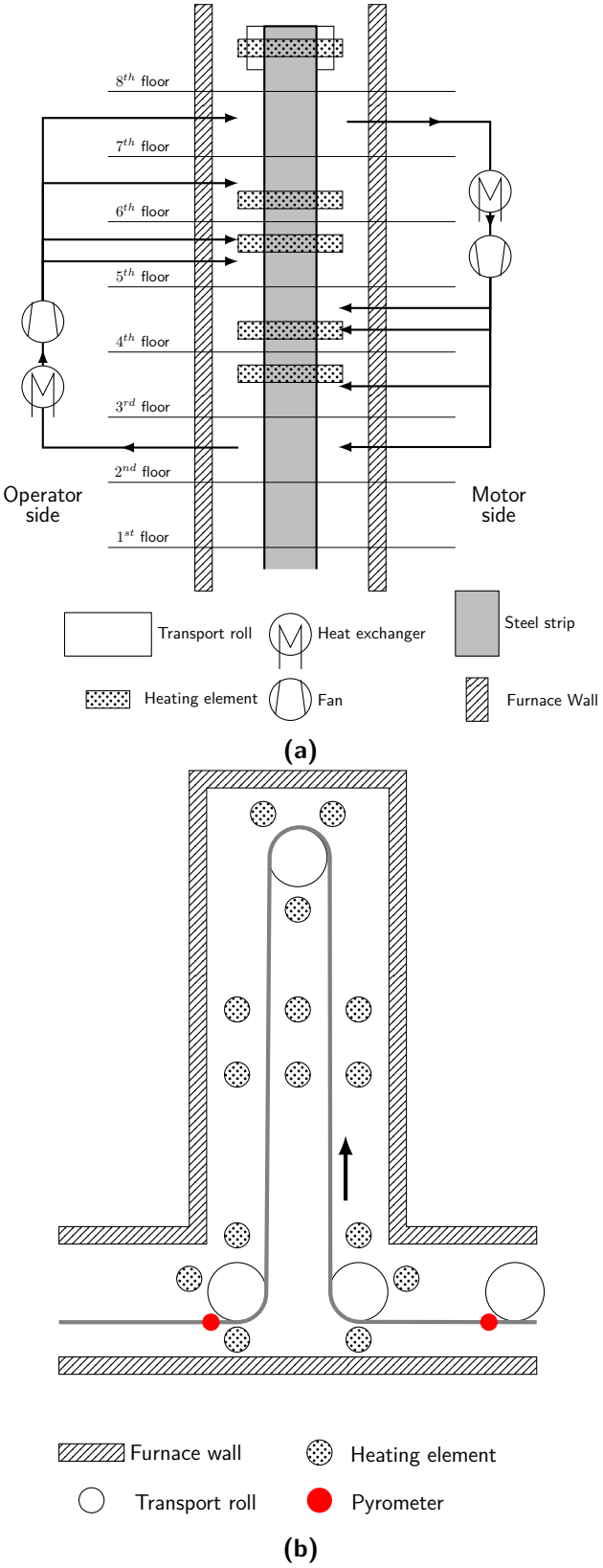

Figure 2-4: Process and instrumentation diagram Slow-Cooling Section.

Chapter 3

Literature Survey on Furnace Control

3-1 Introduction

This chapter provides a summary of research related to furnace modelling and furnace control. Relevant modelling techniques used for modelling of annealing furnaces are discussed in Section 3-2. In Section 3-3 relevant furnace controllers are discussed. Both sections are concluded in Section 3-2-3 and Section 3-3-5.

3-2 Furnace Modelling

A lot of research is done into the modelling and control of annealing furnaces. However, the focus of the available literature, including a few published by Wu et al. [46–48] is mainly on the first couple of sections in the annealing furnace. The first sections involve the fast heating of the steel to higher temperatures, which is very important for the quality of the final steel products and yet difficult to control. The modelling techniques described in the found literature to model the first sections can be used for the development of the model in this research.

3-2-1 Theoretical Modelling

Since the processes inside annealing furnaces are relatively well-known, the vast majority of the literature uses a theoretical approach for the modelling of annealing furnaces. The advantage of a theoretical modelling approach is that it gives physical insight into the process. A theoretical model leads to clear physical interpretations, such that control variables are easily selected. Tata Steel IJmuiden has several processing lines to which Model Predictive Control can be applied. By using a theoretical approach, process models can easily be extended and applied to comparable systems.

In [32–35] mathematical models for direct- and indirect-fired furnaces are proposed by Niederer et al. The strip motion is described based on Lagrangian coordinates. Niederer et al. present the use of Lagrangian coordinates as a good alternative to Eulerian coordinates. The use of Eulerian coordinates requires a relatively fine spatial discretisation of the strip and therefore increases the computational demand. In [32] Only the radiative heat transfer is considered. Many papers neglect the longitudinal direction of the furnace, when modelling the radiative heat transfer. Niederer et al. describe the heat exchange due to radiation based on the net-radiation method. The solution is approximated by means of the Galerkin weighted residual method. In the direct-fired furnace the chemical reactions of the fuel and air are taken into account. The dynamics of the flue gas are considered fast and count as input for the slower subsystem, describing the dynamics of the steel, transport rolls and furnace walls. In [33] a model of an indirect-fired furnace is derived. In an indirect-fired furnace, the steel is mainly heated by radiant tubes. In contrast with direct-fired furnace, where the gas medium is considered an participating medium for radiation, the atmosphere in an indirect-fired furnace is filled by an inert gas. The inert gas is transparent for thermal radiation, comparable to the atmosphere in the Slow-Cooling Section. The solution of the extensive mathematical model is approximated by use of Euler's explicit method. In [34], Niederer et al. switch from the Lagrangian coordinates to Eulerian coordinates to describe the evolution of the strip temperature.

A research group of Vienna University developed a mathematical model of a slab reheating furnace in [40]. The steel is pushed through the furnace, where fuel-fired burners serve as heat sources. Since temperature measurement possibilities are limited in such a furnace, the temperatures are estimated by an extended Kalman filter. In most studies, the temperature profile inside the steel is assumed 1-dimensional. In [40] also a 1-dimensional temperature profile is assumed, based on the fact that the length and width of the steel slabs are much larger compared to the thickness. The heat transfer modes considered in this research are conduction and radiation. The radiative heat transfer is approximated by the net radiation method, comparable to [32].

Yoshitani et al. present in [49] a furnace model by applying the heat balance equation. The model is divided into two sub-models. The first is a dynamic model, derived from the heat balance equation. The second sub-model is a static model, obtained by curve-fitting approximation. The heating section of an annealing furnace is modelled in this paper. Since Model Predictive Control is an on-line control system and the computation time required to solve the optimisation routine relies on the size and complexity of the internal model. By using a combination of two models, a dynamic and static model, the computational demand is quite large.

Besides using a furnace model as basis for on-line control systems, models can also be used in new furnace design and off-line studies to investigate the operating parameters that affect the furnace perfomance, as shown in [11]. Chapman et al. developed a mathematical model of a batch reheating furnace. Comparable to the Slow-Cooling Section, the furnace was modelled as a well-stirred enclosure. Obtaining a model for off-line studies or new furnace design is typically done by applying computational fluid dynamics.

In [1] an experimental and computational fluid dynamics studies is reported on combustion and radiation heat transfer from radiant tube heaters, comparable to the heaters in the Radiant-Tube Furnace in DVL3. A three dimensional CFD model was developed, to analyse

the heat transfer and combustion phenomenon in a radiant heater. The use of computational fluid dynamics allows high-resolution evaluations of the heat and mass flows in the furnace. In the literature, computational fluid dynamics models typically take into account the furnace geometry, energy exchange between all the elements and possible heating or cooling processes, such as combustion. A model based on computational fluid dynamics are usually not applicable suitable for real-time control design, due to their complexity and high dimensions. Depree et al. study an annealing furnace comparing two methods in [13]. A three dimensional model is used to investigate the temperature dynamics of the steel strip inside the annealing furnace. The results from the three dimensional model are compared to thermocouple measurements. The information obtained from the high-fidelity model is used to develop a simplified one dimensional model. The finite element modelling package COMSOL is used for the full three dimensional model. The software package allows the complex geometries inside the furnace to be modelled in detail. The model solves the heat equation for conduction inside the furnace and the radiative exchange is described using a hemicube radiosity algorithm. It is mentioned that the strip edges heat faster than the strip centre. This could be important when temperatures approaches the recrystallisation temperature. Depree et al. claim that this can be modelled in the three dimensional model in COMSOL, but not in a simplified one dimensional model. Since the three dimensional model is computationally expensive to solve, a simplified one dimensional model is approximated. The simplified model uses mesh spacing in both width and thickness direction of the strip and can therefore also be considered a two dimensional model. The results from the three dimensional and one dimensional models are compared. The simplified model shows good agreement with the high-fidelity COMSOL model. The simplified model can be applied in an on-line controller. But the use of such modelling software shows that the system can be modelled in detail and then simplified for use in an on-line controller. In [8, 45] it is stated that the calculating time of conventional computational fluid dynamics modelling techniques is reduced by combining the computational fluid dynamics simulation with classical zone method. In [21] Hu et al. combine the advantages of the classical zone method and computational fluid dynamics. The computation time is 21 - 170 times faster than real-time. By combining these two modelling methods, such a model can be used in real-time control methods.

3-2-2 Experimental Modelling

In contrast to the studies presented above, some studies use an experimental approach for modelling of annealing furnaces. The developments of modelling algorithms and advances in computing power give rise to the use of experimental modelling methods. Experimental modelling is also known as black-box modelling or system identification. The major advantage of these techniques is that only input and output data is needed for the estimation of the model. The system dynamics and parameters are estimated by the use of the input and output data. This directly yields a disadvantage. If a system changes, the model becomes less applicable to the new situation. The reproducibility of such models is low, compared to models based on first principles. Unforeseen disturbances and process dynamics are however captured and limited knowledge of the system is required to obtain a process model.

In [39] the dynamics of a galvannealing section are approximated by a Radial Basis Function Network with on-line learning capabilities, by Schiefer et al. The network is composed of three layers, an input and output layer and between those two layers a nonlinear hidden

layer. Each neuron inside this layer has a radial activation function. Such a function maps the input-output behaviour of the system. Unpredictable and unmeasurable influences are dealt with by using Radial Basis Function Networks. Input and output data are used to train the neural network. The initial centre vectors in the hidden layers are selected randomly. Weighting functions are implemented and updated to prioritise the neurons in the hidden layers. A major downside of using neural networks is the ability to deal with new process conditions, outside of the training data. Schiefer et al. present in [39] a method to on-line update the neural network by using the new process data.

Chen et al. developed a quality model of a continuous annealing process. The quality of the steel is influenced by the overall process, which can be divided in sub-processes. The mapping between the set points of these sub-processes and the quality of the steel are complex nonlinear functions. Chen et al. state [12] that it is important to update the model by using input-output data. Comparable to [39] a Radial Basis Function Network is applied. Training of the model is preferably done by sequential learning algorithms instead of batch learning algorithms. Chen et al. apply the Generalized Growing and Pruning Radial Basis Function Neural Network to model a heating furnace. The advantage of this method is that it can be used for on-line learning, when applied in real-time controllers. New furnace data is used for the allocation of new hidden neurons and the adaptation of network parameters. Only when the furnace data is outside the operating range of the current neural network. The parameters adaptation is done by using an extended Kalman filter. The ability to update the model using new input-output data measured from the heating furnace is a big advantage over classical neural networks without on-line training capabilities. However, large data sets are required to build and train such a network model. In the previous sections, the use of extensive theoretical models for off-line studies or new furnace design is briefly explained. Since neural networks require actual furnace data, neural networks cannot be used for new furnace design. In [37] a comparable robust neural network is developed by Pernía-Espinoza et al. The presence of corrupted or outliers in the training data can lead to an inaccurate model. The research by Pernía-Espinoza et al. reports the effectiveness of robust learning algorithms compared to classical mean-squared error based learning algorithms. Historic data of the galvanising process, with over 6.000 variables, are collected. The relevant process parameters are selected and approximately 30.000 data points per variable are used to train and validate the network model.

3-2-3 Summary of Furnace Modelling

In the previous sections, a literature survey on furnace modelling is given. Furnace modelling is done in one of two ways. Either by theoretical modelling or by experimental modelling. Theoretical modelling typically leads to a set of differential equations, that can be approximated by using numerical methods. The advantage of using a theoretical approach is the clear physical interpretation of the model parameters, large insight is gained into the process and theoretical models are easily extended to similar plants or changed in case of plant adaptation. Theoretical modelling requires fundamental knowledge of the process inside the plant. Unforeseen effects or disturbances are not taken into account when applying theoretical modelling.

The second approach is based on experimental modelling, also known as system identification. Experimental models are developed by using input-output data from the plant to describe

the relation between the inputs and outputs. Artificial intelligence techniques are widely applied, due to the developments in modelling algorithms and advances in computing power. An advantage of developing a model by experimental modelling is that limited knowledge of the process is required. If physical effects are indistinct or affected by unknown disturbances, these dynamics are still captured by the input-output data. A disadvantage of experimental modelling is the lack of insight gained of the process. No clear physical interpretation of process parameters can be identified from an experimental model.

It is important to note that no publications are found to explicitly model the hybrid process, involving both heating and cooling and the associated process dynamics.

3-3 Furnace Control

The second part of this research involves the development of a furnace controller. Until recently the annealing furnace was controlled by conventional PID-controllers. Due to the complexity and diversity of product batches, obtaining precise temperature control using these conventional controllers is near impossible. Some literature can be found on these conventional control techniques

3-3-1 PID Control

Bitschnau et al. developed a mathematical model in state space formulation in [6], specifically suitable for controller design. The furnace is divided into heating zones. The strip temperature control is done by classical PID control. A simple yet effective combination of the PID control with feed-forward compensation is proposed. A PID controller is developed for each heating zone. However, these controllers are not able to react to parameter variations in time. Therefore, the feed-forward compensation is added. A reduction of the temperature deviations of 50% is obtained by adding the feed-forward compensation.

3-3-2 PID Control and Fuzzy Theory

In [14] a combination of fuzzy PID control and expert decision is used to control the strip temperature, proposed by Shi et al. The gains of the PID controller are adjusted by a fuzzy reasoning algorithm. The control action depends on the error and error change rate and the relationship between these factors and the PID gains are established based on fuzzy control theory. If the error between measured and desired temperature is smaller than a certain set temperature, the expert control system is used. Otherwise, the PID controller with fuzzy adaptation is applied as furnace control. A decrease in overshoot and adjusting time is the result of implementing the expert fuzzy PID algorithm instead of the classical PID algorithm. Comparable to the research by Shi et al., in [22] a fuzzy self-tuning PID controller is proposed. Based on expert's experience, the set of linguistic rules are defined. The error and change in error between measurements and desired temperatures are translated by the linguistic rules to a control action. The disadvantage is that an expert's experience is required to define the linguistic rules, also known as membership functions. Esmin et al. propose in [16] the use of the particle swarm optimisation algorithm is used to obtain the fuzzy membership functions.

3-3-3 LQR

A first step to modern control is made by Kelly et al. in [24]. A predictor is used to calculate strip temperature changes caused by process perturbations in real-time. A Kalman filter is added to adjust predictive errors due to unforeseen disturbances or model errors. To calculate the control gains, the Riccati equation is solved. An LQR controller is developed, with cost-weighting values, to minimise the magnitude of error in the strip temperature and magnitude of control action. The cost-weighting values were tuned using off-line simulations. For the controller to operate over the entire operating range of the furnace, gain sets were calculated and appointed to certain operating conditions. The appropriate gain set is used when the furnace is operating in the corresponding operating condition. The implementation of LQR is a predecessor of Model Predictive Control. A certain cost function is optimised over the entire time span. The controller gains are selected beforehand.

3-3-4 Model Predictive Control (MPC)

The vast majority of recent literature describes the design of an MPC for temperature control inside annealing furnaces. MPC was first coined by Richalet et al in [38]. In the past decades a lot of research is dedicated to this advanced control system. Implementation of MPC to process industries showed an explosive growth due to its conceptual simplicity and ability to handle complex constrained systems. Research and implementation of MPC can be seen as parallel developments. The industries did not investigate the conditions that ensured stability during implementation. In previous studies a system is assumed robust stable if an only if it admits a Lyapunov function [26, 27]. One of the major advantages of MPC is that process constraints can be handled explicitly. However, these constraints limit the guarantee on continuity of the Lyapunov function. And by this, closed loop stability cannot be guaranteed.

Stability and Robustness

Various studies investigate the stability of MPC. In [10] a new formulation is discussed, which ensures that the objective function is monotonically decreasing, guaranteeing closed-loop stability. In [30] several issues are handled. The Lyapunov stability and robustness to disturbances are researched in theory. The performance of the MPC depends on the accuracy of the model. Disturbances and model errors complicate the performance. The controller should be able to deal with these disturbances and model errors. Due to the trade-off between controller performance and robustness, the optimal control law does not always ensure closed-loop stability. It is remarkable that MPC is widely accepted in the process industry, while stability and robustness are not proven yet. A method to ensure closed-loop stability is by adding a terminal term to the objective function. The final state, predicted in the optimisation routine, is penalised based on the difference with the target state. A second method is by adding a terminal constraint. A constraint on the final state is added to the list of constraints. This method is elaborated in [4]. The final state has to be in a region where the optimisation problem is feasible.

Linear MPC

The most common way to use Model Predictive Control is by linearising a nonlinear model around the steady-state or operating point. By using a linear model, the computational effort required to solve the optimisation decreases significantly. If the system is close to the steady-state or operating point, the output of the model can be predicted fast, without losing accuracy. But if the system moves away from the operating point at which it is linearised, the predicted output might deviate from actual output. As mentioned, the operating conditions of the Slow-Cooling Section are highly variable. Therefore, different approaches might by interesting for this application, which are discussed next.

Hybrid MPC

Models of many industrial applications involve both continuous dynamical models, describing the process of the application by means of differential or difference equations, and discrete models, describing the software of the process. A hybrid model is a model with both continuous and discrete variables. The temperature changes continuously, but is controlled with discrete inputs. Discrete aspects in the Slow-Cooling Section are the recirculation fans and electric heating elements. These hybrid aspects can be translated into different modelling frameworks. These hybrid models can be controlled with hybrid MPC control systems. Two possible hybrid modelling frameworks are discussed next, Piecewise Affine and Mixed Logical Dynamical systems.

Nonlinear dynamic systems are difficult to implement in MPC [30], due to the loss of convexity of the optimisation problem and increase in computational effort. The loss of convexity poses problems for stability and robustness as discussed before. To circumvent these problems, piecewise linearisation of the nonlinear system can be applied to obtain a set of local linear models. Modelling via Piecewise Affine (PWA) is the most studied modelling framework for discrete-time hybrid systems. PWA systems can model nonlinear and non-smooth processes and are capable of dealing with hybrid effects.

In [47], the nonlinear model, describing the heat transfer in the annealing furnace, is translated to a finite set of piecewise affine systems, such that it can be implemented in the MPC system. The disadvantage of approximating the nonlinear system by a finite set of piecewise affine systems, is that it is only an approximation. Piecewise affine systems partition the state and input space into $i = 1, \ldots, N$ polyhedral regions Ω, where each region has a unique affine state-update and output equation. Stability criteria for PWA systems are investigated in [28]. In [5] the observability and controllability of PWA and hybrid systems are investigated. A second framework to model hybrid systems is Mixed Logical Dynamical (MLD) systems. The MLD formalism has proven successful to model a system described by interdependent physical laws, logic rules and operating constraints. MLD hybrid models can be controlled by hybrid MPC techniques [4]. One widely known hybrid MPC technique is known as MLD-MPC, which uses an MLD model as prediction model. The use of MLD systems in MPC requires an objective function, similar to the one discussed in previous sections. The added auxiliary variables are possibly included in the cost function. Positive definite matrices, for states and inputs, and non-negative definite matrices, for outputs and auxiliary variables, are introduced to apply weighing on the associated variables. Optimal control by MLD-MPC can be solved by recasting the problem as a Mixed Integer Linear Programming (MILP) problem,

if the objective function only contains 1-norms and ∞-norms, or otherwise as a Mixed Integer Quadratic Programming (MIQP) problem. The control law is obtained by solving a MILP or MIQP, which depends on the current state $x(k)$ only, and not on future states. Several techniques have been developed to solve mixed-integer linear and quadratic programs, such as branch-and-bound and cutting plane algorithms.

3-3-5 Summary of Furnace Control

In the previous section, a literature survey on furnace control is given. Although some literature describe the use of conventional control techniques, such as PID and LQR control, to control process comparable to the Slow-Cooling Section, the majority of papers proposes the use of Model Predictive Control to improve the control of the processes of interest. Model Predictive Control seems to be an appropriate successor to the conventional control systems. In the literature, several variants of MPC are described and implemented on annealing furnaces. Most often, a linear MPC is implemented. Besides the different MPC frameworks, also stability and robustness of MPC systems is briefly described in the previous section.

3-4 Conclusions

The Slow-Cooling Section of DVL3 was originally designed for stable processes. However, due to the ongoing diversification of the product portfolio, the Slow-Cooling Section operates more often under transient conditions. The found literature describes the modelling and control of the first sections in annealing furnaces. No publications are found to explicitly model the hybrid process, involving both heating and cooling and the associated process dynamics, which is directly the added value of this research.

Model Predictive Control is investigated further in this research. This also contributes to the general development in Tata Steel to gradually upgrade the conventional control system to the model-based predictive control. As the application of MPC demands firstly an appropriate process model, the detailed modelling of the slow cooling process is described in the subsequent chapter.

Chapter 4

Furnace Modelling

4-1 Introduction

The application of Model Predictive Control to the Slow-Cooling Section requires a process model, describing the heat transfer in the furnace. Therefore, before the control system can be designed, the process model of the Slow-Cooling Section has to be developed. In [36], different frameworks for the development of such a process model are described. The development of a process model can be classified into one of the two following frameworks:

- White box modelling
- Black box modelling

A white box model, also known as a first principle or rigorous model, requires that all information about the system is available. The advantages of white box modelling are that large insights in the process are gained, model parameters have a clear physical meaning for control and changes can be made easily in case of adaptations to the system. Therefore, when all information is available, using the white box modelling framework is preferred over the black box modelling framework. If the information is correct and the relations are described accurately, the model will behave accordingly. Therefore, the behaviour of the model depends on the correctness of the information and the accuracy of the description of the functions relating all the variables in the system. In [33–35, 42] the process model of an annealing furnace is developed based on this white box modelling framework. During the design of new systems, white box modelling can be used to estimate the behaviour of the system prior to the actual realisation of the system and improvements can be executed accordingly.

On the contrary, a black box model requires only input and output data from the process. The black box model is developed by estimating the relations between variables and the parameters in these relations. Popular methods for black box modelling, also known as system identification, are neural networks, particle swarm optimisation techniques or NARMAX (nonlinear autoregressive moving average model with exogenous inputs) algorithms. Black box modelling is preferred when little or no information about the system is available.

In [24, 43, 49, 50], the black box modelling framework is used for the development of the process model of an annealing furnace. The advantages of black box modelling are that only limited theoretical knowledge of the system and process is required to develop the model, the model can directly be implemented to Model Predictive Control and unpredictable effects are accounted for. Disadvantages are that limited insights in the process are gained, a large and diverse process data set is required to estimate the model and in case of adaptations to the system, a new model has to be estimated, with new data. Thus, black box modelling can only be used when the entire system is already manufactured. Black box modelling cannot be used in the design phase.

However, in engineering cases, often a combination of the two modelling frameworks is used. This combination between white and black box modelling, also known as grey box modelling, combines a theoretical basis with process data to account for the unknown parameters. Very often, not all parameters are known or parameters are hard to describe using a pure theoretical approach. In practice, the vast majority of process models are developed using the grey box modelling approach. This research is founded on the white box modelling framework, with parameter estimation for some unknown parameters. For this reason the modelling of the Slow-Cooling Section can be seen as an example of grey box modelling.

In Appendix A fundamental theory for the development of the nonlinear process model is given.

4-2 Nonlinear Process Model

In this chapter the development of the nonlinear process model, that describes the Slow-Cooling Section, is discussed. The starting point is the general form of a nonlinear state space model, given by:

$$\dot{x} = f(x, u) \tag{4-1}$$

which describes the dynamics of temperature, as a function of the temperature of all the elements and process parameters, such as line speed and strip dimension. Since almost all information on the system is available, the physical relations are fairly well known and to ensure a clear physical meaning for the inputs and outputs, the white box modelling framework is used to describe the Slow-Cooling Section. The basis of the nonlinear model is a special form of the energy conservation principle, also known as the First Law of Thermodynamics. The energy conservation principle is given by:

$$\rho V c_p \frac{dT}{dt} = \dot{Q} \tag{4-2}$$

where $\dot{Q}$ describes the heat transfer between the element of interest with the other surrounding elements in the Slow-Cooling Section. Eq. (4-2) can be cast in the general form of a state space model Eq. (4-1), given by:

$$\dot{T} = \frac{dT}{dt} = \frac{\dot{Q}}{\rho V c_p} \tag{4-3}$$

which describes the dynamics of the temperature of an element over time, dependent on the rate of heat transfer and density, volume, specific heat capacity of the said element.

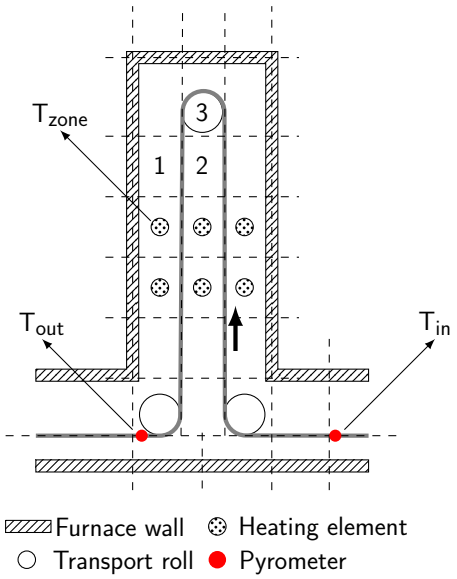

Figure 4-1: Schematic overview of matrix of computational cells and the location of pyrometers.

Describing the dynamics of the Slow-Cooling Section as a whole is complex, due to its dimension and complex geometry. Therefore, the Slow-Cooling Section is divided into a finite number of computational cells. Each cell describes a small part of the Slow-Cooling Section. As depicted in Figure 4-1, a matrix of cells arises. Each cell contains a combination of elements, dependent on the location of the cell in the Slow-Cooling Section. The following elements can be distinguished:

- Steel strip
- Protective Gas
- Transport Roll
- Furnace Wall

The steel cools down by blowing cooled protective gas against it, which is cooled by a water-cooled heat exchanger. No valid information on the heat exchanger can be found. Therefore the dynamics of the heat exchanger is not modelled in this work. The temperature drop of the gas over the heat exchanger is assumed constant and not dependent on the gas flow. Thus, the boundary of the system is set at the outside of the furnace wall of the Slow-Cooling Section.

As described in Appendix A, the dominant heat transfer modes are conduction, convection and radiation. Every cell is modelled as an open system, where the steel flows according to the line speed. The heat balance of an element is the sum of heat exchanges between the element with the other surrounding elements in the cell through the heat transfer modes. For each of the above mentioned elements, the energy conservation principle is applied. The heat transfer in a cell are described as by the following relations:

$$
\begin{aligned}
\dot{Q}_{\text{strip}}(T,u) &= \dot{Q}_{\text{strip}}^{\text{radiation}}(T,u) + \dot{Q}_{\text{strip}}^{\text{convection}}(T,u) + \dot{Q}_{\text{strip}}^{\text{conduction}}(T,u) + \dot{Q}_{\text{strip}}^{\text{enthalpy}}(T,u) \\
\dot{Q}_{\text{wall}}(T,u) &= \dot{Q}_{\text{wall}}^{\text{radiation}}(T,u) + \dot{Q}_{\text{wall}}^{\text{convection}}(T,u) + \dot{Q}_{\text{wall}}^{\text{heat loss}}(T,u) + \dot{Q}_{\text{wall}}^{\text{electric}}(T,u) \\
\dot{Q}_{\text{gas}}(T,u) &= -\left(\dot{Q}_{\text{strip}}^{\text{convection}}(T,u) + \dot{Q}_{\text{wall}}^{\text{convection}}(T,u) + \dot{Q}_{\text{roll}}^{\text{convection}}(T,u)\right) + \dot{Q}_{\text{gas}}^{\text{enthalpy}}(T,u) \\
\dot{Q}_{\text{roll}}(T,u) &= \dot{Q}_{\text{roll}}^{\text{radiation}}(T,u) + \dot{Q}_{\text{roll}}^{\text{convection}}(T,u) + \dot{Q}_{\text{roll}}^{\text{conduction}}(T,u)
\end{aligned}
\tag{4-4}
$$

The heat transfer $\dot{Q}_n$ of element n depends on the temperatures T of the involving elements and the heat exchanges between the elements, as depicted in Figure 4-2. Also additional parameters u, such as strip dimensions, line speed and actuator settings for the heating and cooling control elements, affect the heat transfer.

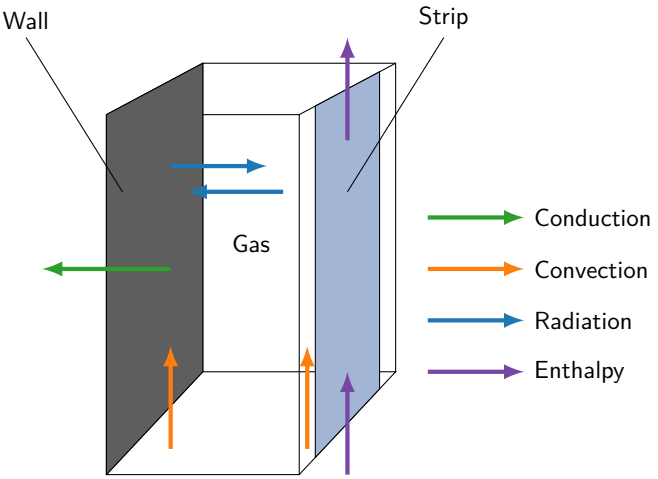

Figure 4-2: Heat exchanges between elements in a typical wall cell.

4-2-1 Cell Types

The Slow-Cooling Section is divided into a matrix of cells. This results in three distinguishable cell types. The presence of specific elements, mentioned above, in each cell depends on the cell type. The three cell types in the Slow-Cooling Section are depicted in Figure 4-3. In Figure 4-1 the different cell types are indicated with numbers. Cell one corresponds to a wall cell, depicted in Figure 4-3a, cell two corresponds to a middle cell, depicted in Figure 4-3b and cell three corresponds to a roll containing cell, depicted in Figure 4-3c. The heat transfer is different for each cell type, depending on the present elements and process parameters. The roll cell can have two configurations, which has to do with the contact area between roll and steel strip. The two bottom transport rolls have contact over 90° of the roll and the top transport roll has contact over 180° of the roll.

4-2-2 Conduction Heat Transfer

Heat transfer through conduction takes place in two situations: heat loss through the furnace wall and contact conduction between the transport roll and strip.

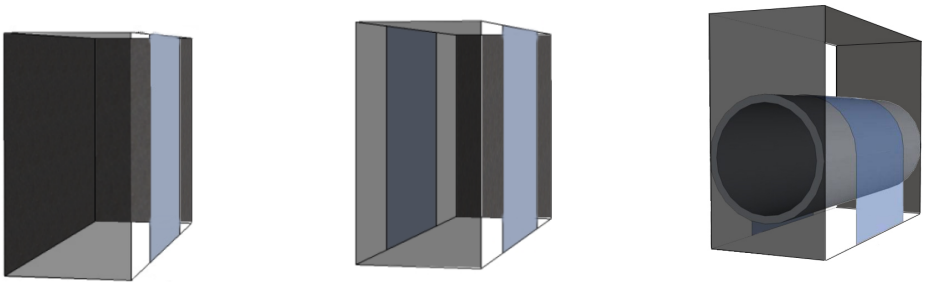

(a) Wall cell: Cell with one strip and wall elements **(b)** Middle cell: Cell with two strip and wall elements **(c)** Roll cell: Cell with one strip, one roll and wall elements

Figure 4-3: Cell types in Slow-Cooling Section.

Heat Loss

The furnace wall separates the furnace inner atmosphere from the ambient. The furnace wall consists of multiple layers of insulation material with different thickness and heat conductance properties. A large amount of heat accumulates in the wall, which has a strong influence on the dynamic calculation of the temperatures in the Slow-Cooling Section. The wall is modelled as a one dimensional heat conduction problem. The net conductive heat flux is described by:

$$\begin{aligned} \dot{Q}_{\text{wall}}^{\text{heatloss}} &= \alpha A_w (T_w - T_a) \\ \alpha &= \left(\sum_{i=1}^{n} R_i \right)^{-1} \\ R &= \frac{L}{\lambda} \end{aligned} \tag{4-5}$$

where n is the number of layers, L is the thickness of the layer and λ is the thermal conductivity of the insulation layer. The thermal conductivity of a layer is highly dependent on the crystalline structure of the material. Insulating materials are known for having a very low conductivity, due to their porous nature.

Contact Conduction

In the roll cell, the strip is in direct contact with the transport roll, depicted in Figure 4-4.The heat transfer between the strip and roll occurs in the contact area, knowing the heat is defined by:

$$Q_{\text{roll}}^{\text{conduction}} = \alpha A_c \left(T_s - T_r \right) \tag{4-6}$$

The heat transfer coefficient for contact resistance, also known as interfacial conductance, depends on various parameters, such as the thermal property of the surfaces and entrapped gas, gas pressure, surface roughness and contact pressure [3]. The heat flow in the interface region is difficult to describe. Therefore a representative value of 5.000 W m^{-2} K^{-1}, given in [29], for typical interfacial conductance, for contact at moderate pressure and usual surface finishes, comparable to the situation in the Slow-Cooling Section is used in the model.

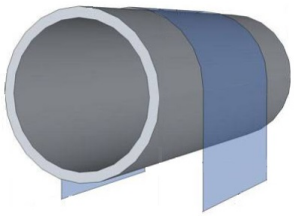

Figure 4-4: Contact conduction between strip and transport roll.

4-2-3 Convection Heat Transfer

The convective heat transfer between the strip element and the gas element can be described by the following equation:

$$\dot{Q}^{\text{convection}} = \alpha A_s (T_s - T_g) \tag{4-7}$$

where α is the convective heat transfer coefficient. The same applies for the wall element. The convective heat transfer coefficient is dependent on the type of convection, as described in Section A-3-2. The convective heat transfer coefficient depends mainly on the volumetric flow rate and thermal properties of the gas. The volumetric flow rate is a function of the rotational speed of the recirculation fans, the discharge dimension and gas pressure. Thus, obtaining the heat transfer coefficient requires detailed information of the system.

A theoretical approach for obtaining the heat transfer coefficient would be a tremendous task, given the limited time and scope of this research. Therefore it is decided to obtain the heat transfer coefficient via parameter estimation, described in Section 4-5.

4-2-4 Radiation Heat Transfer

Radiation heat exchange between surfaces depends on the surface temperatures, radiation properties, such as the emissivity, and the geometry of the enclosure. In an ideal situation, the heat exchange between two infinite parallel surfaces is simple: all radiation leaving one surface is absorbed by the other surface and no radiation is reflected, given by:

$$\dot{Q} = \sigma (T_1^4 - T_2^4) \tag{4-8}$$

However, in reality this problem is complex. To simplify the computation, the following assumptions, while describing the radiation heat exchange, are made:

- Each surface is grey
- Emission and reflection from each surface is diffuse
- Emissivity of the surfaces is constant through the process

The first assumption proposes that radiation incident on surfaces is not entirely absorbed, but partially reflected and independent of wavelength. The second assumption suggests that the radiation has no preferred direction. The third assumption describes that the emissivity

of each surface can be characterised by a single value of emittance and is not temperature dependent through the process.

The protective gaseous atmosphere in the Slow-Cooling Section is a mixture of hydrogen and nitrogen and thus; the protective gas is transparent, also known as nonparticipating for radiation and does not affect the radiation heat exchange in the Slow-Cooling Section.

In the Slow-Cooling Section, heat is exchanged between a number of surfaces via radiation. From the summation rule Eq. (A-24), the radiation incident on surface i is equal to:

$$A_i G_i = J_1 A_1 F_{1i} + J_2 A_2 F_{2i} + J_3 A_3 F_{3i} + \dots \tag{4-9}$$

where J_i is the radiation surface i. Using the reciprocal rule (Eq. (A-21)), this can be rewritten to:

$$\begin{aligned} A_i G_i &= J_1 A_i F_{i1} + J_2 A_i F_{i2} + J_3 A_i F_{i3} + \dots \\ &= A_i \sum_{j=1}^{n} F_{ij} J_j \end{aligned} \tag{4-10}$$

The total radiation leaving surface i, or radiosity, J_i is the sum of the radiation emission E_i of the surface itself and the reflected fraction of radiation incident on the surface. The radiosity is described by the following equation and using the result from Eq. (4-10), the following is obtained:

$$\begin{aligned} J_i &= \varepsilon_i E_i + (1 - \varepsilon_i) G_i \\ &= \varepsilon_i E_i + (1 - \varepsilon_i) \sum_{j=1}^{n} (F_{i,j} J_j) \end{aligned} \tag{4-11}$$

This can be rewritten to:

$$E_i = \frac{1}{\varepsilon_i} \left(J_i - (1 - \varepsilon_i) \sum_{j=1}^{n} (F_{i,j} J_j) \right) \tag{4-12}$$

which proves to be a very useful form. For an enclosure of 3 participating surfaces, the equation above is used to obtain the following matrix form:

$$\begin{bmatrix} E_1 \\ E_2 \\ E_3 \end{bmatrix} = \underbrace{\begin{bmatrix} \varepsilon_1^{-1} & 0 & 0 \\ 0 & \varepsilon_2^{-1} & 0 \\ 0 & 0 & \varepsilon_3^{-1} \end{bmatrix} \begin{bmatrix} 1 - (1 - \varepsilon_1) F_{1,1} & -(1 - \varepsilon_1) F_{1,2} & -(1 - \varepsilon_1) F_{1,3} \\ -(1 - \varepsilon_2) F_{2,1} & 1 - (1 - \varepsilon_i) F_{2,2} & -(1 - \varepsilon_2) F_{2,3} \\ -(1 - \varepsilon_3) F_{3,1} & -(1 - \varepsilon_3) F_{3,2} & 1 - (1 - \varepsilon_3) F_{3,3} \end{bmatrix}}_{\mathrm{V}} \begin{bmatrix} J_1 \\ J_2 \\ J_3 \end{bmatrix}$$

$$E = V \cdot J \tag{4-13}$$

with $E \in \mathbb{R}^{n \times 1}$, $V \in \mathbb{R}^{n \times n}$ and $J \in \mathbb{R}^{n \times 1}$, where n is the number of surfaces in the enclosure under consideration. This result can be used to describe the net heat flux leaving a surface.

The net heat flux leaving surface i can be calculated using the energy balance method, described in Section A-3-3. Substituting the above result, where $J = V^{-1}E$, into Eq. (A-26), the following is obtained:

$$\begin{aligned} \dot{Q} &= \left(\frac{\varepsilon A}{1-\varepsilon}\right)(E - J) \\ &= \left(\frac{\varepsilon A}{1-\varepsilon}\right)\left(E - V^{-1}E\right) \\ &= \underbrace{\left(\frac{\varepsilon A}{1-\varepsilon}\right)\left(1 - V^{-1}\right)}_{\mathrm{M}} E \end{aligned} \tag{4-14}$$

Since $E = \sigma T^4$, the above equation is now a function of the temperature of the elements in the enclosure. So the radiation heat flux is given by:

$$\begin{aligned} \dot{Q}^{\text{radiation}} &= M \cdot E \\ \begin{bmatrix} Q^{\text{rad}}_{\text{strip}} \\ Q^{\text{rad}}_{\text{wall}} \\ Q^{\text{rad}}_{\text{roll}} \end{bmatrix} &= \begin{bmatrix} + & - & - \\ - & + & - \\ - & - & + \end{bmatrix} \begin{bmatrix} T^4_{\text{strip}} \\ T^4_{\text{wall}} \\ T^4_{\text{roll}} \end{bmatrix} \end{aligned} \tag{4-15}$$

where $M \in \mathbb{R}^{n \times n}$ contains the surfaces, emissivities shape factors, as described below, and Stefan-Boltzmann coefficient, and $E \in \mathbb{R}^{n \times 1}$ contains the surface temperatures, where n is the number of elements. For every cell configuration the M matrix is constructed once.

Shape factors

The geometry of the Slow-Cooling Section plays a role in the radiation heat exchange. The shape factor, described in Section A-3-3, is the fraction of radiation leaving a surface, intercepted by another surface. For calculation of shape factors, the following integral can be used:

$$F_{1\to 2} = \frac{1}{A_1} \int_{A_1} \int_{A_2} \frac{\cos(\theta_1) \cdot \cos(\theta_2)}{\pi \cdot R^2} dA_1 dA_2 \tag{4-16}$$

where A_1 and A_2 represent surface areas, θ_1 and θ_2 represent angles between the normal to the surface and the direction of the other surface and R represents the distance between the two surfaces. The Slow-Cooling Section is filled with parallel and perpendicular shapes, as depicted in Figure 4-5. The following assumptions are made for calculation of the view factors:

- The strip and wall surfaces are infinitely long
- Radiation exchange between cells is neglected
- Gaps between strip and wall are seen as diffuse reflectors

The first assumption states that the fraction of radiation leaving the top and bottom of the cell is negligible. To simplify the analysis, radiation exchange between cells is neglected, following the second assumption. In this research, the middle cells account partially for this assumption. The third is based on the assumption that the radiation leaving the cell through the gaps is equal to the radiation coming into the cell through the gaps. The gaps can therefore be modelled as diffuse reflectors. In [29] shape factors for a variety of two and three-dimensional configurations are available and are used to determine the view factors for the different configurations in the Slow-Cooling Section.

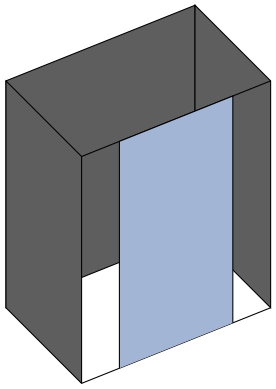

Figure 4-5: Slow-Cooling Section consists of parallel and perpendicular configurations.

Emissivity

In radiation heat exchange, a blackbody is defined as a surface that absorbs all incident radiation and thus, reflects none. A blackbody surface is considered an ideal surface. In real life, surfaces absorb less radiation compared to these ideal surfaces. Surfaces also emit less radiation. The ratio of emitted radiation compared to blackbody surfaces is known as the emissivity, ε of a surface. In [29], approximate values of emittance for selected materials are given. For the emissivity of steel, $0,3$ is used and for the emissivity of the walls, $0,85$ is used. The emissivity is very dependent on the surface condition. In this research, a constant value is selected for the materials playing a role in the radiation heat exchange. Further investigations are undertaken to study the emittance of steel as a function of the temperature and thickness of the oxidation layer.

4-2-5 Strip Enthalpy Heat Transfer

The steel strip is modelled as a flow of steel. The mass flow of steel is equal to the line speed multiplied by strip width, thickness and density of the material. The strip element in each cell contains a certain amount of heat. This property is known as specific enthalpy, h, and is dependent on the temperature of the material. From one cell to another, this can be modelled as heat transfer between adjacent strip elements, equal to:

$$\dot{Q}^{\text{enthalpy}} = \dot{m}\Delta h \tag{4-17}$$

The specific enthalpy can be approximated by:

$$\Delta h = \int_{T_1}^{T_2} c_p dT \tag{4-18}$$

where c_p is the specific heat of a material. Typical values for the specific heat for a list of materials is given in [29]. The specific heat grows with an increase in temperature [23]. However, as described in Appendix B, transition of the steel phase occurs, according to Figure B-1. During this phase transition, a peak on the curve of specific heat can be seen.

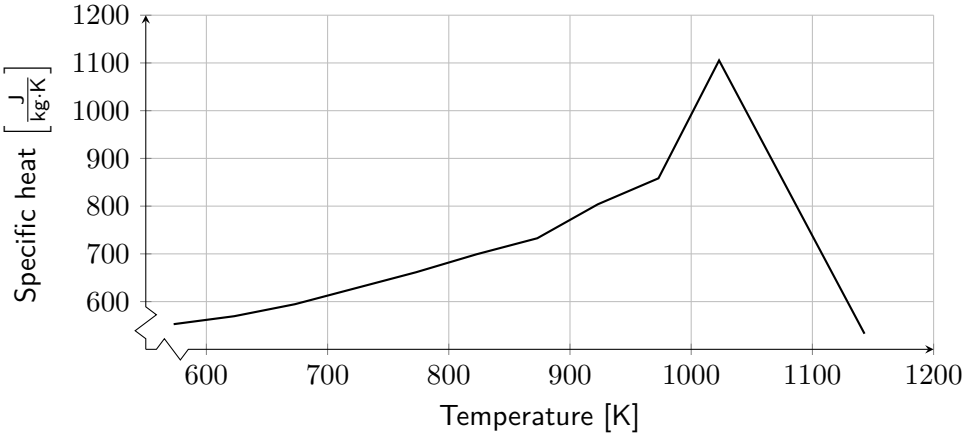

Figure 4-6: Specific heat dependency on temperature for low-carbon steel.

In Figure 4-6, the dependence of specific heat on temperature for low-carbon steel is depicted. Before the phase transition, the specific heat grows with temperature. The peak indicates the phase transition, after which the specific heat significantly drops. Every steel type has its own specific heat graph. In this research, the specific heat for low-carbon steel is used throughout the modelling.

4-2-6 Gas Enthalpy Heat Transfer

The strip in the Slow-Cooling Section is cooled down by blowing protective gas against it. The protective gas is a mixture of hydrogen and nitrogen (HNX) and is circulated by fans. The gas is cooled in a water cooled heat exchanger. The cooled gas mixes with the hotter gas inside the furnace, which results in a desired gas temperature. It is assumed that the protective gas is well-mixed. Therefore, it is decided to group the gas elements of all cells into one element. The heat required to cool the gas to the desired temperature is given by:

$$\dot{Q}_{\text{gas}}^{\text{enthalpy}} = \dot{m} c_p \Delta T \tag{4-19}$$

where $\dot{m}$ is the mass flow of the cooled gas. The fans circulate the gas and enable the cooled gas to mix with the gas inside the furnace. The rotational speed of the fans is linearly dependent on the mass flow of the gas, according to the fan affinity laws [20]. In this research the heat exchanger is not included in the model. The temperature of the cooled gas is assumed to have a constant incoming temperature.

4-2-7 Electric Heat Transfer

The steel is transported in the annealing furnace by transport rolls. To prevent the strip from buckling, these transport rolls have to be at the same temperature as the steel. The temperature of the rolls is regulated by electric heating elements During line starts or a sudden increase in desired temperature, the electric heating elements can also be used. The electric heating elements used to regulate the temperature of the transport rolls are located in a different control system and lie therefore outside the scope of this research. The remaining electric heating elements are in the middle part of the Slow-Cooling Section and are a part of the nonlinear furnace model.

In the furnace model, heating power is evenly distributed to the cells and integrated into the heat balance of the wall cell. The heat from the electric heating elements is modelled by:

$$\dot{Q}_{\text{wall}}^{\text{electric}} = L\left(P_{\max} - P_{\min}\right) \tag{4-20}$$

where L is the electric load supplied to the heating elements and $P_{\max}$ and $P_{\min}$ are the maximum and minimum electrical power released by the elements onto the wall surface.

4-3 Dynamic Solution

The heat exchanges of all the elements in all cells are grouped and form a vector of nonlinear equations, given by

$$\dot{Q}(T,u) = \begin{bmatrix} \dot{Q}_{\text{cell 1,strip}} \\ \vdots \\ \dot{Q}_{\text{cell n,strip}} \\ \dot{Q}_{\text{cell 1,wall}} \\ \vdots \\ \dot{Q}_{\text{cell n,wall}} \\ \dot{Q}_{gas} \\ \dot{Q}_{\text{cell 1,roll}} \\ \vdots \\ \dot{Q}_{\text{cell n,roll}} \end{bmatrix} \in \mathbb{R}^{m\times 1} \tag{4-21}$$

where m is the number of elements. The heat transfer vector Eq. (4-21) is substituted in Eq. (4-3) to describe the temperatures in the Slow-Cooling Section over time. The temperature of each element n is described by:

$$\begin{aligned} \dot{T}_n &= \frac{dT_n}{dt} = \frac{Q_n}{\rho_n V_n c_{p_n}} \\ &= f_n(T_n, u) \end{aligned} \tag{4-22}$$

As in most modelling cases, the nonlinear model, $f_n(T_n, u)$, is described by a set of differential equations. The model involves combining various heat transfer modes in a high temperature environment, with difficult geometries and boundary conditions, resulting in an extensive mathematical model. Unfortunately, due to these difficulties, analytical techniques cannot be applied or are very complicated to use. An alternative approach to solve the model is by using numerical methods. In the literature several numerical methods appear for solving a nonlinear model describing annealing furnaces. In [36] the most common methods are compared with each other. Finite Difference Methods (FDM) and Finite Element Methods (FEM) are widely used in engineering, due to their simplicity. The exact solution to Eq. (4-22) is approximated by using numerical methods. Numerical methods are categorised into one of two following categories, i.e. linear multistep method and Runge-Kutta methods. These categories can be subdivided in implicit and explicit methods. Both linear multistep methods and Runge-Kutta methods are elaborated in [15]. Eq. (4-22) is transformed from a differential equation to a difference equation, given by:

$$T_n(t+1) = T_n(t) + f_n\Big(T_n(t), u(t)\Big) \cdot \Delta t \tag{4-23}$$

where Δt is the step size. Eq. (4-23) is a simple numerical approximation method, i.e. the well-known Euler's method, a linear one-step explicit method. The method consists of repeated evaluation of the difference equation. The temperatures of the elements are calculated for each time step by solving the differential equation.

The step size Δt in Eq. (4-23) defines the accuracy of the approximation. As the step size goes to zero, the numerical approximation will approach the exact solution. The step size should be small enough to ensure the desired accuracy. But step size that is too small results in increased computational efforts, while is does not increase the accuracy significantly.

The accuracy of Euler's method improves linearly with step size. However, the accuracy of the improved Euler method, also known as Euler-Heun method, improves quadratically with step size. The Euler-Heun method is a two-step method. The average of two values is used instead of one value, given by:

$$T_n(t+1) = T_n(t) + \frac{f_n + f_n(t + \Delta t, T_n(t) + \Delta t f_n)}{2} \cdot \Delta t \tag{4-24}$$

The Euler-Heun method is also an explicit method, which results in a higher accuracy at the expense of more computational effort.

In the literature a second class of methods is described, i.e. the Runge-Kutta methods. The most widely known is the classic fourth order four-stage Runge-Kutta method. From here on this will be called the Runge-Kutta method. The accuracy is increased by three orders of magnitude compared to the Euler method and by two orders of magnitude compared to the Euler-Heun method. The Runge-Kutta method is a four-stage method, given by:

$$T_n(t+1) = T_n(t) + \Delta t \left(\frac{k_{1_n} + 2k_{2_n} + 2k_{3_n} + k_{4_n}}{6} \right) \tag{4-25}$$

where the parameters k_{1_n}, k_{2_n}, k_{3_n} and k_{4_n} are given by:

$$
\begin{aligned}
k_{1_n} &= f_n(T_n(t), u(t)) \\
k_{2_n} &= f_n(T_n(t) + \frac{1}{2}\Delta t k_{1_n}, u(t)) \\
k_{3_n} &= f_n(T_n(t) + \frac{1}{2}\Delta t k_{2_n}, u(t)) \\
k_{4_n} &= f_n(T_n(t) + \Delta t k_{3_n}, u(t))
\end{aligned}
\tag{4-26}
$$

A weighted average of values of the differential equation at different points on an interval is used. The Runge-Kutta involves more steps and is therefore more complicated compared to Euler's method and the Euler-Heun method. However, the Runge-Kutta method is not hard to implement and use for the approximation of the differential equation. For comparison, both the Euler method and the Runge-Kutta method will be used to approximate the nonlinear differential equation Eq. (4-22).

4-4 Model Validation

In the previous sections, the development of the nonlinear model is described. In this section the model is validated, against actual furnace data from DVL3, to check the accuracy of the model. Identical process parameters, as applied to the actual furnace, are used for the simulation. It is important to note that the simulation is open loop, also known as free run simulation. This means that no control or adaptation is applied during the simulation. The temperature of the steel is measured by a pyrometer at two locations in the Slow-Cooling Section, at the entrance and at the exit of the furnace. Some installed thermocouples give insight in the zone temperature inside the Slow-Cooling Section.

The first step is to collect temperature measurements and associated process parameters. In the Slow-Cooling Section, the temperature measurements and process parameters are collected and stored every two seconds. The following process parameters can be distinguished:

- Strip width
- Strip thickness
- Strip temperature at entrance of Slow-Cooling Section T_{in}
- Line speed
- RPM of lower and upper recirculation fans
- Power supplied to electric heating elements

These process parameters are inputs to the nonlinear furnace model. However, during the controller design a distinction between process parameters and control inputs is made. Control inputs are the actuator signals that are used to actively regulate the process. The control inputs in the Slow-Cooling Section are:

- RPM of lower recirculation fan
- RPM of upper recirculation fan
- Power supplied to electric heating elements

The outputs from the nonlinear furnace model are the following:

- Strip elements temperatures
- Gas element temperature
- Wall elements temperature
- Transport roll elements temperatures

The second step is to prepare the simulation properly, so that equal settings and parameters are used as during the actual operation of the furnace. One of the outputs of the model, the calculated steel temperature corresponding to the temperature at the exit of the Slow-Cooling Section, is compared to the measured steel temperature at the exit of the Slow-Cooling Section. The calculated zone temperature is also compared to the measured zone temperature. The two numerical methods described before are used to solve the numerical approximation of Eq. (4-22).

4-4-1 Process Data

In order to simulate and validate the entire operating range of the Slow-Cooling Section, data from a day with different process conditions are selected. For the simulation, data from 6 April 2017 are used, equal to approximately 43.000 samples. The operating conditions of this day are depicted in Figure 4-7.

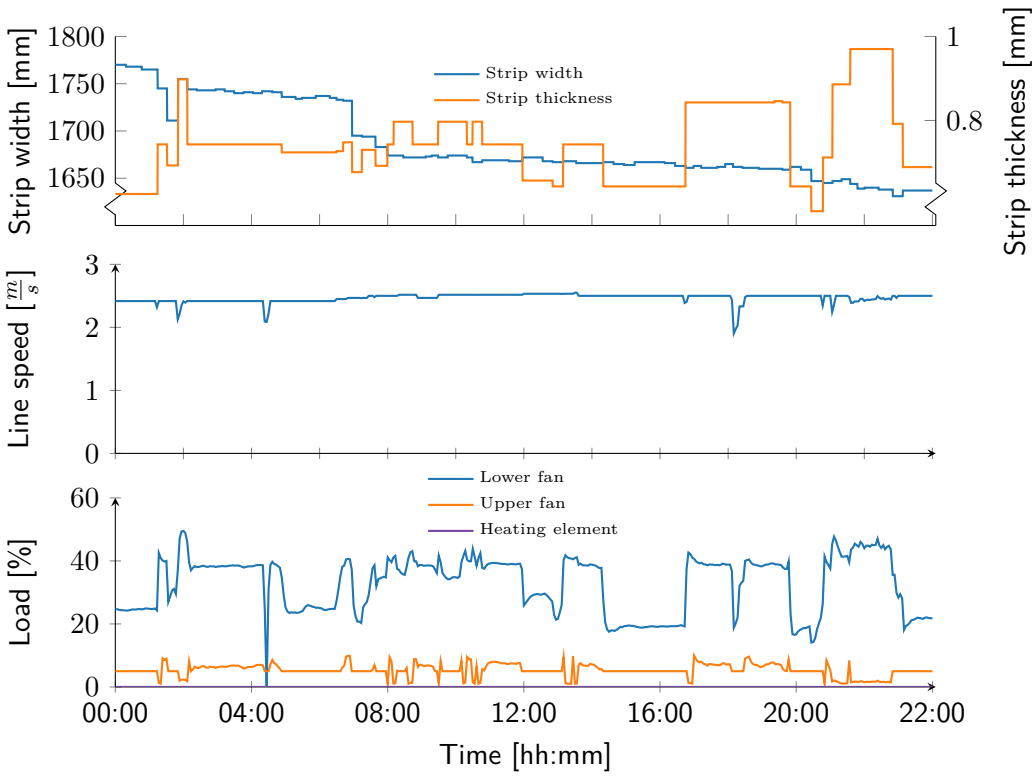

Figure 4-7: Process parameters of 6 April 2017 used for simulation. Top: Strip dimensions. Middle: Line speed. Bottom: Actuator load percentage.

The top graph shows the strip dimension. As can be seen, the width decreases during the day and the thickness varies between 0,5 mm and 1,0 mm. The middle graph shows the line speed. The line speed is kept at a maximum, when possible, to maximise the throughput of the plant. The line speed is, as can be seen, equal to 2,5 m s^{-1} almost the entire day. In the bottom graph, the load percentages for the actuators are depicted. The heating elements are not used throughout the entire day, which is very common. The lower and upper fan are operational at varying loads.

The operating conditions on 6 April 2017 are representative of common operating conditions of the plant. The varying process parameters ensure that the simulation covers the operating range of the Slow-Cooling Section.

4-4-2 Euler's Method

First, Euler's method is used to solve the nonlinear model. A step size, Δt, of 0,1 s is used, corresponding to 20 times the sample rate in the Slow-Cooling Section. The results are depicted in the top graph of Figure 4-8. The measured and calculated temperature, corresponding to the steel temperature at the exit of the Slow-Cooling Section, are indicated by the orange and purple line, respectively. The blue line indicates the measured steel temperature at the entrance of the Slow-Cooling Section. The calculated zone temperature is also compared to the measured zone temperature, depicted in the bottom graph of Figure 4-8. The blue line indicates the temperature measured by the thermocouple and the orange line indicates the calculated zone temperature.

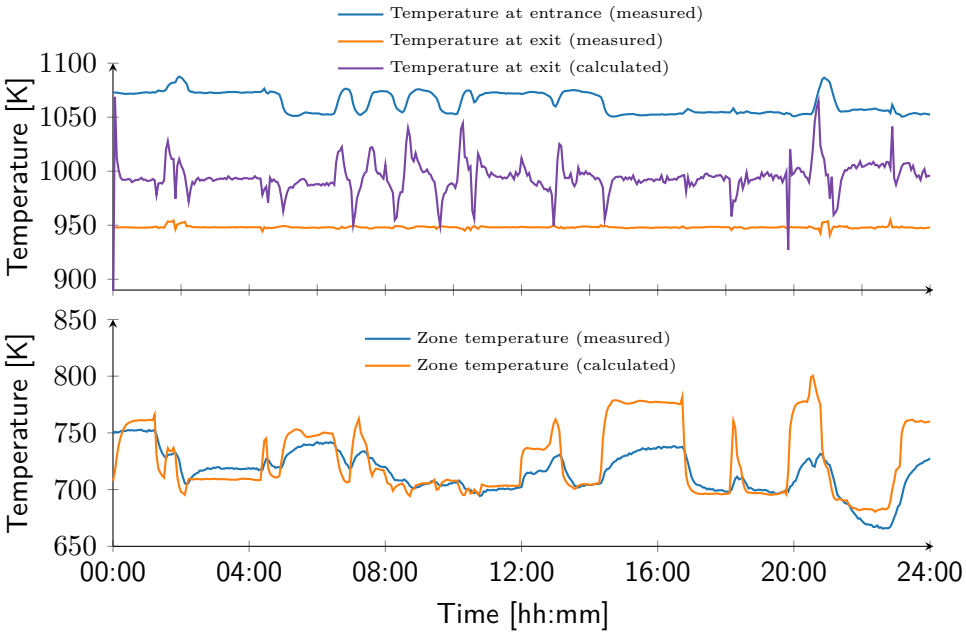

Figure 4-8: Simulation of 6 April 2017, solved by using Euler's method. Top: Measured and calculated steel temperature. Bottom: Measured and calculated zone temperature.

As can be seen in Figure 4-8, the dynamics of the calculated steel temperature do not follow the dynamics of the measured steel temperature closely in the simulation solved by Euler's

method. A lot of spikes and an offset of approximately 40 K can be seen. However, the dynamics of the calculated zone temperature do follow the dynamics of the measured zone temperature. At some points the calculated zone temperature deviates from the measured zone temperature, but in general the dynamic behaviour of the calculated and measured zone temperature are comparable.

4-4-3 Runge-Kutta Method

For the Runge-Kutta method, as well as with Euler's method, a step size of 0,1 s is used. Exactly the same data and process parameters are used for the simulation. The calculated steel temperature is compared to the measured steel temperature. The results are depicted in the top graph of Figure 4-9. The measured and calculated temperature at the exit of the Slow-Cooling Section are indicated by the orange and purple line, respectively. The blue line indicates the measured steel temperature at the entrance of the Slow-Cooling Section. The measured zone temperature is compared to the calculated zone temperature, depicted in the bottom graph of Figure 4-9. As can be seen, the calculated steel temperature is predicted accurately by the model.

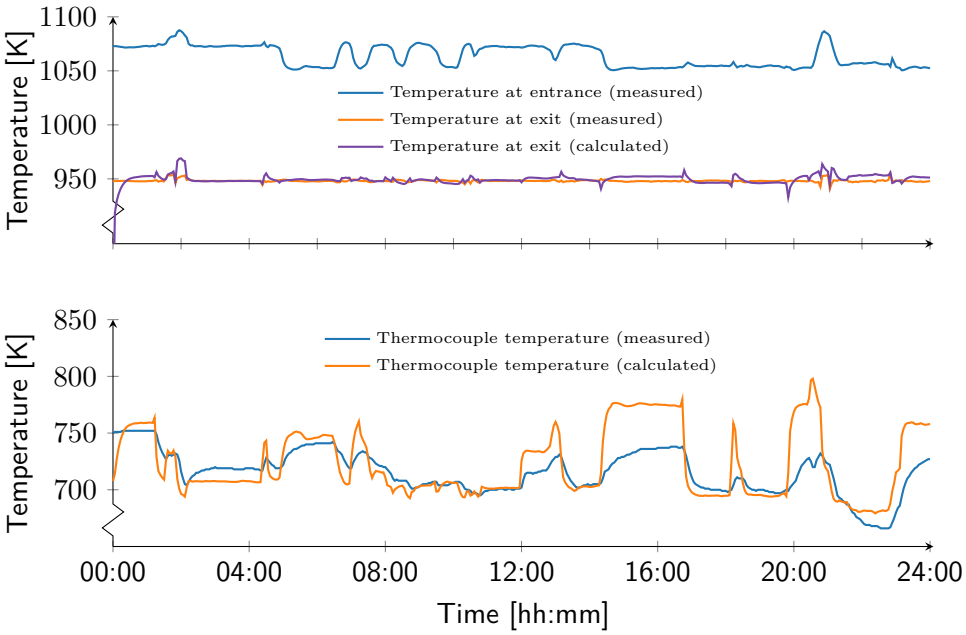

Figure 4-9: Simulation of 6 April 2017, solved by using the Runge-Kutta method. Top: Measured and calculated steel temperatures. Bottom: Measured and calculated zone temperatures.

4-4-4 Comparison

Both numerical methods are used to solve the nonlinear model and simulations have been performed to check the validity of the model and the applicability of the numerical method. The results of the two methods are compared, by looking at the on-target temperatures and the distribution of the deviation from the calculated temperatures compared to the measured

temperatures. The error bar chart, depicted in Figure 4-10, shows the distribution of the difference between the calculated and measured steel temperature. In Figure 4-11 the differences between the calculated and measured steel temperatures from Euler's method and the Runge-Kutta method are depicted. As can be seen very clearly in both graphs, the results from the Runge-Kutta method are much more accurate compared to the results from Euler's method. When looking at the results from the Runge-Kutta method, it can be seen that more than 90% of the calculated temperatures lie within a range of +/− 5 K of the measured temperatures and 96% of the calculated temperatures lie within a range of 10 K of the measured temperatures. But when looking at the results from Euler's method, it can be seen that more than 50% of the calculated temperatures deviate -30 to -40 K from the measured temperatures. It is expected that the results of Euler's method are less accurate compared to Runge-Kutta method. But the results show that Euler's method, with a step size of 0,1 s, is not applicable for solving this nonlinear model. Solving the nonlinear model with the Runge-Kutta method gives more accurate results compared to solving with Euler's method, using the same step size. Therefore, the Runge-Kutta method is used for during the next parts of this research.

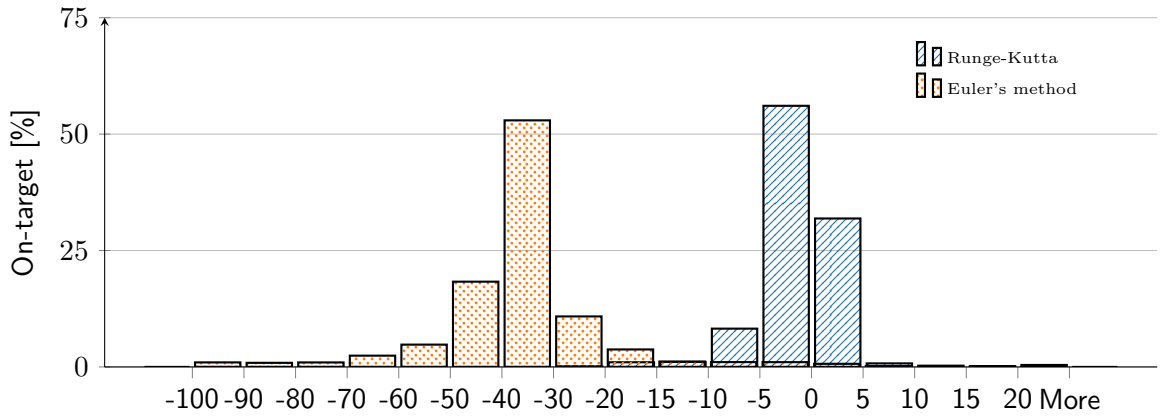

Figure 4-10: Error bar chart on the difference between measured and calculated temperature in Kelvin.

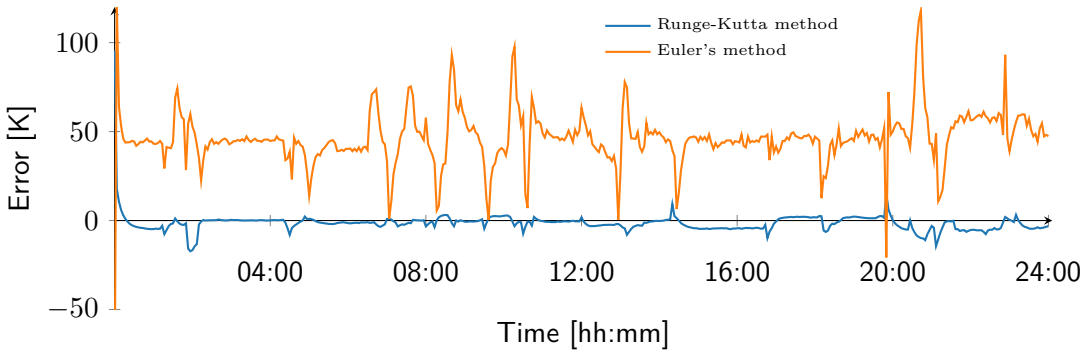

Figure 4-11: Error between calculated and measured steel temperatures for two methods.

4-5 Parameter Estimation

The steel is cooled down by blowing cooled protective gas against the steel. The gas is cooled by a water-cooled heat exchanger and recirculated by fans. At the end of the ventilation ducts, the gas is blown into the Slow-Cooling Section through small nozzles that aim in various directions . The convection heat transfer depends on the heat transfer coefficient and the temperature difference between the gas and surfaces, given by Eq. (4-7). The heat transfer coefficient is a function of various process parameters, such as the flow rate and direction of the gas, the geometrical shape of the nozzle and the line speed. Since limited information and drawings are available regarding the cooling installation, describing the heat transfer coefficient based on available theory is less practical.

Therefore, it is decided to estimate the heat transfer coefficient. The heat transfer coefficient is mainly a function of line speed and flow rate of the incoming circulated protective gas. The gas is circulated by the fans and thus the flow rate is a function of the rotational speed of the fans. According to the fan affinity laws [20], the flow is linearly dependent on the rotational speed of the fans. When the fans do not rotate, the protective gas becomes stationary inside the Slow-Cooling Section and therefore the heat transfer coefficient depends mainly on the line speed. This is called the free convection. When the fans do circulate the gas, an additional form of convection is added, which is called the forced convection. Both the free and forced convection heat transfer coefficient are estimated in the next section.

The parameters are estimated by using the `lsqnonlin`-function in MATLAB. Nonlinear least squares is used to fit furnace data with the nonlinear model, in the unknown parameters. The nonlinear optimisation problem is in the form of:

$$\min_x f(x) \tag{4-27}$$

where f is the nonlinear furnace model and x is the unknown heat transfer coefficient. Several methods are available to solve the nonlinear optimisation problem. The `lsqnonlin`-function can be solved by the *Trust-region-reflective* or *Levenberg-Marquardt* algorithm. Trust-region reflective requires that the system of equations in the nonlinear model is not under determined. Levenberg-Marquardt cannot handle bounds on the estimated parameter. Since the system is not under determined and no specific bounds have to be given, both methods could be used. The Trust-region-reflective method is, as the name suggests, based on trust regions [31]. The Levenberg-Marquardt method searches in a direction, which is a combination of the Gauss-Newton method and the steepest descent direction [25]. Similar results are obtained using both methods and therefore the more standard Trust-region-reflective method is used in this parameter estimation.

4-5-1 Free Convection

Free convection is in this research considered the convection due to the line speed, the moving of the steel strip through the stationary protective gas in the Slow-Cooling Section. Before the free convection heat transfer coefficient can be estimated, the right data has to be selected.

As mentioned, the free convection is only influenced by the line speed when the protective gas is not actively circulated by the fans. Therefore, data is selected from when the recirculation

fans were not operating. In Figure 4-12 the process parameters of 11 May 2017 are depicted. Between approximately 18:00 h and 22:00 h, the recirculation fans are not operating and thus the gas is not circulated.

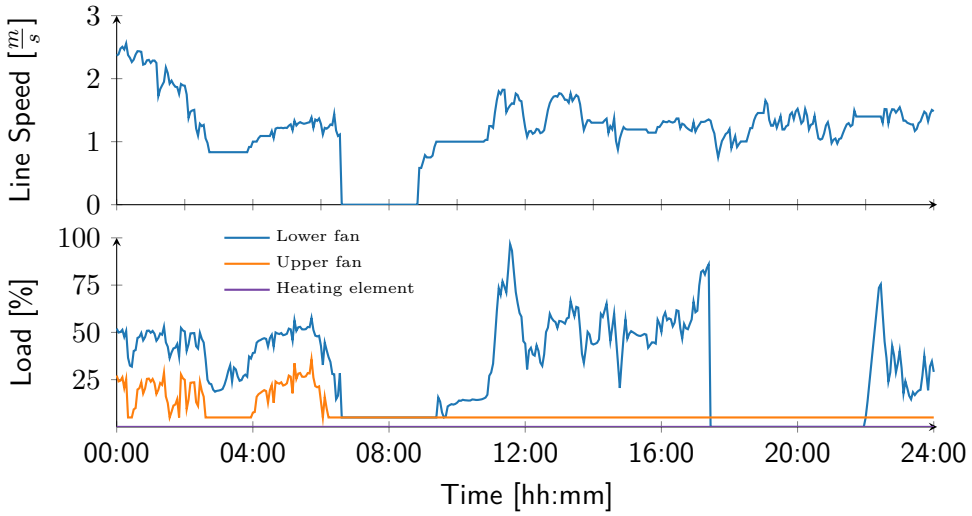

Figure 4-12: Process parameters of 11 May 2017, used for free convection heat transfer coefficient parameter estimation: line speed and fans load percentage.

In [29], order of magnitude of average convective heat transfer coefficients are given. For free convection, the heat transfer coefficient lies between $3-25$ W m^{-2} K^{-1}. This is the starting point for the parameter estimation. The data from 11 May 2017, between 18:00 and 21:00 h, is used for the estimation. The free convection heat transfer coefficient is given by $\alpha_{\text{free}} = 1.2 \cdot v + 6$, where v is the line speed in m s^{-1}. The calculated steel temperature is compared with measured steel temperature, corresponding to the temperature at the exit of the Slow-Cooling Section for the said data. In Figure 4-13, the incoming, calculated and measured temperature are depicted. As can be seen, the calculated temperature follows the measured temperature accurately. In the next section, the estimation of the forced convection is elaborated.

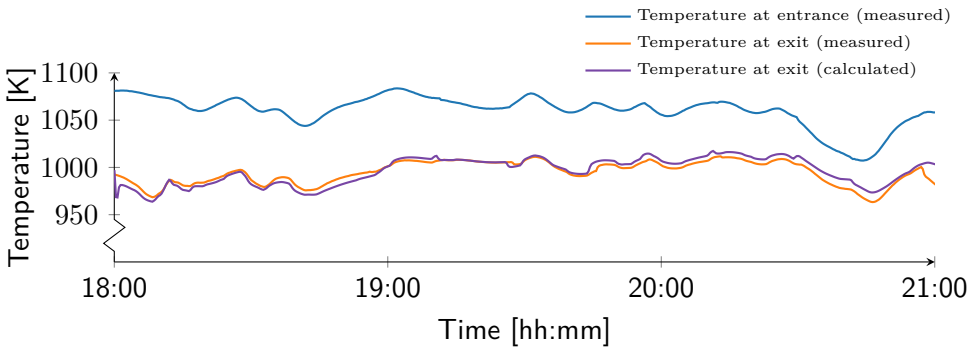

Figure 4-13: Simulation of 11 May 2017 between 18:00 - 21:00 h for free convection heat transfer coefficient estimation.

4-5-2 Forced Convection

The convection heat transfer is a combination of free and forced convection. Now that the free convection heat transfer coefficient is estimated, the forced convection heat transfer coefficient can be estimated. The forced convection heat transfer coefficient can be considered as a function of the rotational speed of the recirculation fans. The volumetric flow rate of protective gas is linearly dependent with the rotational speed. Data from multiple days is used to estimate the forced convection heat transfer convection. The data of 13 April 2017 is used for the estimation of the forced convection heat transfer coefficient, depicted in Figure 4-14.

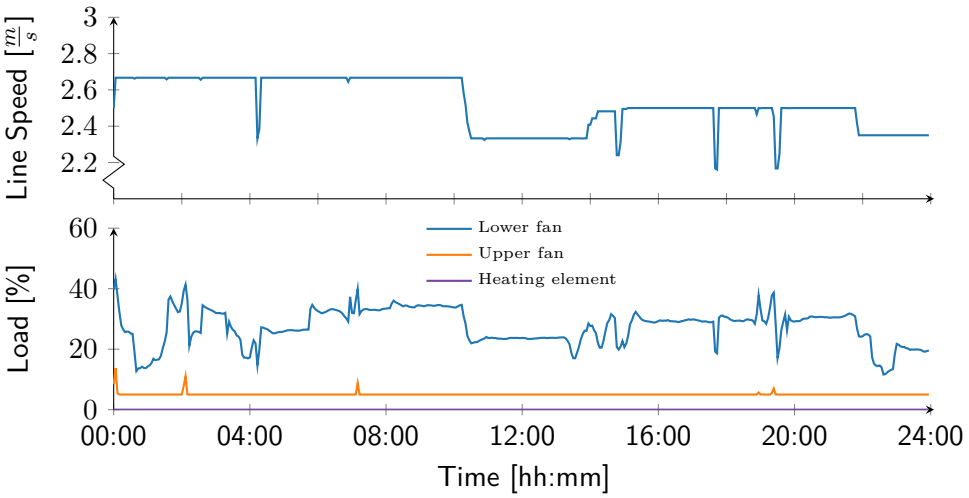

Figure 4-14: Process parameters of 13 April 2017, used for forced convection heat transfer coefficient parameter estimation: line speed, fans and heating elements load percentage.

The forced convective heat transfer coefficient is linearly dependent on the rotational speed of the recirculation fans, given by $\alpha_{\text{forced}} = 0.0129 \cdot \omega$, where ω is the rotational speed in RPM. The calculated steel temperature is compared with measured steel temperature, corresponding to the temperature at the exit of the Slow-Cooling Section for the said data. In Figure 4-15, the incoming, calculated and measured temperature are depicted. As can be seen, the calculated temperature follows the measured temperature accurately.

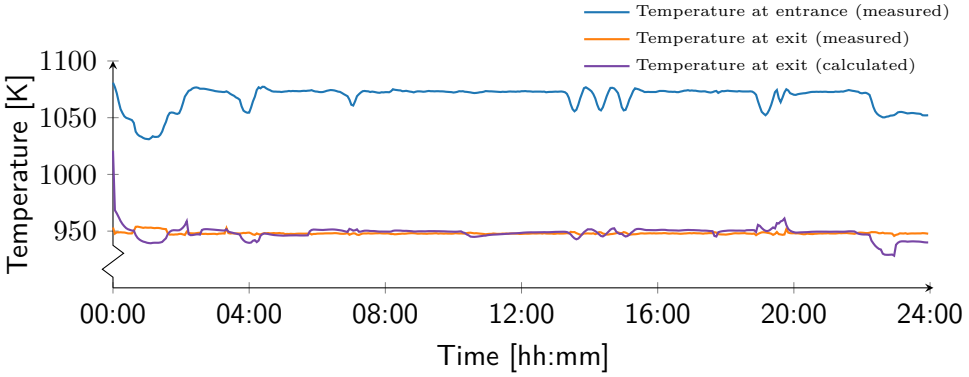

Figure 4-15: Simulation of 13 April 2017 for forced convection heat transfer coefficient estimation.

4-6 Conclusions

In this chapter the development of a nonlinear model describing the Slow-Cooling Section is elaborated. The model is described based on first principles, using a special form of the first law of thermodynamics. The Slow-Cooling Section is divided into computational cells. The heat transfer inside each cell between the steel, protective gas, furnace wall and transport rolls is described by convection, conduction and radiation.

The modelling resulted in a set of differential equations. It is very difficult to solve these differential equations analytically. Therefore it is decided to approximate the solution of the nonlinear model by using a numerical method. The model is validated by using two numerical methods, Euler's method and Runge-Kutta method. After a comparison between Euler's method and Runge-Kutta method, the latter is used to solve the model throughout the remainder of this research. The validation using the Runge-Kutta method yields satisfactory results with temperature errors within $+/-$ 10 K, compared to the measured strip temperatures.

Since limited information and drawings of the Slow-Cooling Section are available, some parameters are estimated in the final section of this chapter. The convection heat transfer coefficient is estimated by using appropriate data sets, which consists of two parts: a line speed dependent free convection and a fan rotation speed dependent forced convection.

In order to simplify the simulations, a typical specific heat curve is used for all the steel grades. However, the specific heat is different for every steel grade and more accurate results can be obtained when all the curves are implemented into the model.

Chapter 5

Design of the Furnace Controller

5-1 Introduction

The control system that is developed for the Slow-Cooling Section, is based on the control methodology Model Predictive Control (MPC). MPC uses a mathematical model of the process. The model consists of a set of differential equations, describing the dynamic behaviour of the temperatures of the elements inside the Slow-Cooling Section. First, the first-principle nonlinear model is prepared such that it can be applied in the MPC framework. The standard nonlinear continuous time state-space model is given by:

$$\frac{dx}{dt} = f(x, u) \tag{5-1}$$

where x and u represent the states and inputs, respectively. The first step is to obtain a linear continuous time state-space representation of the nonlinear model. The state-space representation is used in control engineering to describe a physical system as a set of state, input and output variables. The most general state-space representation is given by the following form:

$$\begin{aligned} \dot{x}(t) &= A(t)x(t) + B(t)u(t) \\ y(t) &= C(t)x(t) + D(t)u(t) \end{aligned} \tag{5-2}$$

where x, u and y are the state, input and output variables. $A \in \mathbb{R}^{n \times n}$, $B \in \mathbb{R}^{n \times p}$, $C \in \mathbb{R}^{q \times n}$, where n, p and q are the number of state, input and output variables, respectively. This form describes a linear time-variant system, where the system matrices depend on time. After linearisation of the nonlinear model, the model is transferred from a continuous time model into the discrete counterpart. A discrete time model is suitable for implementation on digital systems. Only the state-update equation, $\dot{x}(t)$, of Eq. (5-2) is elaborated in the next sections. The output equation, $y(t)$, is trivial, since the only output of this system is the steel

temperature at the exit of the Slow-Cooling Section. This results in the output matrix C as a row of zeros and only one 1, corresponding to the relevant state. The direct feed-through matrix D is the zero matrix for this system.

5-2 Linearisation

In order to use the furnace model in linear MPC, a linear model is needed. The nonlinear state space model is linearised by using the first-order Taylor expansion, given by:

$$f(x,u) \approx f(x_s,u_s) + \left.\frac{\partial f}{\partial x}\right|_{(x_s,u_s)} (x - x_s) + \left.\frac{\partial f}{\partial u}\right|_{(x_s,u_s)} (u - u_s) \tag{5-3}$$

where x_s ad u_s are the states and inputs at the operating point. Often, the model is linearised around a steady-state. The offset term $f(x_s,u_s)$ is then approximately equal to zero. But in this case, the model is not linearised around a steady-state, but around an operating point. From the first-order Taylor expansion the continuous time state matrix A and input matrix B are obtained, given by:

$$A = \left.\frac{\partial f}{\partial x}\right|_{(x_s,u_s)} \qquad B = \left.\frac{\partial f}{\partial u}\right|_{(x_s,u_s)} \tag{5-4}$$

Since the model is not linearised in steady-state but in an operating point, an additional offset term X_c appears in the state-space. The standard state-space model Eq. (5-2) is extended by the offset term. The state update equation is now given by:

$$\dot{x}(t) = Ax(t) + Bu(t) + X_c \tag{5-5}$$

This offset term can be determined by:

$$X_c = f(x_s,u_s) - Ax_s - Bu_s \tag{5-6}$$

where $f(x_s,u_s)$ is calculated using the nonlinear model. The system matrices A and B are time-invariant. However, the process parameters do appear in the matrices. Therefore, the system matrices are parameter varying. The state update equation is rewritten to the following linear parameter varying format:

$$\dot{x}(t) = A(p)x(t) + B(p)u(t) + X_c(p) \tag{5-7}$$

Thus, the state depends on the process parameters, p, at the moment of evaluation. In Chapter 4 the process parameters that can be distinguished are listed. There is a difference between process parameters and control input signals. The MPC developed in Chapter 5 calculates the optimal control input signals. The control input signals that can be distinguished in the Slow-Cooling Section are:

- Rotational speed of lower recirculation fan
- Rotational speed of upper recirculation fan
- Power supplied to electric heating elements

5-3 Discretisation

In order to make the model suitable for evaluation and implementation on a digital system, discretisation must take place. The continuous time model from Eq. (5-5) can be discretised by making use of the matrix exponential, e^{At} [19]. For any A matrix, the unique solution of $\dot{x}(t) = Ax(t)$, with $x(0) = x_0$ is $x(t) = e^{At}x_0$. For existence of this, check that $x(t)$ is a solution by:

$$x(0) = e^{A0}x_0 = x_0 \qquad \text{and} \qquad \dot{x}(t) = \frac{d}{dt}e^{At}x_0 = Ae^{At}x_0 = Ax(t) \tag{5-8}$$

To show the uniqueness, another solution $y(t)$ is used, given by:

$$\begin{aligned} \frac{d}{dt}\left(e^{-At}y(t)\right) &= \left(\frac{d}{dt}e^{-At}\right)y(t) + e^{-At}\left(\frac{d}{dt}y(t)\right) \\ &= -Ae^{-At}y(t) + e^{-At}Ay(t) \\ &= e^{-At}\left(-A + A\right)y(t) = 0 \end{aligned} \tag{5-9}$$

The above shows that the derivative of $e^{-At}y(t)$ is zero and therefore must be a constant. If it is evaluated at $t = 0$, this constant has to be equal to x_0. Thus the following holds:

$$e^{-At}y(t) = x_0 \quad \text{which leads to} \quad y(t) = e^{At}x_0 = x(t) \quad \text{for all } t \in \mathbb{R} \tag{5-10}$$

With Eq. (5-8) - Eq. (5-10), it is proven that the matrix exponential is a solution. The matrix exponential function is created by:

$$e^{At} = I + At + A^2\frac{t^2}{2} + A^3\frac{t^3}{3!} + \dots \tag{5-11}$$

The derivative of the matrix exponential can be rewritten by:

$$\frac{d}{dt}e^{At} = Ae^{At} = e^{At}A \tag{5-12}$$

The offset term X_c is left out of the following proof. The term is inserted back later, but is not important for showing the theory behind discretisation. When the result from Eq. (5-12) is used in Eq. (5-2), the following is obtained:

$$e^{-At}\dot{x}(t) = e^{-At}Ax(t) + e^{-At}Bu(t) \tag{5-13}$$

According to the chain rule, this is equal to:

$$\frac{d}{dt}\left(e^{-At}x(t)\right) = e^{-At}Bu(t) \tag{5-14}$$

Thus, the desired function $x(t)$ can be obtained by integration of the above, which leads to:

$$\begin{aligned} e^{-At}x(t) - e^0 x(0) &= \int_0^t e^{-A\tau}Bu(\tau)d\tau \quad \text{and multiplying with } e^{At} \text{ gives} \\ x(t) &= e^{At}x(0) + \int_0^t e^{A(t-\tau)}Bu(\tau)d\tau \end{aligned} \tag{5-15}$$

which is the analytical solution to the continuous time model. But as said, for evaluation and implementation on computers, discretisation of the continuous time model is required. From the definition that $x[k] \equiv x(kT_s)$, the discrete time solution is obtained:

$$x[k] = e^{AkT_s}x(0) + \int_0^{kT_s} e^{A(kT_s-\tau)}Bu(\tau)d\tau \tag{5-16}$$

and:

$$\begin{aligned} x[k+1] &= e^{A(k+1)T_s}x(0) + \int_0^{(k+1)T_s} e^{A((k+1)T_s-\tau)}Bu(\tau)d\tau \\ &= e^{AT_s}\underbrace{\left[e^{AkT_s}x(0) + \int_0^{kT_s} e^{A(kT-\tau)}Bu(\tau)d\tau\right]}_{x[k]} + \int_{kT_s}^{(k+1)T_s} e^{A(kT_s+T_s-\tau)}Bu(\tau)d\tau \end{aligned} \tag{5-17}$$

Under the assumption that the input u is constant during the integral, the more manageable form is obtained:

$$\begin{aligned} x[k+1] &= e^{AT_s}x[k] + \left(\int_0^T e^{Av}dv\right)Bu[k] \\ &= e^{AT_s}x[k] + A^{-1}\left(e^{AT_s} - I\right)Bu[k] \end{aligned} \tag{5-18}$$

Eq. (5-18) is the exact solution to the discrete time model. However, it is not preferred, for computational reasons, to have the matrix exponential and a matrix inversion in the solution. This can be circumvented by using an approximation of the exact solution. The matrix exponential is generally approximated by one of three methods. In Table 5-1 the three methods and the corresponding approximation of the matrix exponential are depicted. The Forward- and Backward Euler methods estimate the gradient based on the current or next time step. The Tustin transformation is based on the current and next time step and therefore preserves stability [2].

The Tustin approximation is elaborated next and the approximation for the matrix exponential is substituted into the exact solution of the discrete time model.

Table 5-1: Approximation of matrix exponential by three methods.

Method	Approximation of matrix exponential
Forward Euler	$I + AT_s$
Backward Euler	$(I - AT_s)^{-1}$
Tustin transformation	$\left(I + \frac{1}{2}AT_s\right)\left(I - \frac{1}{2}AT_s\right)^{-1}$

The Tustin approximation is given by:

$$\begin{aligned} x[k+1] &= e^{AT_s}x[k] + A^{-1}\left(e^{AT_s} - I\right)Bu[k] \\ &= (I + \frac{1}{2}AT_s)(I - \frac{1}{2}AT_s)^{-1}x[k] + A^{-1}\left((I + \frac{1}{2}AT_s)(I - \frac{1}{2}AT_s)^{-1} - I\right)Bu[k] \\ &= (I + \frac{1}{2}AT_s)(I - \frac{1}{2}AT_s)^{-1}x[k] + \left(T_s(I - \frac{1}{2}AT_s)^{-1}\right)Bu[k] \end{aligned} \tag{5-19}$$

The Tustin approximation is used to transform Eq. (5-5) from continuous time to discrete time. This results in the discrete time state-space model, which can be used in MPC. The offset term is inserted back in the state update equation, now given by:

$$\begin{aligned} x[k+1] =&(I + \frac{1}{2}AT_s)(I - \frac{1}{2}AT_s)^{-1}x[k] + \left(T_s(I - \frac{1}{2}AT_s)^{-1}\right)Bu[k] + \\ &\left(T_s(I - \frac{1}{2}AT_s)^{-1}\right)X_c[k] \end{aligned} \tag{5-20}$$

Finally, the discrete time state-space representation is obtained in Eq. (5-20). The discrete system matrices, A_d, B_d and X_d, are the following:

$$\begin{aligned} A_d &= (I + \frac{1}{2}AT_s)(I - \frac{1}{2}AT_s)^{-1} && \in \mathbb{R}^{n\times n} \\ B_d &= \left(T_s(I - \frac{1}{2}AT_s)^{-1}\right)B && \in \mathbb{R}^{n\times p} \\ X_d &= \left(T_s(I - \frac{1}{2}AT_s)^{-1}\right)X_c && \in \mathbb{R}^{n\times 1} \end{aligned} \tag{5-21}$$

where n and p are the number of state and input variables, respectively. The discrete system matrices are substituted in the discrete state-space representation, which gives the following result:

$$\begin{aligned} x[k+1] &= A_d x[k] + B_d u[k] + X_d \\ y[k] &= Cx[k] \end{aligned} \tag{5-22}$$

This discrete state-space is used to predict the dynamic behaviour of the Slow-Cooling Section.

5-4 Model Predictive Control (MPC)

MPC was originally developed for the control of large chemical process industries [38]. The advanced control system calculates the optimal control inputs at each times step, based on a plant model, past information, the current state and an optimisation routine. The predicted behaviour of the process is optimised such that the desired output is obtained, while respecting given constraints. The main advantages of MPC are:

- MPC is a model based control system, which can easily deal with multiple input and multiple output systems, time-delays and unstable processes.
- MPC is able to predict future behaviour of the process. The predictive ability is a major improvement from the more classic control systems, such as PID controllers.
- Processes come with constraints, such as maximum actuator signals or safety limits. MPC can handle such constraints and safety limits explicitly.
- By optimising over a finite prediction horizon, optimal control inputs are obtained, with respect to an user-defined objective function. The use of an user-defined objective function enables maximising or minimising, not only primary objectives, but also secondary objectives. The components in the objective function are prioritised by using weighting functions.

The control system calculates the optimal control input by using an optimisation routine. The optimisation routine deals with on-line solving of a finite horizon open-loop optimisation problem. The current state of the system is used as initial condition. From the obtained optimal control sequence only the first is applied to the system and the procedure starts from the beginning. This procedure is depicted in Figure 5-1. The optimisation routine has to solve the problem within a feasible time. The computation time required for the optimisation routine depends mainly on the size and complexity of the model, objective function and constraints. Therefore, a trade-off between accuracy and computational burden is made. As said, MPC also has some drawbacks:

- MPC is based on a mathematical model and therefore the performance of the control system depends primarily on the quality of the model.
- The optimisation routine has to be solved in real-time. The computation time is related to the size and complexity of the model. A large and complex model is conflicting with the real-time solving of the optimisation problem

Developments in the field of MPC resulted in different frameworks and approaches [27], as described in the literature survey [36]. However, in all of these frameworks the same building blocks can be distinguished:

- *Prediction model.* The future states of the system are predicted by a dynamic model, describing the plant under control over a finite time prediction horizon. An optimal control sequence is calculated and only the first control action is implemented.

- *Objective function.* At every time instance, the MPC controller optimises a certain objective function, which is often a trade-off between reference tracking and required control input. This optimisation is performed at every time step for a finite prediction horizon, while respecting the constraints. This results in a optimal control sequence, from which only the first input is implemented in the system.
- *Constraints.* An MPC controller is able to respect constraints present in the plant explicitly.
- *Receding prediction horizon.* Optimisation of the objective functions occurs iteratively. After every optimisation, the first control input is implemented. The optimisation is repeated started from the new system state, yielding a new optimal control input. This results in a receding prediction horizon, depicted in Figure 5-1.

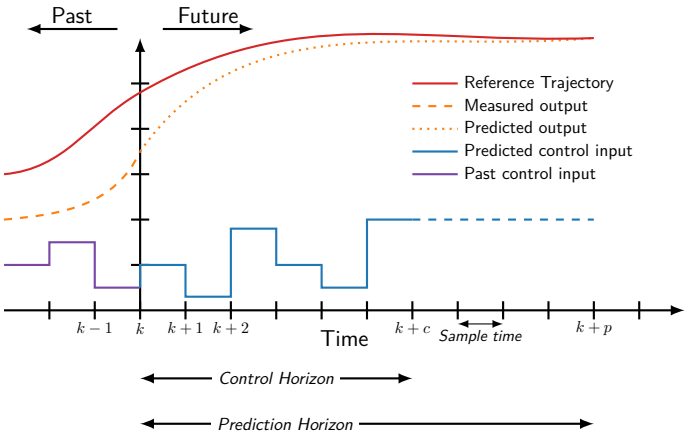

Figure 5-1: Model Predictive Control scheme.

The red solid line in Figure 5-1 shows the process reference. The solid purple and blue lines show the control input signals in the past and future, respectively. The orange dashed and dotted lines indicate the measured and predicted process output. The goal is to track the process reference as close as possible, by applying the calculated control input. Tracking the process reference can be one of the components in the objective function. The predicted output might differ from the corresponding measured output, due to unforeseen disturbances or model errors. Therefore, the optimisation routine is repeated at every time step. The real process outputs are taken into account while calculating the next optimal control input.

In the next sections, the objective function and process constraints are elaborated and adjusted to fit the system at hand, the Slow-Cooling Section.

5-4-1 Objective Function

The goal of MPC is to find the optimal control input sequence for a finite prediction horizon that fulfils a certain objective, at each time step. Most often, the objective of a system is satisfactory reference tracking behaviour of the output and minimising the required input effort, while respecting process constraints [9]. The constrained optimisation problem is described in a objective function, which is a mathematical expression of the desired process

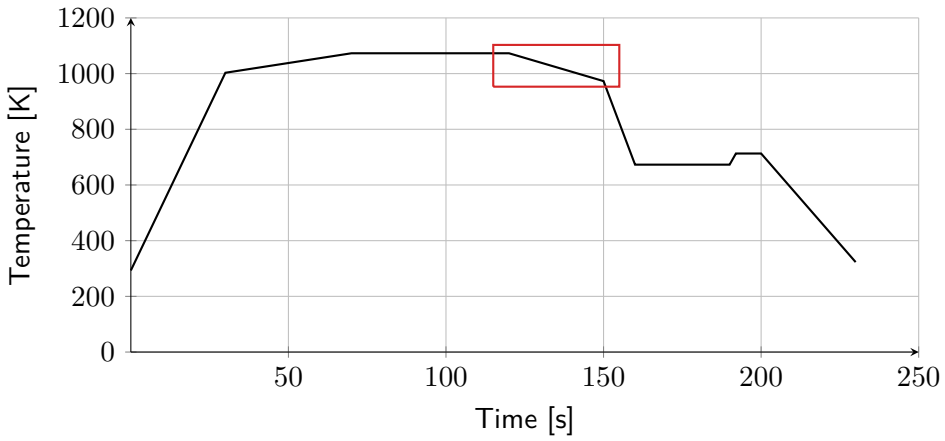

Figure 5-2: Temperature target throughout the entire annealing furnace. Temperature profile for Slow-Cooling Section is indicated by red rectangle.

performance. The objective function for the Slow-Cooling Section is a sum of various process performance targets. In the following sections, the components included in the objective function for the Slow-Cooling Section are listed.

Reference Trajectory Tracking

The most important process performance target in the Slow-Cooling Section is reaching the desired steel temperature at the exit of the Slow-Cooling Section. This performance target is also known as reference trajectory tracking. The reference for the steel temperature in the Slow-Cooling Section is indicated in Figure 5-2 by the red rectangle. The steel comes in at approximately 1073 K and has to leave at approximately 948 K, dependent on the requirements. The reference trajectory, or in this case a target temperature, for a production period of 7 hours of 13 May 2017 is depicted in Figure 5-3.

The main objective is reaching the strip target temperature at the exit of the Slow-Cooling Section. The mathematical expression for this objective is given by:

$$J_T = \sum_{i=1}^{N_p} \Big(T_{\text{steel}}(i) - T_{\text{target}}(i) \Big)^2 \tag{5-23}$$

If the steel temperature is on-target for the entire prediction horizon N_p, this part of the objective is minimised and the primary objective is accomplished. One advantage of MPC is that not only primary objectives can be taken into account, but also secondary objectives can play a role in the control system.

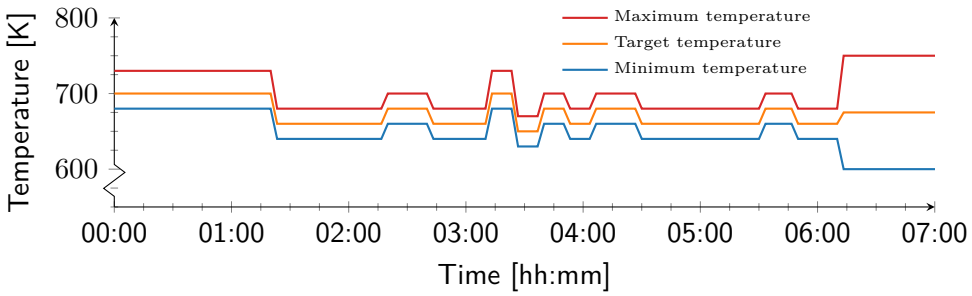

Figure 5-3: Minimum, maximum and target steel temperature.

Actuator Penalisation

The main objective is to reach the desired steel temperature. In the Slow-Cooling Section the steel temperature is controlled by recirculation fans and heating elements. If as little as possible control input is needed to reach the desired steel temperature, energy consumption is minimised and thereby the efficiency of the Slow-Cooling Section is maximised. In other words, one of the secondary objectives is to maximise the efficiency. The mathematical expression for this objective is given by:

$$J_u = \sum_{i=1}^{N_p} \Big(u_{\text{input}}(i) \Big)^2 \tag{5-24}$$

The control input signals, u, that can be distinguished in the Slow-Cooling Section are:

- Rotational speed of lower recirculation fan
- Rotational speed of upper recirculation fan
- Power supplied to electric heating elements

Throughput maximisation

An important performance target for the entire annealing furnace is throughput. The throughput of the furnace is expressed in terms of line speed, v. A high line speed results in high throughput. Besides the mentioned actuators, also the line speed is used to control the steel temperature throughout the furnace. The mathematical expression for the line speed objective is given by:

$$J_v = \sum_{i=1}^{N_p} \Big(v_{\max}(i) - v(i) \Big)^2 \tag{5-25}$$

However, this objective is not used in the Slow-Cooling Section. Other sections in the annealing furnace are more important to the quality of the steel. In these sections, the line speed is used as control signal to reach the desired steel temperature. Therefore, throughput maximisation is not included in the optimisation problem of the Slow-Cooling Section.

Actuator Movement Penalisation

In some systems a steady operation can be desirable. Therefore, besides actuator penalisation also actuator movements, or control input increments, are penalised. The control input increment is given by $\Delta u(i) = u(i) - u(i-1)$, where i is the time instant. The mathematical expression for the penalisation of the actuator movement is given by:

$$J_{\Delta u} = \sum_{i=1}^{N_p} \Big(\Delta u(i)\Big)^2 \tag{5-26}$$

Weighting factors

In the above subsections, the components of the objective function are elaborated. The objective function of the optimisation problem of the Slow-Cooling Section is the sum of these components, given by:

$$J_{\text{total}} = J_T + J_u + J_{\Delta u} \tag{5-27}$$

As said, the most important performance objective is to reach the desired steel temperature. By using weighting factors, W, the different components in the objective function can prioritised according to their importance. A large weighting factor should be used for the primary objectives, while smaller weighting factors should be used for secondary objectives. Adding these weighting factors to Eq. (5-27) yields the objective function for the Slow-Cooling Section, given by:

$$J_{\text{total}} = W_T \cdot J_T + W_u \cdot J_u + W_{\Delta u} \cdot J_{\Delta u} \tag{5-28}$$

5-4-2 Constraints

An aforementioned advantage of MPC is that process constraints or safety limits can be handled explicitly by the control system. The standard form used in the optimisation routine is given by:

$$Eu \leq b \tag{5-29}$$

where u is the optimisation variable. Appropriately defined coefficient matrices E and b represent the constraints in the Slow-Cooling Section. Constraints define the feasibility region of the optimisation problem. Several constraints can be identified in the Slow-Cooling Section, discussed next.

Table 5-2: Minimum and maximum operating conditions for actuators in Slow-Cooling Section.

Actuator		Minimum	Maximum
Lower recirculation fan	[RPM]	77,5	1.550
Upper recirculation fan	[RPM]	77,5	1.550
Heating elements	[kW]	0	240

Actuator constraints

The steel temperature in the Slow-Cooling Section is regulated by the use of recirculation fans and heating elements. These actuators have minimum and maximum operating conditions. In Table 5-2 these constraints are summarised.

In the Slow-Cooling Section 12 electric heaters, of 30 kW each, are installed, that are used for regulating the steel temperature. Typically, the heaters are used only during line starts or extreme conditions. For unknown reasons, the power applied to the heating elements is limited to a maximum of 60% or approximately 20 kW.

Actuator variation constraints

Ideally, the actuators respond instantaneous upon request. However, in reality this is never the case. For instance, the acceleration rate of the rotational speed of the recirculation fans are limited to a maximum. Besides the minimum and maximum actuator constraints from the previous section, the acceleration rate of the actuator is also constrained. The acceleration rate is expressed as the difference between the control input at the current and previous time instant divided by the time step, given by:

$$-a_{\max} \leq \frac{u_{\text{input}}(i) - u_{\text{input}}(i-1)}{\Delta t} \leq a_{\max} \tag{5-30}$$

The acceleration rates are expressed as percentage of the maximum rotational speed or supplied power. For both the recirculation fans and the heating elements, the maximum acceleration or deceleration rate is 5% per 60 seconds.

Temperature constraints

Besides a reference trajectory for the steel temperature, minimum and maximum steel temperatures are active in the Slow-Cooling Section also, depicted in Figure 5-3. These minimum and maximum steel temperatures are considered as constraints. The target temperature lies in between. The control system is able to handle these constraints and can take future temperature constraints into account as well. These minimum and maximum temperatures are expressed as a function of the control signals, which is elaborated Section 5-5-2.

5-5 Optimisation Routine

Now that the building blocks of the MPC are determined, the next step is the development of the optimisation routine. The objective function, constructed in the previous section, is not directly applicable in an optimisation routine. All of the objectives are quadratic, and the constraints are linear. An optimisation routine fit for these kinds of optimisation problems is a quadratic programming framework. The standard form of a quadratic programming problem is:

$$\begin{aligned} \min_{u} \; J(u) =& \frac{1}{2} u^{\intercal} H u + f^{\intercal} u \\ \text{subject to } & Eu \leq b \end{aligned} \tag{5-31}$$

The optimisation problem of the Slow-Cooling Section can be cast into this form. Several steps have to be taken in order to obtain this form. The control input is used to minimise the objective function. Therefore, all the components in the objective function have to be related to the control input sequence. Input vector u contains the three input signals, lower and upper recirculation fans and electric heating elements, for every time step over the length of the prediction horizon N_p:

$$u = \begin{bmatrix} \begin{bmatrix} u_{\text{lower fan}}(1) \\ u_{\text{upper fan}}(1) \\ u_{\text{heating}}(1) \end{bmatrix} \\ \begin{bmatrix} u_{\text{lower fan}}(2) \\ u_{\text{upper fan}}(2) \\ u_{\text{heating}}(2) \end{bmatrix} \\ \vdots \\ \begin{bmatrix} u_{\text{lower fan}}(N_p) \\ u_{\text{upper fan}}(N_p) \\ u_{\text{heating}}(N_p) \end{bmatrix} \end{bmatrix} \in \mathbb{R}^{(N_p \cdot 3) \times 1} \tag{5-32}$$

5-5-1 Prediction Equation

By using the output equation from Eq. (5-22), the behaviour of the states can be predicted over the length of the prediction horizon, N_p. The future states are predicted, based on the current state and the future control inputs. Thus, at time step k the current state $x(k)$ is known and the control inputs $u(k)$, $u(k+1) \dots u(k+N_p-1)$ are chosen to fulfil the objective as well as possible. The aim is to write the optimisation problem in an explicit form. Therefore the future states have to be written as a function of the current state and the control inputs over the prediction horizon. The structure of Eq. (5-22) is exploited to obtain the prediction equation. The initial condition for the prediction is the current state of the system, $x(0)$ at $k = 0$. The state update equation is written as a function of the initial condition and control inputs, given by:

$$
\begin{aligned}
x(1) &= A_d x(0) + B_d u(0) + X_d(0) \\
x(2) &= A_d x(1) + B_d u(1) + X_d(1) \\
&= A_d\Big(A_d x(0) + B_d u(0) + X_d(0)\Big) + B_d u(1) + X_d(1) \\
x(3) &= A_d x(2) + B_d u(2) + X_d(2) \\
&= A_d\Big(A_d\Big(A_d x(0) + B_d u(0) + X_d(0)\Big) + B_d u(1) + X_d(1)\Big) + B_d u(2) + X_d(2)
\end{aligned} \tag{5-33}
$$

The result from Eq. (5-33) is used in the output equation from Eq. (5-22), given by:

$$
\begin{aligned}
y(1) &= Cx(1) \\
&= C\Big(A_d x(0) + B_d u(0) + X_d(0)\Big) \\
y(2) &= Cx(2) \\
&= C\Big(A_d x(1) + B_d u(1) + X_d(1)\Big) \\
&= C\Big(A_d\Big(A_d x(0) + B_d u(0) + X_d(0)\Big) + B_d u(1) + X_d(1)\Big) \\
&= C\Big(A_d^2 x(0) + \Big) \\
y(3) &= Cx(3) \\
&= C\Big(A_d x(2) + B_d u(2) + X_d(2)\Big) \\
&= C\Big(A_d\Big(A_d x(1) + B_d u(1) + X_d(1)\Big) + B_d u(2) + X_d(2)\Big) \\
&= C\Big(A_d\Big(A_d\Big(A_d x(0) + B_d u(0) + X_d(0)\Big) + B_d u(1) + X_d(1)\Big) + B_d u(2) + X_d(2)\Big) \\
&\vdots \\
y(N_p) &= CA_d^{N_p} x(0) + \sum_{i=0}^{N_p-1} CA^{N_p-i-1} B_d u(i) + \sum_{i=0}^{N_p-1} CA^{N_p-i-1} X_d(i)
\end{aligned} \tag{5-34}
$$

The prediction equation is required for solving the optimisation problem using a quadratic programming algorithm. The prediction equation from Eq. (5-34) can be rewritten into the following matrix form:

$$y = \begin{bmatrix} y(1) \\ y(2) \\ \vdots \\ y(N_p) \end{bmatrix} = \overbrace{\begin{bmatrix} CA_d \\ CA_d^2 \\ \vdots \\ CA_d^{N_p} \end{bmatrix}}^{F} x_0 + \overbrace{\begin{bmatrix} CB_d & 0 & \dots & 0 \\ CA_dB_d & CB_d & \dots & 0 \\ \vdots & \vdots & \ddots & \vdots \\ CA_d^{N_p-1}B_d & CA_d^{N_p-2}B_d & \dots & CB_d \end{bmatrix}}^{G} \begin{bmatrix} u(0) \\ u(1) \\ \vdots \\ u(N_p-1) \end{bmatrix} + \overbrace{\begin{bmatrix} CX_d \\ C(I+A_d)X_d \\ \vdots \\ C(\sum_{i=0}^{N_p-1} A_d^i)X_d \end{bmatrix}}^{h}$$

$$= F \cdot x_0 + G \cdot u + h \tag{5-35}$$

where $F \in \mathbb{R}^{n \times 1}$, $G \in \mathbb{R}^{N_p \times (N_p \cdot p)}$ and $h \in \mathbb{R}^{N_p \times 1}$ where n, p and N_p are the number of state and input variables and the prediction horizon, respectively.

5-5-2 Quadratic Programming

The components of the objective function, defined in Section 5-4-1, are all quadratic. The constraints are linear, and therefore a quadratic programming (QP) solver can be used to solve the optimisation problem. The objectives and constraints cannot directly be applied in a quadratic solver. The transformations of the objectives and constraints are discussed next.

Objectives

The components of the objective function have to be cast into the standard form of the quadratic programming algorithm, given by:

$$\min_u J(u) = \frac{1}{2} u^\intercal H u + f^\intercal u \tag{5-36}$$

The reference trajectory tracking component, stated in Eq. (5-23), including weighting factors, can be rewritten and cast into the standard form, given by:

$$\begin{aligned} J_T W_T &= \sum_{i=1}^{N_p} \Big(T_{\text{steel}}(i) - T_{\text{target}}(i) \Big)^2 W_T \\ &= (y - r)^\intercal \cdot W_T \cdot (y - r) \end{aligned} \tag{5-37}$$

where y is the output of the model, which represents the steel temperature at the exit of the Slow-Cooling Section and r is the reference target temperature. The other components from the objective function, Eq. (5-24) and Eq. (5-26) are transformed in a similar way. The actuator constraints is rewritten to:

$$\begin{aligned} J_u W_u &= \sum_{i=1}^{N_p} \Big(u_{\text{input}}(i) \Big)^2 W_u \\ &= u^\intercal W_u u \end{aligned} \tag{5-38}$$

The actuator variation constraints is rewritten to:

$$\begin{aligned} J_{\Delta u} W_{\Delta u} &= \sum_{i=1}^{N_p} \Big(\Delta u(i) \Big)^2 W_{\Delta u} \\ &= \Delta u^\intercal W_{\Delta u} \Delta u \end{aligned} \tag{5-39}$$

where u is a vector containing the control sequence and Δu is the vector representing the increment of the control signal. The objective function can be applied in QP after the transformation. The objective has the following form:

$$J(u) = (y - r)^\intercal W_T (y - r) + u^\intercal W_u u + \Delta u^\intercal W_{\Delta u} \Delta u \tag{5-40}$$

The prediction equation in matrix form is substituted in Eq. (5-40), which yields:

$$J(u) = (F \cdot x_0 + G \cdot u + h - r)^\intercal \cdot W_T \cdot (F \cdot x_0 + G \cdot u + h - r) + u^\intercal \cdot W_u \cdot u + \Delta u^\intercal \cdot W_{\Delta u} \cdot \Delta u \tag{5-41}$$

Every component in the objective function is either known or is linked to the minimisation parameter, the control signal. Thus, minimising the objective function results in close tracking of the target temperature, with a low amount of control input needed and not much variations in the control signals. In order to solve the above objective function using with the `quadprog`-function from MATLAB, it has to be cast into the following form:

$$\begin{aligned} \min_u \ J(u) =& \frac{1}{2} u^\intercal H u + f^\intercal u \\ &\text{subject to } Eu \leq b \end{aligned} \tag{5-42}$$

To cast Eq. (5-40) into the `quadprog`-form, we take the following steps and transform Eq. (5-41) into:

$$\begin{aligned} \min_u \ J(u) &= (F \cdot x_0 + G \cdot u + h - r)^\intercal \cdot W_T \cdot (F \cdot x_0 + G \cdot u + h - r) + u^\intercal W_u u + \Delta u^\intercal W_{\Delta u} \Delta u \\ &= x_0^\intercal F^\intercal W_T F x_0 + x_0^\intercal F^\intercal W_T G u + x_0^\intercal F^\intercal W_T h - x_0^\intercal F^\intercal W_T r \\ &\quad + u^\intercal G^\intercal W_T F x_0 + u^\intercal G^\intercal W_T G u + u^\intercal G^\intercal W_T h - u^\intercal G^\intercal W_T r \\ &\quad + h^\intercal W_T F x_0 + h^\intercal W_T G u + h^\intercal W_T h - h^\intercal W_T r \\ &\quad - r^\intercal W_T F x_0 - r^\intercal W_T G u - r^\intercal W_T h + r^\intercal W_T r \\ &\quad + u^\intercal W_u u + \Delta u^\intercal W_{\Delta u} \Delta u \end{aligned} \tag{5-43}$$

The coefficient matrices H and $f^\intercal$ are obtained from Eq. (5-43). H and $f^\intercal$ contain the following elements:

$$\begin{aligned} H &= 2 \cdot (G^\intercal \cdot W_T \cdot G + W_u + W_{\Delta u}) \quad &\in \mathbb{R}^{(N_p \cdot p) \times (N_p \cdot p)} \\ f^\intercal &= 2 \cdot (x_0^\intercal F^\intercal + h^\intercal - r^\intercal) \cdot W_T \cdot G \quad &\in \mathbb{R}^{1 \times (N_p \cdot p)} \end{aligned} \tag{5-44}$$

where N_p and p are the prediction horizon and the number of input variables, respectively. Not all the terms from Eq. (5-43) are captured in the coefficient matrices H and $f^\intercal$. Only the terms that are linked to the minimisation parameter u are considered. The remaining terms in the objective function that are not linked to the control input u are not important for optimisation, since these terms cannot be optimised by adjusting the control input.

Constraints

Besides the objective function, the constraints, described in Section 5-4-2, have to be cast into a form suitable for `quadprog` function of MATLAB. The constraints have to be in the following form:

$$Eu \leq b \tag{5-45}$$

where u is the vector containing the control input sequence. Matrices E and b have to be described appropriately. The actuator constraints, describing the minimum and maximum settings are transformed to fit the standard form, given by:

$$\begin{aligned} 77,5 \leq \text{RPM} &\leq 1.550 \\ 0 \leq P_{\text{heat}} &\leq 20 \end{aligned} \tag{5-46}$$

where RPM is the rotational speed of the recirculation fans and P_{heat} is the power supplied to the electric heating elements in kilowatt. Only $\leq$ can be used in `quadprog`, so the above inequalities are rewritten to:

$$\begin{aligned} -\text{RPM} &\leq -77,5 \\ \text{RPM} &\leq 1.550 \\ -P_{\text{heat}} &\leq 0 \\ P_{\text{heat}} &\leq 20 \end{aligned} \tag{5-47}$$

This yields matrix E_{input} and b_{input}, given by:

$$E_{\text{input}} = \begin{bmatrix} -I \\ I \\ -I \\ I \end{bmatrix} \qquad b_{\text{input}} = \begin{bmatrix} -77,5 \\ 1.550 \\ 0 \\ 20 \end{bmatrix} \tag{5-48}$$

As mentioned before, the acceleration rate of the recirculation fans is constrained also. The acceleration rate is described as the difference in control input signals between the current and previous time step, divided by the time step, displayed in Eq. (5-30). The power applied to the electric heating elements is limited by the same acceleration rate. The acceleration rate is expressed as a percentage of the maximum rotational speed or supplied power. The input is limited to an increase or decrease of 5% every 60 seconds. Dependent on the used time step, Δt, the acceleration constraint is given by:

$$-5 \cdot \frac{\Delta t}{60}\% \leq \Delta u \leq 5 \cdot \frac{\Delta t}{60}\% \tag{5-49}$$

where $\Delta u = u(i) - u(i-1)$. Again, this is rewritten so that only $\leq$ is used given by:

$$\begin{aligned} u(i) - u(i-1) &\leq 5 \cdot \frac{\Delta t}{60}\% \\ u(i-1) - u(1) &\leq 5 \cdot \frac{\Delta t}{60}\% \end{aligned} \tag{5-50}$$

The coefficient matrices $E_{\Delta\text{input}}$ and $b_{\Delta\text{input}}$ are defined appropriately, such that it represents the acceleration constraints, in the following way:

$$E_{\Delta\text{input}} = \begin{bmatrix} 1 & 0 & 0 & -1 & 0 & 0 & \dots & 0 & 0 & 0 & 0 & 0 & 0 \\ 0 & 1 & 0 & 0 & -1 & 0 & \dots & 0 & 0 & 0 & 0 & 0 & 0 \\ 0 & 0 & 1 & 0 & 0 & -1 & \dots & 0 & 0 & 0 & 0 & 0 & 0 \\ \vdots & \vdots & \vdots & \vdots & \vdots & \vdots & \ddots & \vdots & \vdots & \vdots & \vdots & \vdots & \vdots \\ 0 & 0 & 0 & 0 & 0 & 0 & \dots & 1 & 0 & 0 & -1 & 0 & 0 \\ 0 & 0 & 0 & 0 & 0 & 0 & \dots & 0 & 1 & 0 & 0 & -1 & 0 \\ 0 & 0 & 0 & 0 & 0 & 0 & \dots & 0 & 0 & 1 & 0 & 0 & -1 \end{bmatrix} \quad b_{\Delta\text{input}} = \begin{bmatrix} 0,05 \\ 0,05 \\ 0,05 \\ \vdots \\ 0,05 \\ 0,05 \\ 0,05 \end{bmatrix} \cdot \frac{\Delta t}{60} \tag{5-51}$$

Eq. (5-51) is the constraint for the acceleration rate. The deceleration rate is constrained by the negative of the coefficient matrices, $-E_{\Delta\text{input}}$ and $-b_{\Delta\text{input}}$.

The main goal of the Slow-Cooling Section is to reach the desired steel temperature. For product quality reasons the temperature cannot be higher or lower than certain temperatures. These temperatures are considered constraints in the optimisation routine. The temperature constraints can be different for every strip, dependent on the steel type and strip dimension, as depicted in Figure 5-3. The constraints are defined by:

$$T_{\min} \leq T_{\text{steel}} \leq T_{\max} \tag{5-52}$$

This is rewritten in a similar way, so that only $\leq$ is used, given by:

$$\begin{aligned} -T_{\text{steel}} &\leq -T_{\min} \\ T_{\text{steel}} &\leq T_{\max} \end{aligned} \tag{5-53}$$

The temperature is predicted by Eq. (5-35). T_{steel} is replaced by the prediction equation. This results in the following constraints:

$$\begin{aligned} -(F \cdot x_0 + G \cdot u + h) &\leq -T_{\min} \\ (F \cdot x_0 + G \cdot u + h) &\leq T_{\max} \end{aligned} \tag{5-54}$$

This can be rewritten to fit the standard constraint form $Eu \leq b$, by:

$$\begin{aligned} -G \cdot u &\leq -T_{\min} + F \cdot x_0 + h \\ G \cdot u &\leq T_{\max} - F \cdot x_0 - h \end{aligned} \tag{5-55}$$

The coefficient matrices E_{temp} and b_{temp} are defined appropriately:

$$E_{\text{temp}} = \begin{bmatrix} -G \\ G \end{bmatrix} \qquad b_{\text{temp}} = \begin{bmatrix} -T_{\min} + F \cdot x_0 + h \\ T_{\max} - F \cdot x_0 - h \end{bmatrix} \tag{5-56}$$

All the constraints are cast into the standard form of Eq. (5-45). The coefficient matrices E and b are given by:

$$E = \begin{bmatrix} E_{\text{input}} \\ E_{\Delta\text{input}} \\ -E_{\Delta\text{input}} \\ E_{\text{temp}} \end{bmatrix} \qquad b = \begin{bmatrix} b_{\text{input}} \\ b_{\Delta\text{input}} \\ -b_{\Delta\text{input}} \\ b_{\text{temp}} \end{bmatrix} \tag{5-57}$$

5-6 Modelling Framework

As mentioned, the name Model Predictive Control indicates a range of control methods, based on a process model, that optimises a certain objective function [10]. Different approaches are the result of research into MPC. The approaches differ mainly in the underlying process model. In this research, two approaches are compared. The first approach uses a linear state-space model as internal model for MPC. Since the process in the Slow-Cooling Section is nonlinear, mainly due to the strip transitions, a second approach is used. The second approach uses a set of piecewise affine models. The use of piecewise affine models approximates the nonlinear model more accurately, as can be seen in Chapter 6. The two approaches are elaborated next and both are used in the simulation studies.

5-6-1 Linear MPC

Linear MPC requires a linear internal model. Since the steel usually enters the Slow-Cooling Section at an average temperature of approximately 1073 K and leaves at a temperature of approximately 948 K, linearising the nonlinear model at an operating point seems justified.

The parameters of the operating point are selected by looking at the steel temperatures throughout the Slow-Cooling Section in a steady operation. Common process parameters for strip dimension, line speed and actuator settings are selected and used as operating point. The state-space used as internal model in the MPC has the following form:

$$x(k+1) = A(x_s, u_s)x(k) + B(x_s, u_s)u(k) + X_d(x_s, u_s) \tag{5-58}$$

where A, B and X_d as the discrete system matrices and x_s and u_s as the process parameters corresponding to the operating point. The state-space is created only once, which reduces the computational burden of the optimisation routine significantly. Another advantage of using only one linear internal model is that the prediction equation is not dependent on the process parameters. The prediction horizon is filled with equal system matrices, which saves time in the prediction of future states. The use of only one internal model simplifies the optimisation routine and it is beneficial for the computation time. In Chapter 6, simulations using only one internal model are performed. By using only one linearised model, prediction of future dynamics is only correct when the process actually operates in the operating point used for linearisation. To circumvent these problems, piecewise linearisation of the nonlinear system can be applied to obtain a set of local linear models. In the next section, the linear internal model is extended to a piecewise affine model, where process parameters used in the optimisation correspond to the actual process parameters in the Slow-Cooling Section.

5-6-2 Piecewise Affine MPC

The process in the Slow-Cooling Section is nonlinear. The difficulty from controlling the Slow-Cooling Section is mainly due to the strip transitions. One of the reasons to use MPC to control the Slow-Cooling Section is that future strip dimension can be accounted for, such that the process is prepared when a steel strip with different dimensions enters the Slow-Cooling Section. The use of piecewise affine models as internal model for MPC complicates the prediction equation. The state-space used as internal model in the MPC has the following form:

$$\dot{x}(t) = A(p)x(t) + B(p)u(t) + X_d(p) \tag{5-59}$$

where p represents the actual process parameters, active in the Slow-Cooling Section. The prediction equation, when using only one linear model, is filled with powers of system matrices, as can be seen in Eq. (5-35). In case of using parameter dependent system matrices, the state update equation and prediction equation are extended, by:

$$\begin{aligned}
x(1) &= A(0)x(0) + B(0)u(0) + X_d(0) \\
x(2) &= A(1)x(1) + B(1)u(1) + X_d(1) \\
&= A(1)\Big(A(0)x(0) + B(0)u(0) + X_d(0)\Big) + B(1)u(1) + X_d(1) \\
x(3) &= A(2)x(2) + B(2)u(2) + X_d(2) \\
&= A(2)\Big(A(1)\Big(A(0)x(0) + B(0)u(0) + X_d(0)\Big) + B(1)u(1) + X_d(1)\Big) + B(2)u(2) + X_d(2)
\end{aligned} \tag{5-60}$$

The system matrices A and B are parameter dependent and are filled with future process parameters. The future process parameters, such as strip dimensions, can be determined by using the current line speed and the production plan. Also the output equation differs from the one given in Eq. (5-34). The output equation is extended, given by:

$$\begin{aligned}
y(1) &= Cx(1) \\
&= C\Big(A(0)x(0) + B(0)u(0) + X_d(0)\Big) \\
y(2) &= Cx(2) \\
&= C\Big(A(1)x(1) + B(1)u(1) + X_d(1)\Big) \\
&= C\Big(A(1)\Big(A(0)x(0) + B(0)u(0) + X_d(0)\Big) + B(1)u(1) + X_d(1)\Big) \\
y(3) &= Cx(3) \\
&= C\Big(A(2)x(2) + B(2)u(2) + X_d(2)\Big) \\
&= C\Big(A(2)\Big(A(1)x(1) + B(1)u(1) + X_d(1)\Big) + B(2)u(2) + X_d(2)\Big) \\
&= C\Big(A(2)\Big(A(1)\Big(A(0)x(0) + B(0)u(0) + X_d(0)\Big) + B(1)u(1) + X_d(1)\Big) + B(2)u(2) + X_d(2)\Big)
\end{aligned} \tag{5-61}$$

The prediction equation becomes parameter dependent, corresponding to future process parameters. At every time step in the optimisation routine, additional steps have to be taken, when using piecewise affine models as internal model for Model Predictive Control. The system matrices A and B and the offset term X_d have to be calculated for the entire prediction horizon. The coefficient matrices F, G and h have to be filled following the semantics of Eq. (5-62), given by:

$$y = \begin{bmatrix} y(1) \\ y(2) \\ y(3) \\ \vdots \\ y(N_p) \end{bmatrix} = \overbrace{\begin{bmatrix} CA_d(0) \\ CA_d(1)A_d(0) \\ CA_d(2)A_d(1)A_d(0) \\ \vdots \\ C\prod_{i=N_p-1}^{0} A_d(i) \end{bmatrix}}^{F} x_0 + \overbrace{\begin{bmatrix} CX_d(0) \\ C\Big(A_d(1)X_d(0) + X_d(1)\Big) \\ C\Big(A_d(2)A_d(1)X_d(0) + A_d(2)X_d(1) + X_d(2)\Big) \\ \vdots \\ C\Big(\sum_{j=0}^{N_p-1}\Big(\prod_{i=N_p-1}^{j+1} A_d(i)\Big)X_d(j) + X_d(N_p-1)\Big) \end{bmatrix}}^{h} +$$

$$\underbrace{\begin{bmatrix} CB_d(0) & 0 & 0 & \dots & 0 \\ CA_d(1)B_d(0) & CB_d(1) & 0 & \dots & 0 \\ CA_d(2)A_d(1)B_d(0) & CA_d(2)B(1) & CB_d(2) & \dots & 0 \\ \vdots & \vdots & \vdots & \ddots & \vdots \\ C\prod_{i=N_p-1}^{1} A_d(i)B_d(0) & C\prod_{i=N_p-1}^{2} A_d(i)B_d(1) & C\prod_{i=N_p-1}^{3} A_d(i)B_d(2) & \dots & CB_d(N_p-1) \end{bmatrix}}_{G} \begin{bmatrix} u(0) \\ u(1) \\ u(2) \\ \vdots \\ u(N_p-1) \end{bmatrix} \tag{5-62}$$

5-7 Control Loop

The Model Predictive Control system, based on the linear or piecewise affine internal model, calculates the optimal control sequence. The optimisation is based on the current state of the system, while keeping future process dynamics in account. The controller is implemented in a feedback control system. The feedback control system is a means of monitoring the behaviour of the process. The MPC calculates the optimal control sequence, but only the first control input of the sequence is sent to the process. Under influence of this control input, the system moves to a new state. In this plant, the temperatures of the steel strip, gas, furnace walls and transport rolls in the Slow-Cooling Section evolve. The nonlinear model, developed in Chapter 4, is used in the simulation study to represent the Slow-Cooling Section. The control loop is depicted in Figure 5-4.

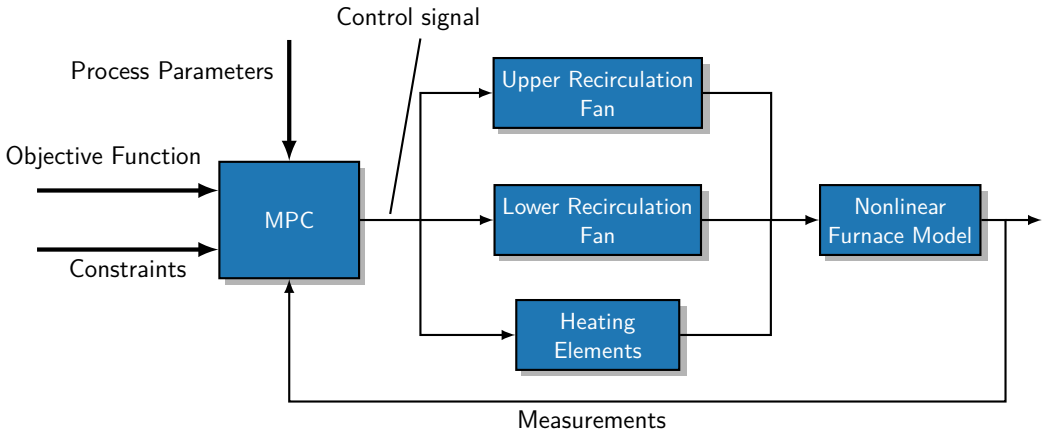

Figure 5-4: Control loop block diagram Model Predictive Control.

The MPC receives the objective function and the constraints. The measurements from the Slow-Cooling Section are send back to the controller and are used as initial condition for the optimisation routine at every time step. The objective function, constraints and measurements are used to calculate the optimal control sequence and the first control input signal is sent to actuator blocks. The actuator blocks translate the control signal to the associated actuator settings and then send it to the Slow-Cooling Section, or in case of the simulation studies to the nonlinear furnace model. In an ideal case, the process evolves exactly as predicted. However, there are always deviations in the model or measurements. The new output is measured and sent to the MPC and the optimisation routine starts again.

5-8 Conclusions

In this chapter the Model Predictive Control (MPC) framework is used to design a control system for the Slow-Cooling Section. The nonlinear model developed in Chapter 4 is linearised and discretised in the first part of this chapter. The Tustin approximation is used for discretisation of the continuous time model.

The use of MPC makes it possible to define the process constraints explicitly. Process constraints, such as actuator settings and safety limits are described in the second part of this

chapter. MPC uses a objective function to optimise the future control inputs. The components defining the objective function are reference tracking, the use of actuators and the change in use of actuators. The objective function and constraints are solved by using the quadratic programming algorithm.

In the next part of this chapter, two methods are used to design an MPC. First, a model linearised in an operating point of common process parameters is used as internal model for the optimisation routine. The advantage of this controller is the simplicity of the design of the prediction horizon and system matrices. The disadvantage is that the process only performs accurate when it actually operates in the operating point. Therefore, a second method is used. The second method uses a set of piecewise affine models as internal model for the optimisation routine. Future process parameters are taken into account, when calculating the future control inputs.

Chapter 6

Simulation Study

6-1 Introduction

In Chapter 5 two MPC are developed, using different internal models. Both MPC are used in simulation studies in this chapter. The results of both developed controllers are compared to the current control system. In Figure 5-4 the control loop, used for the simulation studies is depicted. The nonlinear model developed in Chapter 4 is used to represent the Slow-Cooling Section during the simulation studies.

Three case studies are performed. The first two case studies compare the performance of the new controllers with the performance of the current controller. The third case study investigates the possibilities of relaxation of actuator constraints to improve the overall performance of the Slow-Cooling Section.

6-2 Data Selection

On some days, the process in the Slow-Cooling Section operates under very steady conditions. On other days, the operating conditions of the Slow-Cooling Section are subject to more variations. The performance of the newly developed controllers is tested for both steady and non steady operating conditions. The following data are used as inputs for the simulations:

- Strip width
- Strip thickness
- Line speed
- Temperature at Slow-Cooling Section entrance

6-2-1 Case Study 1: 6 April 2017

Data from 6 April 2017 show very steady process conditions. A prediction period of 4 hours is simulated. The process parameters for these 4 hours are depicted in Figure 6-1. As can be seen, the variations of the strip dimensions are very limited. The line speed is equal to approximately 2,4 m s^{-1}, almost the entire production period. However, some sudden decreases in line speed can be seen. The target temperature during this production period is very steady and only switches two times by 5 K.

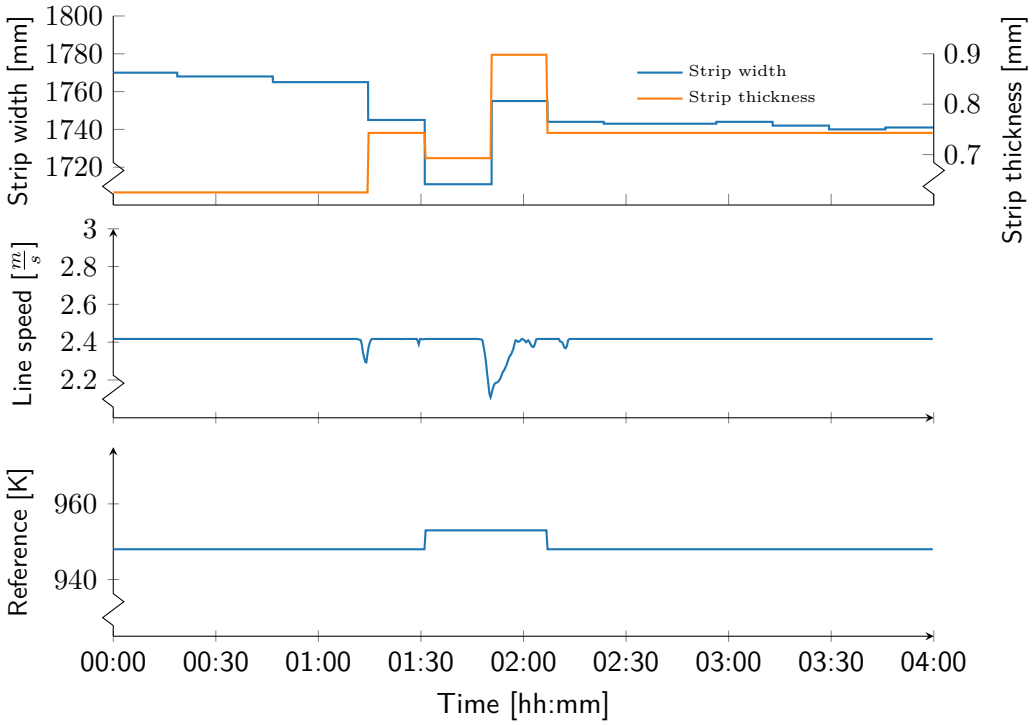

Figure 6-1: Process parameters of 6 April 2017 used for simulation studies.
Top: Strip dimensions. Middle: Line speed. Bottom: Target Temperature.

6-2-2 Case Study 2: 13 May 2017

The second simulation is performed with data from a production period of 8 hours of 13 May 2017. The operating conditions vary throughout this day, as depicted in Figure 6-2. The width and thickness of the steel varies a lot during this production period, the strips become wider and thicker. Next to some sudden bigger decreases, the line speed is not steady throughout this production period also. The target temperature is different for almost every strip. Altogether, this production period can be seen as very challenging to control. But these variations do yield the possibility of testing the performance of the controllers for non steady operating conditions.

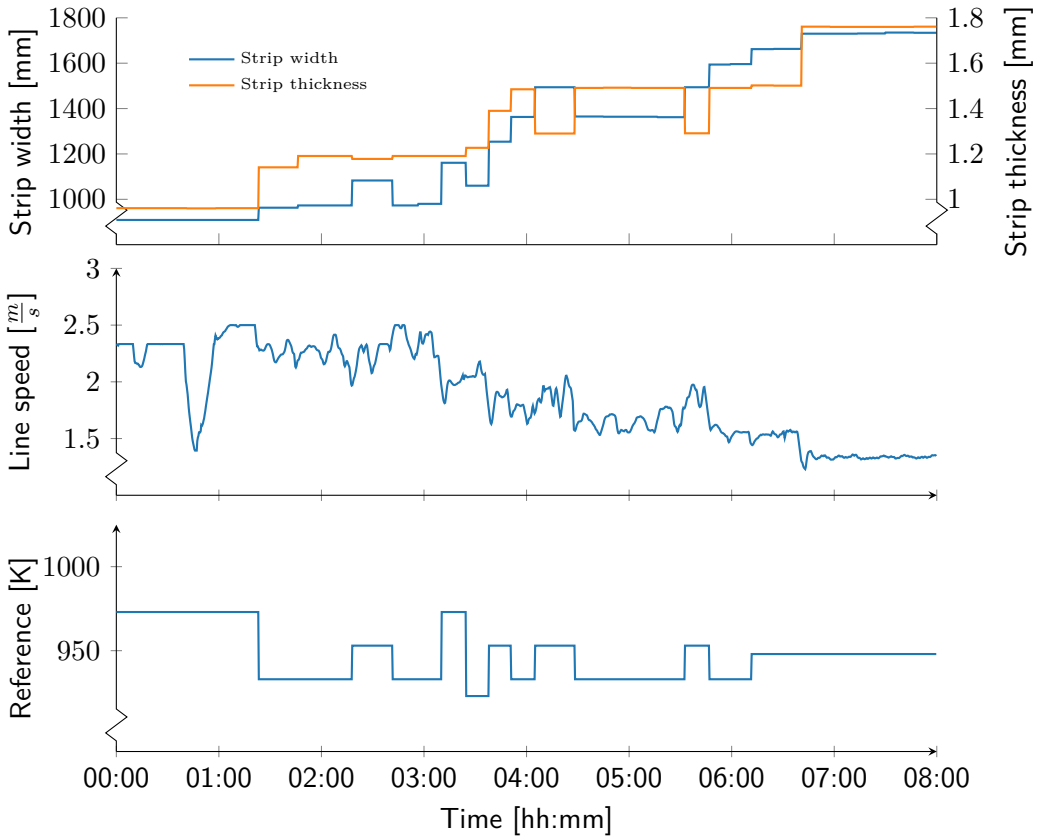

Figure 6-2: Process parameters of 13 May 2017 used for simulation studies. Top: Strip dimensions. Middle: Line speed. Bottom: Target Temperature.

6-3 Simulation Set-up

The data of the two cases are ready for simulation. It is chosen to use the nonlinear furnace model, developed in Chapter 4 to represent the Slow-Cooling Section, i.e. it represents the "real" world. A regular strip of approximately 1.800 m traverses the Slow-Cooling Section in approximately 720 s. The Runge-Kutta method is used to solve the nonlinear process model. The time step used for this numerical method is set to 0,1 s, equal to time step used for model validation. The sampling time for the Model Predictive Control system is set to 4 s. The prediction horizon is set to 300 s. As indicated in Section 5-4-2, the actuators are limited in acceleration rate. The actuators can accelerate with 5% every 60 seconds. By choosing a prediction horizon of 300 s, the controller can adjust the actuator by 25%. A prediction horizon of 300 s results in that when the current strip is approximately halfway through the Slow-Cooling Section, the dimensions and corresponding parameters of the next strip appear in the prediction horizon. This gives the controller enough time to prepare for the operating condition. The simulations are performed using MATLAB R2016b on a HP Z-Book with a 2,4 GHz Intel Core i7 processor and 8 GB of RAM.

6-4 Case Study 1

The performance of the Linear MPC and that of the Piecewise Affine MPC is tested with data from 6 April 2017. The Linear MPC requires an operating point, representing common process conditions for the simulation. The system matrices are created based on this operating point. The system matrices depend on temperatures of the elements, strip dimensions, line speed and actuator settings. For the temperatures and actuator settings average values are used. For line speed a value of 2,4 m s^{-1} is used, corresponding to the line speed of the majority of the data. The strip dimensions that are selected for the operating point are depicted in Figure 6-3.

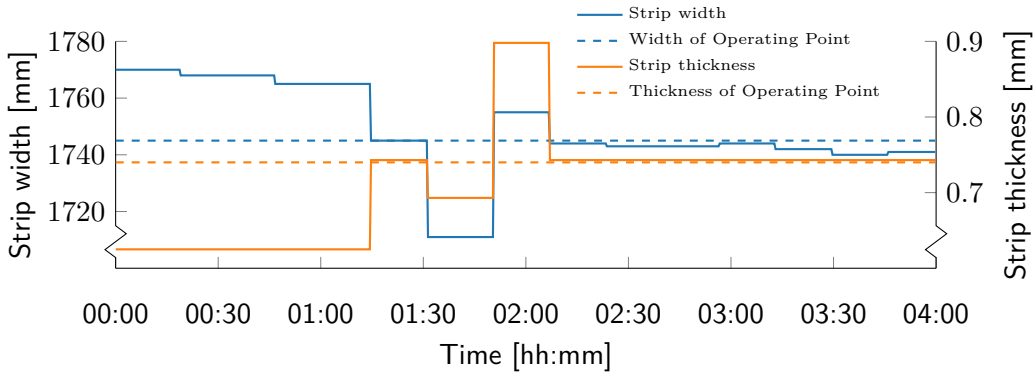

Figure 6-3: Strip dimensions used in the operating point. Solid lines indicate the actual strip dimension during the production period. Dashed lines indicate the dimensions used for the operating point.

6-4-1 Results of Case Study 1

The target temperature, measured temperature and the calculated temperatures by the Linear MPC and Piecewise Affine MPC are depicted in Figure 6-4.

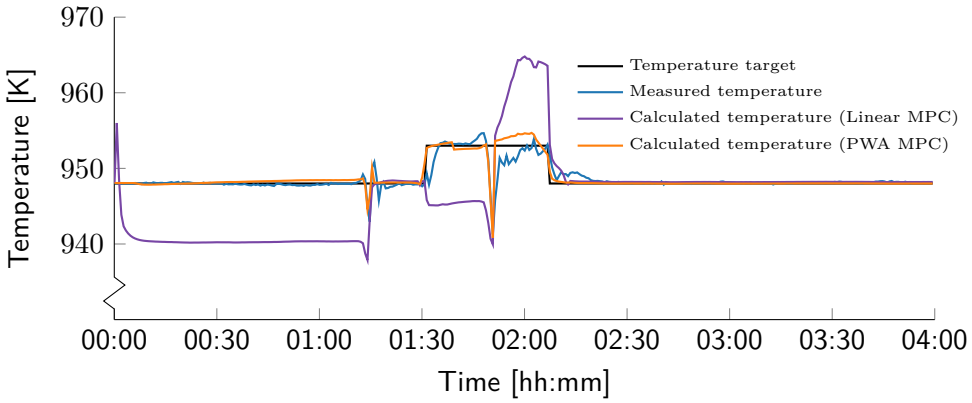

Figure 6-4: Target, measured and calculated temperatures from simulation of 6 April 2017 with Linear MPC and Piecewise Affine MPC.

6-4-2 Discussion of Results of Case Study 1

The results of the simulation of a production period of 4 hours of 6 April 2017 are depicted in Figure 6-4. It can be seen that both the Linear MPC and the PWA MPC follow the trend of the measured temperature. However, the Linear MPC has a small deviation. When taking a closer look, it is noticed that the temperature calculated by the Linear MPC tracks the target temperature only when the strip dimensions used as operating point are equal to the actual dimensions of the strip inside the Slow-Cooling Section. When the strip thickness used in the operating point is larger than the actual strip thickness, the calculated temperature is lower than desired, and vice versa. The Linear MPC assumes there is more steel than actually is present in the Slow-Cooling Section. This results in more cooling of the steel than actually necessary. The temperature calculated by the PWA MPC tracks the target temperature closely. Even at transient conditions, the calculated temperature stays on target. Between 01:00 h and 01:30 h a sudden decrease in line speed can be seen. This results in a drop in temperature also. The steel resides longer than planned in the cooler environment of the Slow-Cooling Section and therefore cools down more. The results clearly show that the Linear MPC only operates as desired when the operating point used for linearisation matches the actual operating conditions of the Slow-Cooling Section. The use of a set of piecewise affine functions as internal model of the MPC proves to give good results.

6-5 Case Study 2

In the previous section a simulation with steady operating conditions is performed. But as explained, the annealing furnaces operate more often under transient operating conditions, due to the ongoing diversification of the product portfolio. Strips with different dimensions and target temperatures succeed each other. The performance of the Linear MPC as well as that of the Piecewise Affine MPC is tested during a simulation of a production period of 8 hours of 13 May 2017. This production period is characterised by non steady operating conditions, as shown in Figure 6-2. Similar as in the previous case study, the Linear MPC is created at a specific operating point. For this case study, a line speed of 2,1 m s^{-1} is used. The strip dimensions used as operating point are depicted in Figure 6-5 by the dashed lines. The solid lines indicate the strip dimensions during the production period.

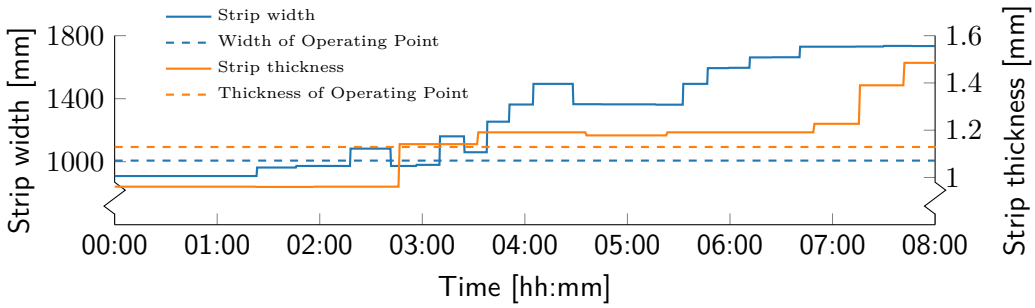

Figure 6-5: Strip dimensions used in the operating point. Solid lines indicate the actual strip dimension during the production period. Dashed lines indicate the dimensions used for the operating point.

As explained, the nonlinear furnace model is used to represent the Slow-Cooling Section. Therefore it seems more accurate to compare the temperatures calculated by using the nonlinear furnace model and using the process data as depicted in Figure 6-2 with the calculated temperatures by the Linear MPC and the Piecewise Affine MPC.

6-5-1 Results of Case Study 2

The calculated temperatures by using the nonlinear furnace model and process data represent the "real" temperatures. The results from the Linear MPC are depicted in Figure 6-6. The results from the Piecewise Affine MPC are depicted in Figure 6-7.

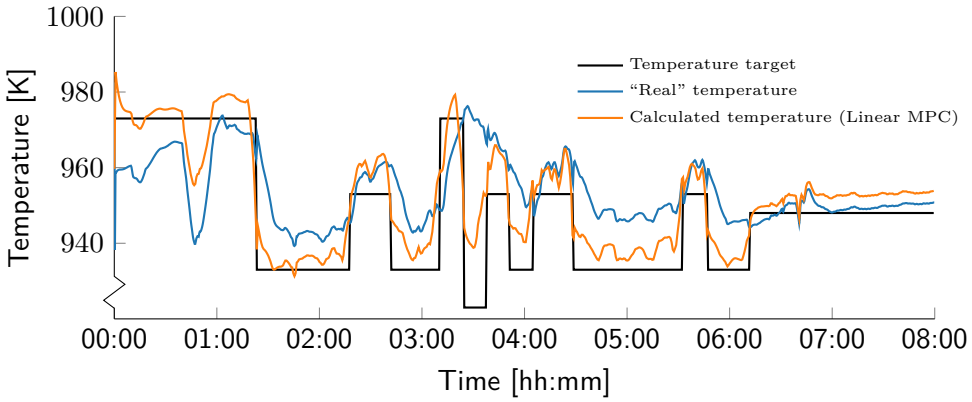

Figure 6-6: Target, measured and calculated temperatures from simulation of 13 May 2017 with Linear MPC.

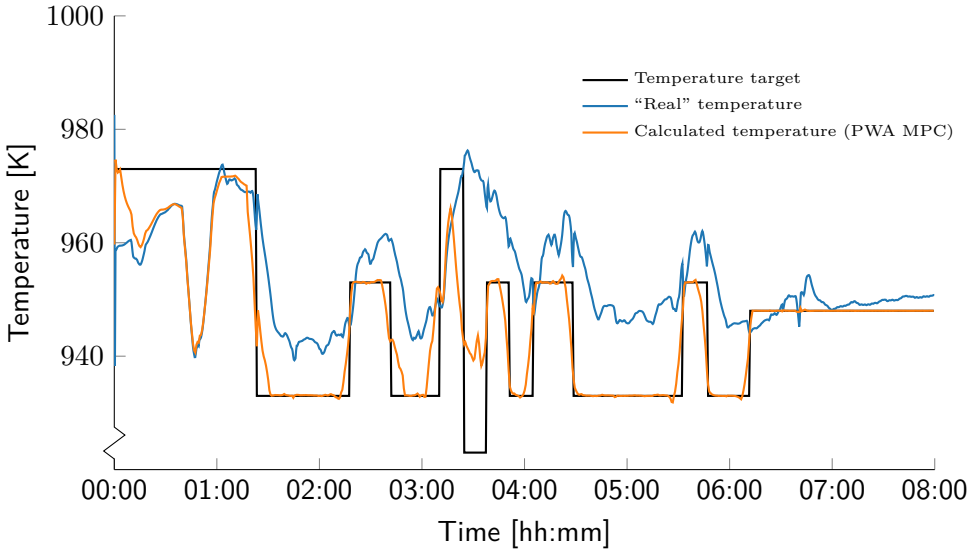

Figure 6-7: Target, measured and calculated temperatures from simulation of 13 May 2017 with Piecewise Affine MPC.

The calculated inputs signals by the PWA MPC and the actual input signals from 13 May 2017 are depicted in Figure 6-8 and Figure 6-9, respectively.

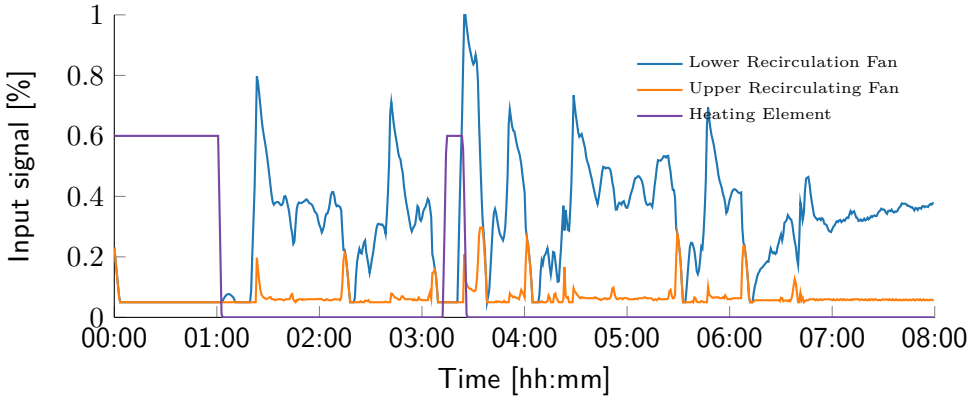

Figure 6-8: Input signals calculated by Piecewise Affine MPC.

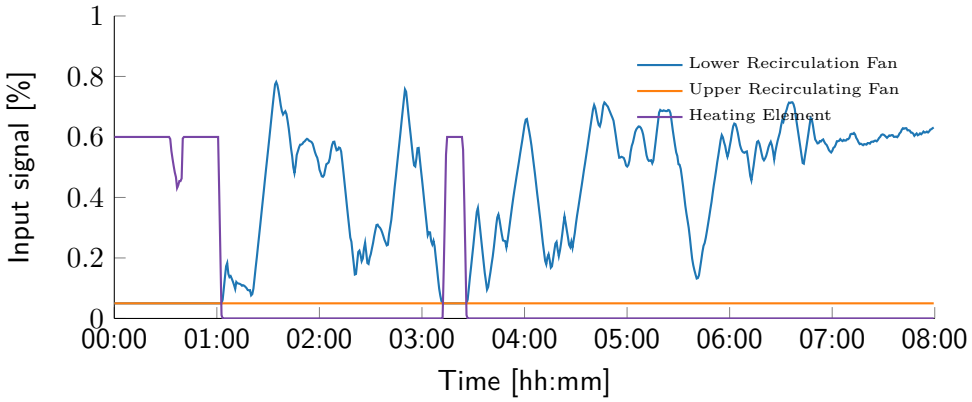

Figure 6-9: Actual input signals from 13 May 2017.

6-5-2 Discussion of Results of Case Study 2

Contrary to the first case study, the operating conditions for this simulation are highly variable. The target temperature for the steel switch frequently and new targets only last for a short period of time. The Linear MPC is not able to accurately track the target temperature. The strip dimensions used as operating point are smaller than the actual strip dimensions in a large part of the production period. The Linear MPC assumes that less steel is present in the Slow-Cooling Section. This leads to not high enough rotational speeds of the recirculation fans to cool the actual wider and thicker strips. The Piecewise Affine MPC is able to track the target temperature closely. When a switch in target temperature is foreseen, the controller prepares at the end of the current strip for the target temperature of the next strip. For example, this phenomena can be seen around 01:30 h of the simulation. However, sometimes the new target temperature is too big a change and the controller is not able to let the steel reach the desired temperature. Between 03:00 h and 04:00 big variations in the target temperature can be seen in a short period of time. The steel approaches the target

temperature. But before it reaches this new target temperature, the MPC already has to prepare for the next target temperature. In the next case study, the acceleration limits of the recirculation fans are relaxed, to investigate the possibilities of increased capacity.

Comparable to the previous case study, in this case study a sudden line speed decrease can be seen. The steel resides longer than planned in the Slow-Cooling Section, which results in a lower steel temperature than desired. The measured temperature and both the calculated temperatures from the Linear MPC and Piecewise Affine show a lower steel temperature than desired. The current controller and the newly developed controllers are not able in the current set-up to deal with these sudden and intense line speed decreases. As mentioned, the effect of relaxation of the actuator constraints is investigated in the next case study.

As explained, the primary objective of the current and new controller is to achieve the desired steel temperature at the exit of the Slow-Cooling Section. Therefore, the performance of the controller can be measured in terms of the error between the steel temperature and this target temperature. In the two case studies, it is seen that the Piecewise Affine MPC outperforms the Linear MPC. The Piecewise Affine MPC is compared to the control system, currently active in the Slow-Cooling Section. The absolute error between the real temperature, calculated by the nonlinear model, using process data and the target temperature and the absolute error between the calculated temperate by thy Piecewise Affine MPC and the target temperature are depicted in Figure 6-10.

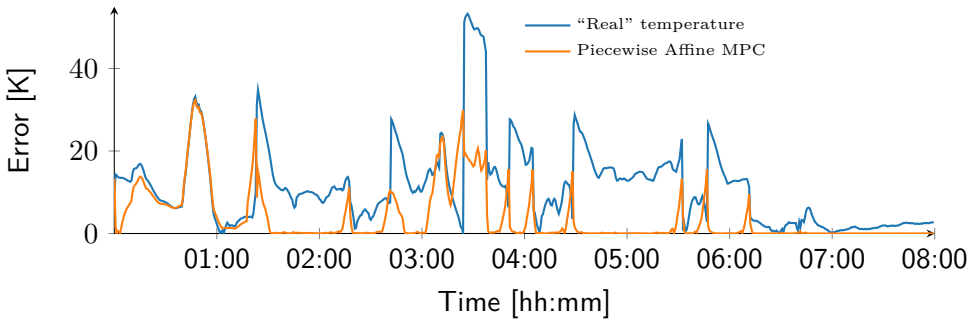

Figure 6-10: Error between target temperature and calculated temperature from the current control system and new Piecewise Affine MPC.

6-6 Case Study 3

The two previous case study show that the new controller is able to track the reference temperature. However, when the target temperature drops significantly, as can be seen around 03:30 hour in Figure 6-7, the temperature of the steel does not reach this new target temperature. As explained in Section 5-4-2, the acceleration rate of the recirculation fans is limited. These acceleration constraints are defined by the manufacturer of the Slow-Cooling Section. Accelerating the recirculation fans too fast could lead to a too low pressure inside the Slow-Cooling Section, which activates the emergency protocol.

Besides testing the performance of the controller, simulations could also be used to investigate the effect of new settings or potential changes to the Slow-Cooling Section. Therefore, in the following case study, the constraints of the acceleration limit of the recirculation fans are

relaxed from 5% to 15% per 60 seconds. If this case study shows that relaxation of the constraints is beneficial for the performance of the Slow-Cooling Section, it might by useful to reinvestigate the possibility of actual relaxation of these constraints.

6-6-1 Results of Case Study 3

The same production period as in case study 2 is simulated. But the acceleration constraints are relaxed for this case study. Only the Piecewise Affine MPC is used for this case study. The results from the Piecewise Affine MPC with original constraints and those from the Piecewise Affine MPC with constraint relaxation are depicted in Figure 6-11.

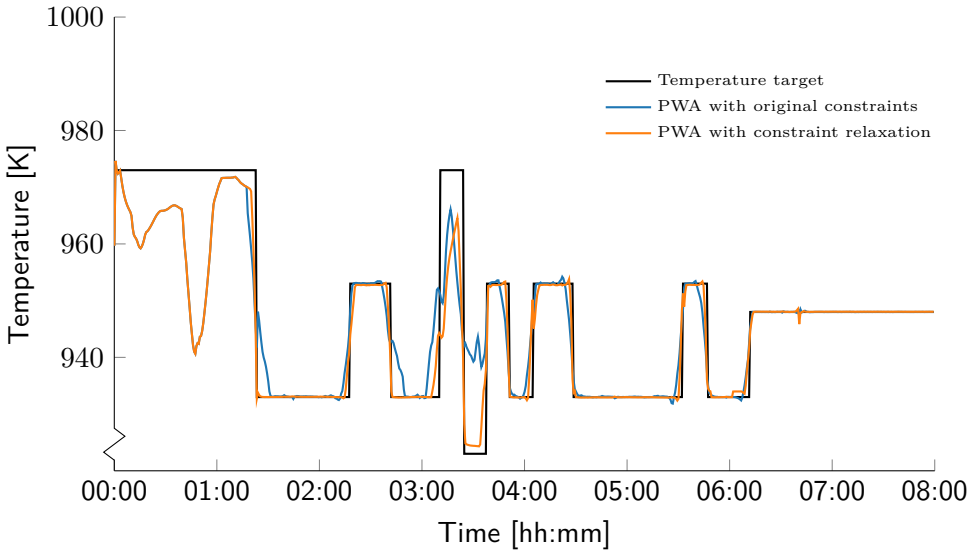

Figure 6-11: Target and calculated temperatures by Piecewise Affine MPC with original constraints and Piecewise Affine MPC with constraint relaxation.

6-6-2 Discussion of Results of Case Study 3

The goal of this case study is to investigate the effect of relaxation of the acceleration constraints. The target temperature decreases from 973 K to 923 K around 03:30 h. With the current settings in the Slow-Cooling Section, it is not possible to reach this new target temperature in time. As can be seen in Figure 6-11, the steel temperature approximates this desired target temperature faster and more closely with constraints relaxation. The constraint relaxation enables faster increase of the rotational speed of the recirculation fans. This case study showed that investigating the possibility of constraint relaxation could be beneficial for the overall performance of the Slow-Cooling Section.

6-7 Conclusions

In this chapter, three cases studies are performed. The first two case studies test the performance of the newly developed controllers. The first case study simulates a production period

with steady operating conditions. The second case study simulates a production period with transient operating conditions.

The third case study investigates the effect of constraint relaxation. If the recirculation fans are allowed to accelerate faster, the cooling capacity could be increased and more transient conditions in the Slow-Cooling Section can be handled.

6-7-1 Linear MPC

In both case studies, the Linear MPC was able to track the desired temperature, only when the parameters used as operating point matched the actual operating conditions in the Slow-Cooling Section. The operating point is chosen such that it is an average value of the actual process parameters. If the Linear MPC is implemented on-line, the operating point can be selected per day by looking at the production schedule. Compared to the Piecewise Affine MPC, the Linear MPC is able to solve the optimisation routine faster. The future process parameters are not taken into account, when optimising the control input. In Figure 6-4 it can clearly be seen that the temperature of the steel tracks the target temperature only when the strip dimensions used as operating point match the actual dimensions of the strip inside the Slow-Cooling Section. One of the motivations for the development of an MPC is that future process parameters and strip dimensions could be taken into account to achieve precise temperature control, also during transient conditions. By using the Linear MPC, precise temperature control is not possible for the variable process conditions in the Slow-Cooling Section.

6-7-2 Piecewise Affine MPC

The Piecewise Affine MPC is able to track the target temperature closely, both for steady and highly variable operating conditions. The development of the Piecewise Affine MPC requires significantly greater effort, compared to the Linear MPC. Especially obtaining the system matrices, as a function of the future process parameters, and then using these system matrices to create the prediction equation, is disadvantageous for the computation effort. The future process parameters are estimated based on the line speed.

The results from both the case studies show that the Piecewise Affine MPC achieves precise temperature control, while respecting the process constraints. In Figure 6-7 it can be seen that in case of a switch in target temperature, the Piecewise Affine MPC starts to prepare for the next steel strip, within temperature limits and maximising the on-target temperature for both strips.

6-7-3 Acceleration Constraints

In case study 3, relaxation of constraints is investigated. For some operating conditions, the temperature of the steel did not reach the target temperature, due to a too big increase / decrease of the target temperature. Relaxation of the acceleration limits proved to be beneficial for the overall performance of the Slow-Cooling Section. It is therefore recommended to investigate if actual relaxation of these constraints is possible, within the safety limits.

6-7-4 Computation Time

An MPC is developed as an on-line control system. This means that the optimisation routine has to be solved within real-time. As explained, the computational effort for the Linear MPC is smaller compared to the Piecewise Affine MPC. Both the Linear MPC and Piecewise Affine MPC can be executed within real-time. It takes 2,5 hours to simulate a production period of 4 hours, comparable to case study 1. And it takes 4 hours to simulate a production period of 8 hours, comparable to case study 2. The simulations are performed with MATLAB R2016b on a HP Z-Book with a 2,4 GHz Intel Core i7 processor and 8GB of RAM. The computing power in DVL3 is much better, compared to this HP Z-Book. This indicates that the controllers are qualified for on-line control in the Slow-Cooling Section.

Chapter 7

Conclusions and Recommendations

7-1 Introduction

The production of Advanced High Strength Steels requires precise temperature control during the cooling process in the annealing furnace. The Slow-Cooling Section is a part of the cooling process, operating at a temperature level between 923 K and 1073 K. It has both cooling and heating capabilities to effectively adjust the temperature required by the metallurgical prescription of a specific strip product. The question to be answered in this research is the following:

"How can the hybrid set-up of the Slow-Cooling Section be modelled and controlled, while respecting all process variations, such that precise temperature control can be achieved"

7-1-1 Nonlinear Process Model

One of the objectives of this research is the development of a generic nonlinear process model, describing the cooling and heating process inside the Slow-Cooling Section and its dynamic relation to the strip transport. The conclusions on furnace modelling in this research are the following

- This research led to a nonlinear furnace model, mathematically describing the dynamics of the thermal process, based on first principles.
- Parameter estimation is used to obtain the convective heat transfer coefficient.
- Runge-Kutta method is used to achieve good accuracy for numerically solving the nonlinear furnace model.
- Validation of the nonlinear furnace model shows good agreement. 90% of the calculated temperatures lie within a range of $+/-$ 5 K, compared to the production data.

The model is developed in a generic way, such that it can be used in future research. The model can easily be extended to fit another process in the annealing furnace or in case of line adjustments.

7-1-2 Linear MPC and Piecewise Affine MPC

The second objective of this research is the development of a model-based predictive controller. The conclusions on furnace control in this research are the following:

- The nonlinear furnace model is linearised and converted to discrete time, to fit the MPC framework.
- A Linear MPC and a Piecewise Affine MPC are designed, with the associated objectives and constraints.
- The Piecewise Affine MPC is selected based on the ability of taking future process parameters into account.
- During simulation studies, the performance of the Linear MPC and Piecewise Affine MPC are tested.
- The Linear MPC yielded, as expected, only satisfactory results for specific conditions.
- The Piecewise Affine MPC yields satisfactory results, for both steady and highly variable process conditions.

7-2 Recommendations and Future Research

Recommendations regarding the extension of the process model are formulated. During this research, several assumptions had to be made due to limited amount of information on several components. If these components are included in the model, more accurate results could be achieved. Besides this modelling recommendations, the results of the simulations indicate the limitations of the Slow-Cooling Sections in terms of cooling and heating capacity. The modelling recommendations and recommendations concerning the limitations of the capacity are explained next.

7-2-1 Heat Exchanger

The protective gas is cooled by a water-cooled heat exchanger. The temperature drop of the protective gas over this heat-exchanger is mainly influenced by the pressure, flow speed and the performance of the heat exchanger. Limited information on these parameters and the heat exchanger could be found. It is therefore decided not to include the dynamics of the heat exchanger in the nonlinear process model. The influence of the heat exchanger is simplified and a constant temperature for the incoming cooled protective gas is assumed. The temperature of the incoming cooled gas affects the process inside the Slow-Cooling Section and better results could be achieved if more is known on the dynamics of the heat exchanger. It is recommended to study the heat exchanger in more detail.

7-2-2 Specific Heat

Specific heat is defined as the amount of heat required to increase the temperature of the steel. The specific heat is temperature dependent also and different for every steel grade. In

this research the relation between specific heat and temperature for low-carbon steel is used for every steel grade. It is recommended to include the specific heat relations for every steel grade into the process model.

7-2-3 Cooling and Heating Capacity

During the simulation, it was noticed that in case of an unexpected decrease of the line speed, the heating elements are not able to deliver enough heat to prevent the steel from cooling down to much. On the other hand, the ramping constraints for the recirculation fans are limiting the cooling capacity inside the Slow-Cooling Section. Simulations showed that relaxation of the ramping constraints could lead to an improved performance of the temperature control inside the Slow-Cooling Section. Therefore, to further improve the control response and accuracy, it is recommended to investigate the capacity of the heating elements and if relaxation of ramping constraints for the recirculation fans is possible.

Appendix A

Fundamentals of Heat Transfer

A-1 Introduction

When the hot steel strip enters the cool environment of the Slow-Cooling Section, the steel strip loses internal energy, while the surrounding elements gain internal energy. This process is known as heat transfer. The heat transfer in the Slow-Cooling Section relies on different heat transfer mechanisms. These mechanisms, also known as modes, are divided into three of the most important heat transfer mechanisms, i.e. conduction, convection and radiation. In this chapter the fundamentals of heat transfer are described, since it forms the basis of the furnace model, developed in Chapter 4.

A-2 First Law of Thermodynamics

The analysis of heat transfer starts with a basic law of physics, the energy conservation principle [29]. This principle states that energy in a closed system cannot be created nor destroyed, but can only transform from one form to another. The energy conservation principle is given by:

$$\begin{gathered}\text{Change in internal energy within the system} = \text{Heat transferred into the system} + \text{Heat generated within the system} \\ \Delta U = \dot{Q}\Delta t + \dot{Q}_v\Delta t\end{gathered} \tag{A-1}$$

After some simplifications, we end up with a special form of the first law of thermodynamics, commonly used in engineering to describe heat flow between objects. The equation that forms the basis of the furnace model is given by:

$$\rho V c\frac{dT}{dt} = \dot{Q} + \dot{Q}_v \tag{A-2}$$

where ρ, V and c represent the density, volume and specific heat respectively, of the object under consideration. Eq. (A-2) gives the rate of change of temperature with time. The change of temperature depends on the net flow towards the system, $\dot{Q}$, and heat generated within the system, $\dot{Q}_v$.

A-3 Heat Transfer Modes

The heat flow towards the system, $\dot{Q}$, from Eq. (A-2) can be divided into the modes of heat transfer: conduction, convection and radiation. The change in internal energy within the system can be described by the change in enthalpy of the object. In the remainder of this chapter, these three modes and the concept enthalpy are further described.

A-3-1 Conduction

Heat transferred through a body by diffusion is known as conduction. In engineering, conduction is often described using phenomenological laws, proposed by Fourier in [18]. Fourier's law of heat conduction states that in a homogeneous substance, the heat flux, in one dimension, is proportional to the negative of the temperature gradient given by:

$$\dot{Q} = qA \quad \text{and} \quad q \propto -\frac{dT}{dx} \tag{A-3}$$

where q is the heat flux, T is the temperature, x is the coordinate in the flow direction and A is the cross-sectional area. By introducing a constant λ, known as thermal conductivity of a substance, Fourier's law is obtained:

$$\dot{Q} = qA = -\lambda A \frac{dT}{dx} \tag{A-4}$$

where λ depends on the microscopic structure and temperature of the material. Heat conduction occurs in various sections of the furnace, e.g. heat transfer through the furnace walls due to the temperature difference between the inside of the furnace and the ambient. The heat flow through two layers of different material is equal in each layer, but results in different temperature gradients. A simple representation is depicted in Figure A-1.

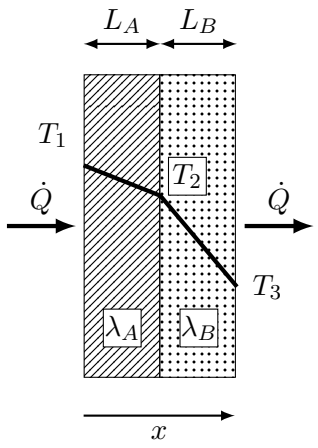

Figure A-1: Heat flow in a wall of two slabs of material and temperature gradient.

By integrating Eq. (A-4), we obtain the standard form

$$\begin{aligned} \frac{\dot{Q}}{A}\int_0^L dx &= -\int_{T_1}^{T_2} \lambda dT \\ \dot{Q} &= \frac{\lambda}{L} A(T_1 - T_2) \end{aligned} \tag{A-5}$$

where L represents the thickness of the insulation layer. If the heat flows through a wall of two types of material, as depicted in Figure A-1, the heat flow through each layer is equal and the following is obtained:

$$\dot{Q} = \frac{\lambda_A}{L_A} A(T_1 - T_2) = \frac{\lambda_B}{L_B} A(T_2 - T_3) \tag{A-6}$$

Often only the two outer temperatures are of interest or known. By rearranging this equation, the interface temperature T_2 can be eliminated, which yields:

$$\dot{Q} = \frac{A(T_1 - T_3)}{L_A/\lambda_A + L_B/\lambda_B} \tag{A-7}$$

Eq. (A-7) can be applied to all kinds of insulation layers and will be used to calculate the heat flow between the inside of the furnace and the surroundings.

A-3-2 Convection

Convective heat transfer relates to the heat flow from a surface to a moving fluid. The flow of the moving fluid can be forced, e.g. a gas blown by a fan, or free, due to buoyancy forces from density differences. Another distinction has to be made between internal, e.g. inside a pipe, or external flow, e.g. flow on the outside of the furnace. Flows can be either laminar, at lower velocities and more viscous fluids, or turbulent. A flow is turbulent when the dimensionless Reynolds number exceeds 2.300. Turbulent flows come with higher heat

transfer rates compared to laminar flows. The heat transfer can be calculated using Newton's Law of Cooling, given by:

$$\dot{Q} = qA = h_c A(T_{\text{surface}} - T_{\text{fluid}}) \tag{A-8}$$

where q is the heat flux at the boundary, A is the area of the surface,h_c is the heat transfer coefficient and $T_{\text{surface}} - T_{\text{fluid}}$ defines the temperature difference between the surface and fluid. The heat transfer coefficient mainly depends on the type of flow, considering the distinctions made above.

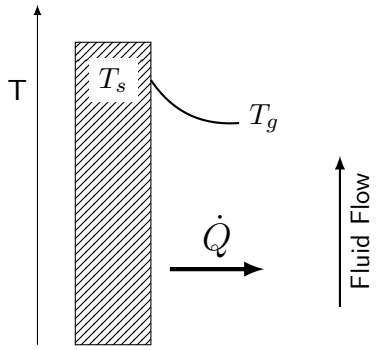

Figure A-2: Schematic overview of convective heat transfer from a surface to a fluid.

Convection also occurs in various section of the furnace, e.g. the protective gas is blown against the strip, which is a form of convection. Inside the furnace, forced convection is more present, compared to the outside of the furnace where free convection is the dominant mode of convection. The heat transfer coefficient varies a lot due to changes in fluid speed for instance. Therefore it is convenient to define an average heat transfer coefficient $\overline{h}_c$, where the heat transfer coefficient is integrated over the entire surface by:

$$\overline{h}_c = \frac{1}{A}\int_0^A h_c dA \tag{A-9}$$

This average heat transfer coefficient is often defined in terms of the Nusselt number, given by:

$$\overline{\text{Nu}} = \frac{\overline{h}_c L}{\lambda} \tag{A-10}$$

where L is the characteristic length of the surface and λ the thermal conductivity of the fluid. The Nusselt number depends on the type of convection, i.e free versus forced and laminar versus turbulent. The Nusselt number for these different situations is described below.

Forced Convection

For forced laminar convection [44] on a plate, the Nusselt number can be approximated by:

$$\overline{\text{Nu}} = 0,664\text{Re}_L^{1/2}\text{Pr}^{1/3} \tag{A-11}$$

For forced turbulent convection [44] on a plate, the Nusselt number can be approximated by:

$$\overline{\mathrm{Nu}} = \frac{0,037\mathrm{Re}^{4/5}\mathrm{Pr}}{1 + 2,443\mathrm{Re}^{-1/10}\left(\mathrm{Pr}^{2/3} - 1\right)} \tag{A-12}$$

Free Convection

The Nusselt number for free, laminar and turbulent, flows near a vertical surface [44] can be approximated by:

$$\mathrm{Nu} = \left\{0,825 + 0,387\left[\mathrm{Ra}f_1(\mathrm{Pr})\right]^{1/6}\right\}^2 \tag{A-13}$$

with the function $f_1(\mathrm{Pr})$ is given by:

$$f_1(\mathrm{Pr}) = \left[1 + \left(\frac{0,482}{\mathrm{Pr}}\right)^{9/16}\right]^{-16/9} \tag{A-14}$$

In the above equation, the non-dimensional Reynolds Re, Rayleigh Ra, Prandtl Pr and Grashof Gr number appear, which are defined by:

$$\begin{aligned}
\mathrm{Re} &= \frac{\rho v L}{\mu} \\
\mathrm{Ra} &= \frac{\beta \Delta T g L^3}{\nu \alpha} \\
\mathrm{Pr} &= \frac{c_p \mu}{\lambda} = \frac{\nu}{\lambda/\rho c_p} = \frac{\nu}{\alpha} \\
\mathrm{Gr} &= \frac{\beta \Delta T g L^3}{\nu^2}
\end{aligned} \tag{A-15}$$

where β is the thermal coefficient of volume expansion [K^{-1}], ν is the kinematic viscosity [m^2 s^{-1}], α is thermal diffusivity [m^2 s^{-1}] and μ is the dynamic viscosity [kg m^{-1} s^{-1}].

A-3-3 Radiation

Radiation is generated by the thermal motion of charged particles. Compared to conduction and convection, no medium is required. Thermal radiation is split in two forms, i.e. irradiation and radiosity. Irradiation is the flux of radiant energy incident on a surface. Radiosity is the flux leaving a surface due to emission and reflection. In the following equation ε represents the emissivity of a body. A perfect emitter and receiver of radiation has an emissivity equal to 1, i.e. nothing can emit or receive more radiation than these so called black bodies. The amount of radiation surface A emits is given by the Stefan-Boltzmann law:

$$JA = \sigma T^4 A \tag{A-16}$$

where σ represents the Stefan-Boltzmann coefficient ($\simeq 5,67 \cdot 10^{-8}$ W m^{-2} K^{-1}). Important to note is that temperature is the absolute temperature in Kelvin. The emissivity for a black body is equal to 1, meaning that all incident radiation is absorbed, and thus none is reflected. The radiation leaving the surface is emitted by the surface. Real surfaces emit less radiation compared to black surfaces. The fraction of radiation emitted is known as the emissivity ε of a surface. The relation between radiation emitted, absorbed and reflected is given by:

$$\varepsilon = \alpha = 1 - \rho \tag{A-17}$$

where ε represents the amount of energy emitted by a surface divided by the amount of energy emitted by a black surface at the same temperature, absorptivity α is the amount of incoming radiation absorbed divided by the total amount of incoming radiation and reflectivity ρ is the amount of incoming radiation reflected divided by the total amount of incoming radiation.

The irradiation G, the flux of radiant energy incident on the surface A_1, depends on the temperature T_2 of emitting surface by:

$$G_1 A_1 = \sigma T_2^4 A_1 \tag{A-18}$$

The net heat flow from surface A_1 is given by the radiosity minus the irradiation by:

$$\begin{aligned} \dot{Q} &= (J_1 - G_1)A_1 \\ &= \sigma(T_1^4 - T_2^4)A_1 \end{aligned} \tag{A-19}$$

In Figure A-3 a schematic overview of thermal radiation between two surfaces is depicted, where A_1 in Eq. (A-19) is the surface area of the circle.

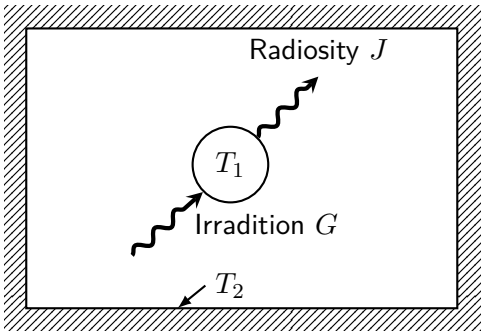

Figure A-3: Net heat flow from one surface.

Shape Factors

Eq. (A-19) assumes that all the radiation from surface 1 reaches surface 2. In most cases this is not realistic. The fraction of energy leaving a surface and intercepted by another surface is defined by the shape factor F, which depends on size, shape, and orientation of the surfaces. The fraction of radiation leaving surface A_1 that is intercepted by A_2 is given by the shape

factor $F_{1\to2}$. The fraction of radiation leaving surface A_2 that is intercepted by A_1 is given by the shape factor $F_{2\to1}$. The heat flow between two finite black surfaces is then given by:

$$\dot{Q}_{12} = \sigma T_1^4 A_1 F_{1\to2} - \sigma T_2^4 A_2 F_{2\to1} \tag{A-20}$$

The reciprocal rule describes the relation between the shape factors and surfaces by:

$$A_1 F_{1\to2} = A_2 F_{2\to1} \tag{A-21}$$

By substituting this in Eq. (A-20), the net heat flow between two black surfaces is given by:

$$\dot{Q}_{12} = A_1 F_{1\to2} \sigma (T_1^4 - T_2^4) \tag{A-22}$$

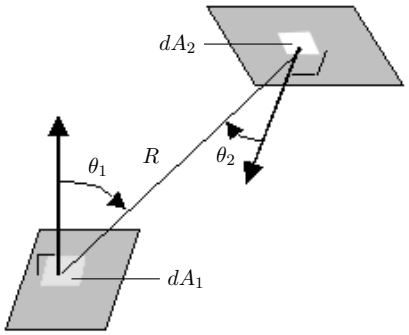

Figure A-4: Shape factors between two surfaces.

The shape factors can be calculated by solving the following double integral:

$$F_{1\to2} = \frac{1}{A_1} \int_{A_1} \int_{A_2} \frac{\cos(\theta_1) \cdot \cos(\theta_2)}{\pi \cdot R^2} dA_1 dA_2 \tag{A-23}$$

where A_1 and A_2 represent surface areas, θ_1 and θ_2 represent angles between the normal to the surface and the direction of the other surface and R represents the distance between the two surfaces, as depicted in Figure A-4. Solving the double integral to obtain the shape factors can be difficult. In [29] shape factors for common two- and three-dimensional configurations are given, which can be used as an approximation of the reality. The summation rule can also be used to obtain shape factors. If surface i lies in an enclosure of n surfaces, all energy leaving surface i must be intercepted by the surfaces in the enclosure, by the summation rule:

$$\sum_{j=1}^{n} F_{i\to j} = 1 \tag{A-24}$$

By combining the reciprocal rule and summation rule and using available shape factors for two- and three-dimensional configurations, determining shape factors is simpler than by using the double integral.

Energy Balance Method

The analysis of radiation heat flow between black surfaces is trivial. However, real surfaces are not black and the emissivity, ε, of a surface also plays a role in the heat flow. The radiant heat flux of a gray surface can be expressed in terms of radiosity J, irradiation G and emissive power E_b. Radiosity is all the radiation leaving the surface, either by reflection or emission, given by:

$$\begin{aligned} J &= \varepsilon E_b + \rho G \\ J &= \varepsilon E_b + (1-\varepsilon) G \\ \text{solving for G gives} & \\ G &= \frac{J - \varepsilon E_b}{1-\varepsilon} \end{aligned} \tag{A-25}$$

By substituting the result for G of Eq. (A-25) in Eq. (A-19), the following is obtained:

$$\begin{aligned} \dot{Q} &= (J - G)\, A \\ &= \left(J - \frac{J - \varepsilon E_b}{1-\varepsilon} \right) A \\ &= \left(\frac{(1-\varepsilon)J - J + \varepsilon E_b}{1-\varepsilon} \right) A \\ &= \left(\frac{\varepsilon A}{1-\varepsilon} \right) (E_b - J) \end{aligned} \tag{A-26}$$

where $E_b = \sigma T^4$. This is also known as the net-radiation method, often used in literature when modelling annealing furnaces [17, 33, 41, 45]. Eq. (A-26) is used to model the radiation heat transfer between the elements in the Slow-Cooling Section in Chapter 4.

A-3-4 Enthalpy

Analysis of heat transfer process depends on the type of system. Eq. (A-1) describes a closed system. In Chapter 4, parts of the Slow-Cooling Section are modelled as an open system, where steel flows in and out of the system boundaries. As mentioned in the introduction of this chapter, the increase in internal energy may result in an increase in temperature. If we consider the steel strip, the increase in internal energy is calculated by the amount of energy of the incoming steel and the heat flow to the steel, minus the amount of the energy of the steel leaving. The Slow-Cooling Section is divided into computational cells, which will be further elaborated in Chapter 4. Such computational cells are also known as control volumes. The amount of energy of the incoming steel and the steel leaving the control volume is given by:

$$\dot{Q} = \dot{m} c_p T \tag{A-27}$$

where $\dot{m}$ is the mass flow of incoming steel, c_p is the specific heat of the steel. T is the temperature of the incoming steel to the control volume or steel leaving the control volume.

Appendix B

Metallurgy

In this chapter the goal of annealing is described and which metallurgical aspects come into play during annealing. The main goal of the annealing treatment is to ensure the desired mechanical properties of the steel strip. The mechanical properties are obtained by the chemical composition en the crystal structure. In an earlier stage of the steel production, the chemical composition of the steel strip is determined. The final crystal structure is obtained by the annealing treatment.

B-1 Crystal Structure

Steel is an alloy of mainly iron and carbon. The crystal structure of iron normally takes on two crystalline forms. The first is body centred cubic (BCC), with an atomic packing factor of 68% and face centred cubic (FCC), with an atomic packing factor of 74%. In iron the BCC appears in the form of Ferrite, and the FCC is in the form of Austenite. The steel grade is created by letting amounts of carbon, and other alloying elements, enter the crystal structure of iron. Dissolution of carbon and alloying elements happens either by substituting iron atoms or by dissolving in-between the iron atoms. Dissolution of these elements ensures a certain hardness and tensile strength of the steel. Dependent on the concentration of carbon, the steel appears in different crystal structures, depicted in Figure B-1[1].

Cementite is a compound of iron and carbon, Fe_3C, also known as iron carbide. It is known for making the steel very hard and wear resistant. The phase diagram in Figure B-1 is the situation in equilibrium, meaning that sufficient time has passed to establish equilibrium. The cooling rate in the annealing furnace is therefore of vital essence for the crystal structure of the steel. The cooling rate determines the grain size and the crystal structure. Slow cooling enables forming of the iron-carbides. Cooling the steel at higher rates results in remaining carbon in the steel. This can be desirable for certain steel grades. Additional crystal structures appear in the phase diagram, but will not be discussed here. The heating furnaces in the

[1] Materials Science and Metallurgy, 4th ed., Pollack, Prentice-Hall, 1988

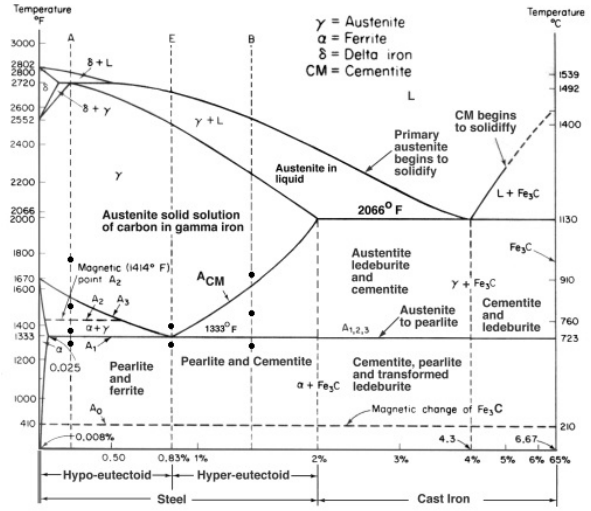

Figure B-1: Iron-carbon phase diagram.

annealing treatment ensure the desired ductility and strength of the steel. Austenite has a higher ductility compared to ferrite, for instance. Four stages, depicted in Figure B-2, occur in the annealing process:

- Recovery
- Nucleation
- Recrystallisation
- Grain growth

B-2 Recrystallisation

Recovery softens the steel by removal or rearrangement of the dislocations into lower energy configurations. The dislocations increase the yield strength of the steel, and thus by removing them, a decrease in yield strength is the result. Recrystallisation takes place above recrystallisation temperature of the steel, slightly higher than the temperature during the recovery stage. In this stage the yield strength and hardness will be further decreased and the ductility of the steel will be increased, as the grain structure grows. Recrystallisation depends on temperature and time. Sufficient time is needed for the steel to fully recrystallise. When keeping the steel at higher temperature, grain growth occurs. The size of the grains in the steel grow, and thereby losing yield strength.

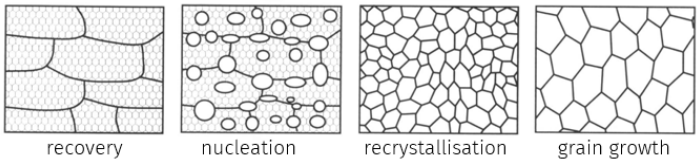

Figure B-2: Process of Recrystallisation.

Glossary

List of Acronyms

AHSS	Advanced High Strength Steel
DVL3	Dompel Verzink Lijn 3
MPC	Model Predictive Control
PWA	Piecewise Affine
QP	Quadratic Programming

List of Symbols

Symbol	Unit	Description
Latin letters		
A	m^2 or $-$	Surface Area or State Matrix
B	$-$	Input Matrix
b	$-$	Constraint Vector
C	$-$	Output Matrix
c_p	$Jkg^{-1}K^{-1}$	Specific Heat Capacity
D	$-$	Feedthrough Matrix
E	Wm^{-2} or $-$	Emissive Power or Constraint Matrix
F	$-$	Shape Factor or Prediction Equation Matrix
$f^\intercal$	$-$	Coefficient vector
G	Wm^{-2} or $-$	Irradiation or Prediction Equation Matrix
H	$-$	Hessian Matrix
h	Jkg^{-1} or $-$	Specific Enthalpy or Prediction Equation Matrix
J	Wm^{-2} or $-$	Radiosity or Cost Function
L	m or $-$	Length or Load
m	kg	Mass
N_p	$-$	Prediction horizon
P	W	Power
Q	J	Thermal Energy
r	°C or K	Target Temperature
T	°C or K	Temperature
t	s	Time
u	$-$	Input
V	m^3	Volume
v	ms^{-1}	Line Speed
W	$-$	Weighting Factors
X	$-$	Offset term
x	$-$	State
y	$-$	Output

Symbol	Unit	Description
Greek Letters		
α	$Wm^{-2}K^{-1}$	Heat Transfer Coefficient
ε	$-$	Emissivity
θ	rad	Angle
λ	$Wm^{-1}K^{-1}$	Thermal Conductivity
ρ	$kg\ m^{-3}$	Density
σ	$Wm^{-2}K^{-4}$	Stefan-Boltzmann constant
ω	RPM	Rotational speed of recirculation fans
Subscripts		
c	$-$	Continuous Time
d	$-$	Discrete Time
g	$-$	Protective Gas
r	$-$	Transport Roll
s	$-$	Steel
w	$-$	Furnace Wall

Bibliography

[1] Mohammad Davood Ahanj, Masoud Rahimi, and Ammar Abdulaziz Alsairafi. CFD modeling of a Radiant Tube Heater. *International Communications in Heat and Mass Transfer*, 39(3):432–438, mar 2012.

[2] K.J Astrom and B Wittemark. *Computer-controlled Systems: Theory and Design*. Prentice-Hall, second edition, 1990.

[3] M Bahrami, JR Culham, and MM Yovanovich. Thermal resistances of gaseous gap for conforming rough contacts. *AIAA Paper(42nd AIAA Aerospaces Meeting and Exhibit)*, (February 2015):1–11, 2004.

[4] A Bemporad and M Morari. Control of Systems Integrating Logics, Dynamics, and Constraints. *Automatica*, 35:407–427, 1999.

[5] Albert Bemporad, G. Ferrari-Trecate, and R. Morari. Observability and controllability of piecewise affine and hybrid systems. In *Proceedings of the 38th IEEE Conference on Decision and Control*, volume 4, pages 3966–3971. IEEE, 1999.

[6] Lukas Bitschnau and Martin Kozek. Modeling and Control of an Industrial Continuous Furnace. In *2009 International Conference on Computational Intelligence, Modelling and Simulation*, pages 231–236. IEEE, 2009.

[7] Lukas Bitschnau, Martin Kozek, Stefan Jakubek, and Florian Leeber. Implementation of Model Predictive Control in an Industrial Continuous Annealing Furnace. In *Control and Applications*, Calgary,AB,Canada, 2011. ACTAPRESS.

[8] P. BOINEAU, C. COPIN, and F. AGUILE. Heat transfer modelling using advanced zone model based on a CFD code. *Modélisation du rayonnement et simulation numérique des fours. Journée*, pages A1–A11.

[9] J Buijs, J Ludlage, W Van Brempt, and B De Moor. Quadratic Programming in Model Predictive Control for Large Scale Systems. *IFAC Proceedings Volumes*, 35(1):301–306, 2002.

[10] E. F. Camacho and C. Bordons. *Model Predictive control*. Advanced Textbooks in Control and Signal Processing. Springer London, London, 2007.

[11] K. S. Chapman, S. Ramadhyani, and R. Viskanta. Modeling and parametric studies of heat transfer in a direct-fired batch reheating furnace. *Journal of Heat Treating*, 8(2):137–146, sep 1990.

[12] Qing Chen, Shaoyuan Li, Yugeng Xi, and Guangbin Huang. Furnace Temperature Modeling for Continuous Annealing Process Based on Generalized Growing and Pruning RBF Neural Network. In *Advances in Neural Networks-ISNN*, pages 755–760. Springer, 2004.

[13] N. Depree, J. Sneyd, S. Taylor, M.P. Taylor, J.J.J. Chen, S. Wang, and M. O'Connor. Development and validation of models for annealing furnace control from heat transfer fundamentals. *Computers & Chemical Engineering*, 34(11):1849–1853, nov 2010.

[14] Shi Dequan, Gao Guili, Gao Zhiwei, and Xiao Peng. Application of Expert Fuzzy PID Method for Temperature Control of Heating Furnace. *Procedia Engineering*, 29:257–261, 2012.

[15] J. W. Dettman, W. E. Boyce, and R. C. DiPrima. Elementary Differential Equations and Boundary Value Problems. *The American Mathematical Monthly*, 74(6):758, jun 1967.

[16] A.A.A. Esmin, A.R. Aoki, and G. Lambert-Torres. Particle swarm optimization for fuzzy membership functions optimization. In *IEEE International Conference on Systems, Man and Cybernetics*, volume vol.3, page 6. IEEE, 2002.

[17] Martin Fein, Michael Böck-schnepps, Stephan Strommer, Martin Niederer, Andreas Steinboeck, and Andreas Kugi. Model-based control and optimization of continuous strip annealing furnaces. *Heat Processing*, 14(01):57–63, 2016.

[18] Jean Baptiste Joseph Fourier. *Théorie Analytique de la Chaleur*. Cambridge University Press, Cambridge, 1822.

[19] Bernard Friedland. *Control System Design: An Introduction to State-Space Methods*. Dover Publications Inc., 2005.

[20] Stephen Hall. Fans, Blowers, and Compressors. In *Branan's Rules of Thumb for Chemical Engineers*, pages 118–133. Elsevier, 2012.

[21] Yukun Hu, CK Tan, Jonathan Broughton, and Paul Alun Roach. Development of a first-principles hybrid model for large-scale reheating furnaces. *Applied Energy*, 173(July):555–566, jul 2016.

[22] Wei Jiang and Xuchu Jiang. Design of an Intelligent Temperature Control System Based on the Fuzzy Self-Tuning PID. *Procedia Engineering*, 43:307–311, 2012.

[23] T. Kargul, E. Wielgosz, and J. Falkus. Application of thermal analysis tests results in the numerical simulations of continuous casting process. *Archives of Metallurgy and Materials*, 60(1):221–225, 2015.

[24] C.D. Kelly, Dhani Watanapongse, and K.M. Gaskey. Application of modern control to a continuous anneal line. *IEEE Control Systems Magazine*, 8(2):32–37, apr 1988.

[25] Kenneth Levenberg. A method for the solution of certain non-linear problems in least squares. *Quarterly of Applied Mathematics*, 2(2):164–168, jul 1944.

[26] David Q. Mayne. Model predictive control: Recent developments and future promise. *Automatica*, 50(12):2967–2986, 2014.

[27] D.Q. Mayne, J.B. Rawlings, C.V. Rao, and P.O.M. Scokaert. Constrained model predictive control: Stability and optimality. *Automatica*, 36(6):789–814, jun 2000.

[28] D Mignone, G Ferrari-Trecate, and M. Morari. Stability and stabilization of piecewise affine and hybrid systems: an LMI approach. In *Proceedings of the 39th IEEE Conference on Decision and Control (Cat. No.00CH37187)*, volume 1, pages 504–509. IEEE, 2000.

[29] A.F. Mills. *Basic Heat and Mass Transfer*. Pearson Education Limited, 2nd edition, 1998.

[30] Manfred Morari and Jay H. Lee. Model predictive control: past, present and future. *Computers & Chemical Engineering*, 23(4-5):667–682, may 1999.

[31] Jorge J. Moré and D. C. Sorensen. Computing a Trust Region Step. *SIAM Journal on Scientific and Statistical Computing*, 4(3):553–572, sep 1983.

[32] M. Niederer, A. Steinboeck, S. Strommer, and A. Kugi. Analysis of Radiative Heat Transfer in an Indirect-Fired Strip Annealing Furnace based on Integral Equations. *IFAC Proceedings Volumes*, 46(16):403–408, 2013.

[33] M. Niederer, S. Strommer, A. Steinboeck, and A. Kugi. A simple control-oriented model of an indirect-fired strip annealing furnace. *International Journal of Heat and Mass Transfer*, 78:557–570, nov 2014.

[34] M. Niederer, S. Strommer, A. Steinboeck, and A. Kugi. Nonlinear model predictive control of the strip temperature in an annealing furnace. *Journal of Process Control*, 48:1–13, dec 2016.

[35] M Niederer, S Strommer, A Steinboeck, A Kugi, M Fein, G Helekal, and Andritz Ag. A Mathematical Model of a Combined Direct- and Indirect-Fired Strip Annealing Furnace. In *Proceedings of the 10th International Conference on Zinc and Zinc Alloy Coated Steel Sheet*, number June, pages 137–144, 2015.

[36] D.R. Nusman. Dynamic Modeling and Control of Hybrid Automotive Systems. Msc. thesis, Delft University of Technology, 2017.

[37] A. Pernía-Espinoza, M. Castejón-Limas, A. González-Marcos, and V. Lobato-Rubio. Steel annealing furnace robust neural network model. *Ironmaking & Steelmaking*, 32(5):418–426, 2005.

[38] J. Richalet, A. Rault, J.L. Testud, and J. Papon. Model predictive heuristic control. *Automatica*, 14(5):413–428, sep 1978.

[39] Christian Schiefer, F.X. Rubenzucker, H.P. Jorgl, and H.R. Aberl. A neural network controls the galvannealing process. *IEEE Transactions on Industry Applications*, 35(1):114–118, 1999.

[40] A. Steinboeck, D. Wild, T. Kiefer, and A. Kugi. A mathematical model of a slab reheating furnace with radiative heat transfer and non-participating gaseous media. *International Journal of Heat and Mass Transfer*, 53(25-26):5933–5946, dec 2010.

[41] A. Steinboeck, D Wild, and A Kugi. Nonlinear model predictive control of a continuous slab reheating furnace. *Control Engineering Practice*, 21(4):495–508, apr 2013.

[42] S. Strommer, M. Niederer, A. Steinboeck, and A. Kugi. A mathematical model of a direct-fired continuous strip annealing furnace. *International Journal of Heat and Mass Transfer*, 69:375–389, feb 2014.

[43] Y.C. Tian, D.C. Levy, and T. Gu. Implementing a Process Model for Real-Time Applications. *Conference on Complex Systems*, (December 2004):287–296, 2004.

[44] Wolfgang Wagner. *VDI Heat Atlas*, volume 1. 2010.

[45] D. Wild, T. Meurer, and A. Kugi. Modelling and experimental model validation for a pusher-type reheating furnace. *Mathematical and Computer Modelling of Dynamical Systems*, 15(3):209–232, jun 2009.

[46] H. Wu, R. Speets, F. Heeremans, O. Ben Driss, and R. van Buren. Non-linear model predictive control of throughput and strip temperature for continuous annealing line. *Ironmaking & Steelmaking*, 42(8):570–578, sep 2015.

[47] H. Wu, R. Speets, G. Ozcan, R. Ekhart, R. Heijke, C. Nederlof, and C.J. Boeder. Nonlinear model predictive control to improve transient production of a hot dip galvanising line. *Ironmaking & Steelmaking*, 43(7):541–549, aug 2016.

[48] Hai Wu, R. Speets, Jos van der Kooij, and Bertie van Benschop. Advanced transitional system optimiser using model predictive control for continuous annealing. In *METEC and 2nd Estad*, 2015.

[49] Naoharu Yoshitani. Modelling and parameter estimation for strip temperature control in continuous annealing processes. In *Proceedings of IECON '93 - 19th Annual Conference of IEEE Industrial Electronics*, number 1, pages 469–474. IEEE, 1993.

[50] Zhou Ming, Yu Datai, and Zhou Jiangang. A new strip temperature control method for the heating section of continuous annealing line. In *2008 IEEE Conference on Cybernetics and Intelligent Systems*, pages 861–864. IEEE, sep 2008.